

Parth Bhatia

pbhatia10a@gmail.com

Education

UNIVERSITY OF MARYLAND, BALTIMORE

Baltimore, Maryland

Degree and Date to be Conferred:

Master's in Human Genetics and Genomic Medicine, Fall 2022

JAMIA HAMDARD UNIVERSITY

New Delhi, India

Bachelor of Pharmacy

Graduation: 2020

Research Experience

- 1. Single nucleus-RNASeq and snATAC-seq transcriptomic study of traumatic brain injury in hippocampi of mice**
November, 2020 – Present
 - Analysed snRNA-Seq and snATAC-seq data generated on TBI mice model in aged and young mice as master's thesis project.
 - Used tools like Seurat, ArchR, LIGER to comprehensively characterize and annotate cell types.
 - Characterized repair vs degenerative processes in different by studying differential gene expression in hippocampal cell-type specific states in the context of TBI and aging
- 2. Computational methods for anti-viral drug repurposing** June, 2019 – July, 2019
 - Worked as a project trainee in the Department of Biological Sciences and Engineering at Maulana Azad National Institute of Technology, Bhopal.
 - Used MEGA X to compute pair-wise distance, calculate evolutionary distance and construct phylogenetic tree.
 - Identified clusters of closely related viruses and conserved genomic segments from aligned sequences.
- 3. Effect of socio-economic factors in understanding the paradigm of general health and autism in Delhi-NCR**
November 2017 – April 2018
 - Conducted a city-wide survey of autism affected families in Delhi-NCR.
 - Analyzed collected data and created a five-pronged model for a policy plan called "A.L.E.R.T." based on the evidence collected.
 - Presented the project to the Drug Controller of Delhi-NCR pitched the A.L.E.R.T model as an actionable policy plan.

Publications

- 1. Title: Recent advancement in the discovery and development of COX-2 inhibitors: Insight into biological activities and SAR studies (2008–2019) – *Bioorganic Chemistry***
(<https://doi.org/10.1016/j.bioorg.2019.103007>)
- 2. Title: Novel quinazoline-based EGFR kinase inhibitors: A review focusing on SAR and molecular docking studies (2015-2019) – *European Journal of Medicinal Chemistry***
(<https://doi.org/10.1016/j.ejmech.2020.112640>)
- 3. Title: Recent advancement of anti-epileptic biomolecules: An insight into structure-activity relationship and Docking – *European Journal of Pharmaceutical Sciences***

(<https://doi.org/10.1016/j.ejps.2020.105494>)

Presentations and Conferences

- 1. 44th Annual UMB Graduate Research Conference** Baltimore, MD
Poster presenter 4th March, 2022
 - Presented poster on “Characterization of cellular phenotypes through single-nucleus transcriptomic and epigenomic changes during TBI in young and aged mice”
- 2. 70th Indian Pharmaceutical Congress** New Delhi, India
Poster presenter December, 2018
 - Presented Poster on the topic “Effect of socio-economic factors in understanding the paradigm of general health and autism in Delhi-NCR”
- 3. International Symposium on Informatics, Drug Discovery and Development** New Delhi, India
Poster presenter 31st January, 2019
 - Presented poster on “Advances in cheminformatics approaches of Class 1HDAC inhibitors”
 - Awarded “**Best Poster**” among 60 participants

Workshops and Training

- 1. GIAN Workshop on “Genome Manipulations, Editing and Interference by VIGS, CRISPR and RNAi” (Instructor: Prof. Marcos Egea-Gutiérrez Cortines)** 5th March-14th March, 2019
 - Learnt bioinformatics and molecular techniques involving CRISPR and scored “A” grade in final evaluation
- 2. Training in Bioinformatics and Computational Biology** Indian Institute of Technology, New Delhi
Trainee – Dr. B. Jayaram’s Lab 28th May-3rd June, 2019
 - Modules covered: Genome analysis, Protein folding, drug design and high-performance computing in bioinformatics

Leadership and Activities

- 1. UMB Writing Center** Baltimore, MD
Graduate Peer Writing Consultant (Paid job) August, 2021
Provided one-to-one peer writing support to graduate students of all schools within the university on scientific drafts.
- 2. UMB Indian Association** Baltimore, MD
General Secretary August, 2021 - Present
- 3. 3rd International Conference of the Society for Interdisciplinary Placebo Studies** Virtually held
Technical Team Member May, 2021

Skills & Interests

Technical: R, Linux, Python, Mega X, ChemDraw, AutoDock, Molecular Flipbook, Shotcut

Language: Hindi (mother tongue) and English

Hobbies: Programming, medical illustrations, poetry, badminton

ABSTRACT

Title: Single-Nucleus Multi-Omic Characterization of Age-Specific Effects of Traumatic Brain Injury in the Mouse Hippocampus

Bhatia Parth, Master of Science, 2022

Thesis Directed by: Seth A. Ament, Ph. D, Associate Professor

Traumatic brain injury (TBI) has been characterized as a silent epidemic with growing incidence rates worldwide. Recently, single cell genomics has revealed multiple microglial subtypes activated during inflammation, and emerging evidence suggests that distinct subtypes contribute to age-related differences in neurodegeneration and neuroprotection. In this thesis, I test the hypothesis that differential microglial activation states contribute to the worsened outcomes to TBI associated with aging. Using single-nucleus RNA and ATAC sequencing, I describe cell type specific transcriptional and epigenomic changes in microglia in the context of TBI in young vs. aged mice. I found substantial transcriptional effects of TBI in microglia in both young and aged mice. Regulatory network models predict common repression of homeostatic genes but differential activation of regulatory activity with transcription factors like *Nfe2l2* and *Runx1* in rescuing and repressing a neuroprotective state of microglia.

Single-Nucleus Multi-Omic Characterization of Age-Specific Effects of Traumatic Brain
Injury in the Mouse Hippocampus

by

Parth Bhatia

Thesis submitted to the Faculty of the Graduate School of the
University of Maryland, Baltimore in partial fulfillment
of the requirements for the degree of
Master of Science
2022

To my mother, who will always be missed
and is as much a part of this work as she is a part of me

Table of Contents

Dedication	iii
List of Figures	vi
List of Abbreviations	xi
Chapter 1: Introduction	1
1.1 Traumatic Brain Injury: Primary Injury.....	2
1.2 Traumatic Brain Injury: Secondary Injury.....	3
1.3 Aging, Alzheimer’s and TBI.....	8
1.4 Microglia: Functions and Subtypes.....	10
Chapter 2: Methods	16
2.1 Animals.....	16
2.2 Experimental Design.....	16
2.3 Nucleus Isolation, snRNA-seq, and snATAC-seq.....	17
2.4 snRNA-seq Data Processing and Quality Control.....	18
2.5 snATAC-seq Data Processing and Quality Control.....	19
2.6 scRNA-seq Clustering and Cell Annotation.....	21
2.7 Differential Gene Expression Testing.....	23
2.8 Pseudotime Ordering Using Monocle.....	24

2.9 snATAC-seq Clustering and Analysis Using ArchR.....	25
2.10 Gene Regulatory Network (GRN).....	28
Chapter 3: Results	30
3.1 A single-cell gene expression and chromatin accessibility atlas for the aging mouse hippocampus and its sensitivity to brain injury.....	30
3.2 Functional heterogeneity of microglia in the context of inflammation and aging.....	46
3.3 Pseudotime trajectory construction and analysis.....	58
3.4 Integration of snRNA-seq and snATAC-seq data.....	65
Chapter 4: Discussion	69
References	74

List of Figures

Figure 1A: Experimental design showing the 4 groups with n=4 mice each in both snRNA-seq and snATAC-seq experiments.

Figure 1B: UMAP consisting of global clusters observed across all samples after clustering in Seurat.....30

Figure 1C: Dotplot of all cell-type specific markers used, representing cell type specific expression for each cell type observed. The “mixed” cluster shows markers of both oligodendrocytes and microglia.....31

Figure 1D: Bar graphs representing number of nuclei per group per cell-type. The percentages are representative of the composition of the specific cell type population per group.....32-33

Figure 1E: Number of significantly upregulated and downregulated DEGs observed in each celltype [FDR < 0.01, |log₂FC| > 0.2].....34

Figure 2A: UMAP showing all global snATAC-seq clusters obtained after clustering with ArchR.....36

Figure 2B: Visualization of marker gene activity scores of microglia on global UMAP embedding37

Figure 2C: Visualization of marker gene activity scores of ependyma cells on global UMAP embedding.....37

Figure 2D: Visualization of marker gene activity scores of choroid plexus cells on global UMAP embedding.....38

Figure 2E: Visualization of marker gene activity scores of combined cluster of endothelial, mural and fibroblast cells on global UMAP embedding.....38

Figure 2F: Visualization of marker gene activity scores of Neuron_Subiculum_Slc17a6 cells on global UMAP embedding.....39

Figure 2G: Visualization of marker gene activity scores of Neuron_Dentate_C1ql2 cells on global UMAP embedding.....40

Figure 2H: Visualization of marker gene activity scores of Neuron_CA2CA3_Pvr13-Rgs15-Calb2 cells on global UMAP embedding.....40

Figure 2I: Visualization of marker gene activity scores of Neuron_CA1_Subiculum_Postsubiculum cells on global UMAP embedding.....41

Figure 2J: Visualization of marker gene activity scores of astrocytes on global UMAP embedding.....41

Figure 2K: Visualization of marker gene activity scores of interneuron cells on global UMAP embedding.....42

Figure 2L: Visualization of marker gene activity scores of oligodendrocytes on global UMAP embedding.....43

Figure 2M: Visualization of marker gene activity scores of OPC (oligodendrocyte progenitor cells) on global UMAP embedding.....43

Figure 2N: Bar graphs representing number of nuclei per group per cell-type. The percentages are representative of the composition of the specific cell type population per group.....44

Figure 3A: UMAP of microglial cells from the snRNA-seq experiment showing microglia and peripheral immune cell populations.....50

Figure 3B: Dotplot of marker genes showing the expression for the observed subtypes of microglia.....51

Figure 3C: Bar graphs representing number of immune cell nuclei per subcluster per group. The percentages are representative of the composition of the specific subcluster populating each group.....51

Figure 3D: Venn diagram depicting the number of differentially expressed genes in 18-month-old and 3-month-old mice contrasting TBI against Sham.....52

Figure 3E: Venn diagram depicting the number of differentially expressed genes in TBI and Sham mice contrasting 18-month-old against 3-month-old.....52

Figure 4A: Number and percentage of differentially accessible peaks by condition and age in microglia.....54

Figure 4B: Venn diagram showing number of DAPs common and unique to 18-month-old and 3-month-old mice in the context of TBI.....55

Figure 4C: Venn diagram showing number of DAPs common and unique to TBI-induced and Sham-treated mice in the context of aging.....55

Figure 5A: Violin plots of the cluster wise gene expression of genes differentially upregulated in TBI. The yellow plots on the right for each cluster show its expression in TBI mice while the blue plots on the left of each cluster show its expression in Sham mice.....57

Figure 5B: Violin plots of the cluster wise gene expression of genes differentially upregulated with age. The yellow plots on the right for each cluster show its expression in 3-month-old mice while the blue plots on the left of each cluster show its expression in 18-month-old mice.....58

Figure 6A: Microglial cells arranged along a trajectory across pseudotime.....60

Figure 6B: Cells arranged along a trajectory showing the arrangement of different clusters of microglia along the branches.....60

Figure 6C: Important areas of the heatmap generated from BEAM analysis. The branch from the middle to the left shows the expression pattern of genes in M3 microglia while the branch going from the middle to the right is showing the same for M4 microglia.....61

Figure 6D: Plots showing the pattern of expression along the branches of the trajectory. The dotted line shows the trajectory branching into a cluster of M3 cells and the solid line shows the branch with M4 cells clustered at the end.....62

Figure 6E: Expression pattern of genes in each experimental group that show change with pseudotime across clusters.....62

Figure 6F: Expression pattern of genes in each cluster that show change with pseudotime.....65

Figure 7A: Clusters of microglia annotated according to the same annotation as the one used for snRNA-seq represented here in a 2D space through a UMAP plot.....67

Figure 7B: UMAP plot showing convergence of cells from snATAC and snRNA-seq across clusters.....67

Figure 7C: Gene expression patterns in each cluster across experimental groups of major regulatory factors observed in the GRN.....68

List of Abbreviations

ARM	activated response microglia
AD	Alzheimer's disease
<i>ApoE</i>	apolipoprotein
BBB	blood brain barrier
BEAM	branched expression analysis modelling
CREB	cAMP responsive element binding protein
<i>Ccl2</i>	C-C chemokine ligand 2
<i>Ccr2</i>	C-C chemokine receptor 2
<i>Rage</i>	advanced glycosylation end product-specific receptor
CDC	Center for Disease Control
CTE	chronic traumatic encephalopathy
<i>Cr1</i>	complement C3b/C4b Receptor 1
<i>Cx3cr1</i>	motif chemokine receptor 1
DAMP	damage-associated molecular patterns
DAM	disease-associated microglia
MGnD	microglial neurodegenerative phenotype
<i>Fth1</i>	ferritin heavy chain 1
FACS	fluorescence activated cell sorting
GABA	gamma-aminobutyric acid
GRN	gene regulatory network
GLM	generalized linear model
<i>GLUT1</i>	glucose transporter protein type 1

<i>GRP75</i>	glucose-regulated protein 75
<i>Inpp5d</i>	inositol polyphosphate-5-Phosphatase D
<i>Itgam</i>	integrin alpha M
LSI	latent semantic indexing
MIF	macrophage inhibition inhibitory factor
MHC II	major histocompatibility complex II
<i>Marco</i>	macrophage receptor with collagenous structure
<i>Mmp9</i>	matrix metalloproteinase 9
MNNs	mutual nearest neighbours
NMDA	N-methyl D-aspartate
PAMPs	pathogen associated molecular patterns
<i>Piezol</i>	piezo type mechanosensitive ion channel component 1
ROS	reactive oxygen species
<i>Siglech</i>	sialic acid binding Ig-like lectin H
scATAC-Seq	single cell Assay for Transposase-Accessible Chromatin)
scRNA-Seq	single cell RNA sequencing
snATAC-Seq	single nucleus assay for transposase-accessible chromatin
snATAC-Seq	single nucleus assay for transposase-accessible chromatin
snRNA-Seq	single nucleus Ribonucleic acid sequencing
snRNA-seq	single nucleus RNA sequencing
<i>St6gal1</i>	ST6 beta-galactoside alpha-2,6-sialyltransferase 1 ()
<i>Cmklr1</i>	chemerin chemokine-like receptor 1
<i>TLR9</i>	Toll-like Receptor 9

TF	transcription factor
TBI	traumatic brain injury
<i>Trem2</i>	triggering receptor expressed on myeloid cells 2),
<i>Clu</i>	Clusterin
TNF- α	tumor necrosis factor- α
UMAP	uniform manifold approximate projection

INTRODUCTION

Every year, around 27 to 69 million cases of traumatic brain injury (TBI) are recorded¹. With the average hospital costs of TBI ranging from \$2,130 to \$401,808² per patient, the economic burden of TBI is considerable, especially considering the fact that there can be an added burden of disability. According to the Center for Disease Control (CDC), in 2014 alone, there were 56,800 TBI-related deaths in the U.S. with 2,529 of them being among children³. Injury to the central nervous system also increases the risk of other neurodegenerative and psychiatric disorders like Alzheimer's disease (AD), chronic traumatic encephalopathy (CTE), depression, suicidal ideation and negative effects on memory and behavior⁴⁻⁶. There are two distinct phases of TBI: Primary and secondary, each with their own distinct pathology. This acute phase is primarily characterized by tissue damage, while the effects of secondary injury comprise the long-term prolonged damage and neuroinflammation persisting for months and years later, as a consequence of the biochemical, cellular and pathological events during primary injury. My master's thesis focuses on the analysis of single-cell transcriptomic and epigenomic profiling of hippocampal tissue in a mouse model of TBI, comparing the effects of brain injury in young vs. aged mice. This study is designed to provide insights into the molecular and cellular mechanisms underlying both good (e.g., repair) and bad (e.g., degenerative) long-term outcomes.

1.1 Traumatic Brain Injury: Primary Injury

TBI needs emergency treatment as soon as it has occurred as delay may cause worsening of condition. There is an initial primary phase which can present different prognoses based on what type of injury has occurred. The injury can be either focal or diffuse, although both might be present at the same time too, especially for patients inflicted with moderate to severe level of injury⁷. In focal brain injury, focal brain damage occurs along with a presentation of skull fracture and localized contusion at the core of the site of injury. As a consequence of neuronal and glial necrosis occurring along with compromised blood supply, confined layers of the brain present with hematoma and epidural, subdural and intracerebral hemorrhages. The area opposite to and surrounding the coup of the injury may also show some secondary contusion due to the brain rebounding and striking the skull⁸. On the other hand, diffuse injury is caused by rapid shearing and stressing of cerebral tissue through non-contact forces. The tensile forces in this type of injury cause damage to axonal tracts, especially in the subcortical and deep white matter tissue which is a distinct feature, oligodendrocytes and blood vasculature resulting in brain edema and ischemia. The damage to axons may persist for months post injury impairing axonal transport and degradation of the cytoskeleton. The degree of this damage and neurodegeneration is the determinant for the severity of TBI. The influx of activated endothelial cells, microglia and astrocytes along with the damage and degradation of axonal transport and cytoskeletal structure due to the production of reactive oxygen species (ROS) and inflammatory cytokines and chemokines^{9,10}. Immediate actions to recuperate include reducing the intracranial pressure which may be caused due to swelling or blood, reducing pressure in the medullary cavity, reducing cerebral edema along with offering

systemic support¹¹. Hypotension and hypoxia are one of the first two things to be managed as even a single episode increases the risk of morbidity¹². An adequate level of sedation can help reduce metabolic stress by decreasing the consumption of oxygen as a result of lower cerebral metabolic activity post-sedation. Mild hyperthermia, hyperglycemia, and occurrence of convulsions are also to be monitored in patients as all and any of these lead to poor outcomes. Decompressive craniectomy to reduce intracranial pressure along with antibiotic therapy and nutritional support is also considered¹³.

1.2 Traumatic Brain Injury: Secondary Injury

The molecular, cellular and physiological events occurring during the primary phase lead to the secondary phase of TBI as they can persist for up to months after primary injury^{9,10}. The secondary phase is marked by neuroinflammation, excitotoxicity, mitochondrial dysfunction, oxidative damage, axonal degeneration and growth inhibition, and neuronal apoptosis^{9,14}.

Excitotoxicity

Elevated extracellular glutamate levels may persist in patients with severe TBI from days to weeks. This is toxic to cells as ATP reserves are spent due to overstimulation and the energy expenditure involved in reuptake¹⁵. Ionic homeostasis of potassium, sodium and calcium are also disrupted leading to exacerbation of ATP depletion due to changes in astrocytic potassium conductance post-TBI¹⁶. Increase in intracellular sodium levels cause increase in osmotic pressure¹⁷ while prolonged increase in calcium levels cause mitochondrial dysfunction, activation of nitric oxide synthase leading to generation of reactive oxygen species (ROS), breaking down of cytoskeletal architecture and increase in

transcription of apoptotic genes¹⁸. Increase in ROS leads to destabilization of cellular and mitochondrial membranes by reacting with polyunsaturated fatty acids¹⁹. These can initiate a passive leakage of intracellular molecules which can act as damage-associated molecular patterns (DAMPs) and trigger immune cell reactivity²⁰.

The N-Methyl D-Aspartate (NMDA) receptor plays a particularly important role as intracellular calcium levels are controlled by multiple routes of entry into the cell. Voltage-gated calcium channels do not allow as much calcium to get into the cell as ligand-gated (glutamate) calcium channels (NMDA), therefore leading to increased cell survival and better tolerance to glutamate-induced calcium influx^{21,22}. This has been explored as a therapeutic target before and in recent studies as well²³⁻²⁵. Only a few studies have explored the effects of increased glutamate in the chronic (>14 days post injury) in TBI, but all have pointed towards altered glutamate as well as GABA levels persisting long after the injury in mice²⁶ as well as humans^{27,28} respectively. In the hippocampus, deregulation of positive regulators of excitatory amino acid transporter 2 (EEAT2 encoded by *Slc1a2*) like Extracellular Signal Regulated Kinase (ERK encoded by *Mapk*) and cAMP Responsive Element Binding Protein (CREB)²⁹, through which 90% of the glutamate reuptake happens³⁰, are a potential mechanism for the cognitive impairment observed in TBI as ERK and CREB are also markers of memory consolidation. Long term potentiation is also critically maintained in the CA1 subfield of the hippocampus through glutamate reuptake³¹. Subsequent astrocytic cell death, failure to maintain synaptic strength and initiating LTP in the hippocampus could be accounted for by the dysregulated glutamate reuptake causing chronic electrophysiological deficits¹⁵.

Mitochondrial Dysfunction

Mitochondria are primarily responsible for producing ATP by the process of oxidative phosphorylation in homeostatic condition. They also release mitochondrial ROS at levels rescued by endogenous enzymes and non-enzymatic antioxidants. Oxidative stress is caused when these ROS levels exceed the balance they have with the endogenous enzymes either due to endogenous factors like aging or immune cell responding to damage or infection or due to exogenous factors like radiation, pollutants or heavy metals entering the body and being metabolized, releasing ROS in the process³². Mitochondria are both a target of inflammation and potentiates inflammatory response. ROS and mutated mtDNA from dysfunctional mitochondria trigger the NOD-, LRR-, and Pyrin domain containing 3 (NLRP3) inflammasome and the production of cytokines through NF- κ B stimulation³³. Additionally, mtDNA can also trigger Toll-like Receptor 9 (*TLR9*) which further sets off pro-inflammatory signaling cascades³⁴. Aging is a process which itself renders the mitochondrial DNA susceptible to lesions with higher production of ROS, impaired oxidative phosphorylation and in general, “primed” mitochondrial health ready to trigger inflammation associated processes. Aged animals have swollen or branched mitochondria, either due to fission or fusion^{35,36}. They also show impairment in normal mitochondrial processes and efficiency while becoming more vulnerable to external sources of stress³⁷. Microglial mitochondria shift from oxidative phosphorylation to glycolysis when needed to react to immune challenges so as to support cell growth and production of cytokines and ROS. This is driven by Glucose Transporter Protein type 1 (*GLUT1*) in the cytoplasm³⁸ but has also been shown to be facilitated through Glucose-regulated Protein 75 (*GRP75*), a mitochondrial chaperone³⁹. Another hypothesis is that mitochondria also play a more direct

role in enable pro-inflammatory signaling in microglia through facilitating the transcription of NF- κ B and IFN- β ^{40,41}. Overall, mitochondria play an important role in the function of microglia and dysfunction of the same impairs the ability of the microglia to respond to injury, especially when already in a susceptible state due to pre-injury priming. Treatment of microglia with mitochondrial division inhibitor, Mdivi-1 has showed reduced ROS production⁴² while the effect of anti-oxidants like Coenzyme Q10, ubiquinol and others have also been documented and shown positive results^{43,44}.

Neuroinflammation

Neuroinflammatory processes involved have been known to exacerbate chronic neurodegenerative outcomes but also help in repair and regeneration after TBI⁴⁵. Breakage of the blood brain barrier (BBB) leads to infiltration systemic neutrophils, monocytes and lymphocytes which help mediate the neuroinflammatory response post TBI along with microglia and astrocytes. These cells react to DAMPs and/or pathogen associated molecular patterns (PAMPs) or as a consequence of high ATP levels induced by the activation of the mTOR pathway^{46,47}. Elevated chemokine production by activated resident glia in the brain are responsible for the recruitment of systemic immune cells at the site of injury. Peripheral leukocytes are largely vacated from the brain parenchyma about 10-14 days post injury (dpi) but the presence of F4/80⁺ macrophages persist for months or even years at sites distal from the primary injury⁴⁸. Some of the chemokines which get expressed are Ccl2/Ccr2 (important for monocyte mobilization), Cxcl12/Cxcr4 (maintains neural stem cell niche), Cx3cl1/Cx3cr1 (regulator of microglial toxicity) among others⁴⁸⁻⁵⁰. Cytokines on the other hand are produced by immune cells like monocytes, lymphocytes and macrophages and can be pro-inflammatory, such as interleukin (IL)-1, IL-6, IL-18,

IFN- γ , Tumor Necrosis Factor (TNF)- α or anti-inflammatory, such as IL-4 and IL-10⁵¹. Microglia play a pivotal role in the neuroinflammatory response to TBI in both primary and secondary phases. Their functionality is discussed in further detail ahead in a separate section of this document.

BBB breakdown

The BBB is a semipermeable layer of endothelial cells that interact with microglia and astrocytes, with its primary function being a barrier to blood-borne pathogens and systemic immune cells. This layer is disrupted in TBI when cell junctions weaken caused by upregulation of Matrix Metalloproteinase 9 (*Mmp9*), which breaks down the tight junctions allowing systemic immune cells to infiltrate⁵². The immune cells then further cause the BBB to become more permeable via disruption of endothelial transport functions and endothelial-pericyte crosstalk, pericyte loss, cerebral blood flow reduction, and tissue hypoxia⁵³. These pathological events contribute to the chronic neurodegeneration observed in mouse models and human patients of TBI.

Axonal Injury

Acute axonal damage cascades into secondary axotomy in the chronic phase of TBI. Wallerian degeneration, a form of evolutionarily conserved cell death pathway in which the distal end of the axon starts fragmenting following a nerve lesion, can start minutes after axonal injury^{54,55} but can persist for weeks later as well^{56,57}. The chronic phase post TBI is characterized by degeneration of myelin sheath, impaired axonal transport, accumulation of axonal transport proteins and the increased expression of amyloid precursor protein^{54,55}. Prolonged swelling of injured axons and eventual apoptosis of

neurons is also observed due to the formation of retraction bulbs as a result of dissociated axonal connections and accumulation of axonal transport proteins. The strongest predictor of post TBI neurodegeneration and infiltration by microglia and macrophages has been the extent of axonal injury caused in white matter tracts like the corpus callosum⁵⁸⁻⁶⁰, ultimately leading to deformation of white matter.

1.3 Aging, Alzheimer's and TBI

Age is a variable that has been shown to matter both in the recovery from TBI as well as the incidence of TBI as most some of the most vulnerable populations to TBI in the United States are children aged 0-4 years, adolescents aged 15-19 years, and adults aged 65 years and over. Those aged 75 years and older are the most vulnerable with the highest rates of hospitalizations and death⁵⁴. On a cellular level, aging exerts a mixed effect on the immune cells and processes in place to respond to events like TBI. Aged microglia and macrophages both display a reduced capacity for phagocytosis and chemotaxis⁶¹, the microglia present a “primed” state which exhibit an exaggerated pro-inflammatory response to immune challenges^{41,62}. This primed state has distinct features including the following – an increased expression of various inflammatory markers like major histocompatibility complex II (MHC II) which in turn produce IL-1 β following activation, Integrin alpha M (*Itgam*), TNF- α , and IL-6 among others⁶³. However, the age specific effects of TBI have not been studied in thorough detail and experiments looking at this effect have only recently begun to emerge. Krukowski et al. found brain lesion and cavitation formation, prolonged BBB breakdown associated with increased microglial number and activity at 30 dpi in a mice model of focal contusion injury. They also found a significant accumulation of Complement component q (C1q) on synapses within the hippocampus, which when

pharmacologically blocked rescued memory deficit in aged animals⁶⁴. A recent study using single nucleus RNA sequencing (snRNA-seq) also demonstrated increased thalamic C1q expression by microglia colocalizing with neuron loss, chronic inflammation, disruption in sleep spindles and appearance of epileptic activity⁶⁵. Ritzel et al. showed aged mice having a higher increase in microglial numbers post TBI with worse behavioral and motor outcomes than the young mice along with a higher production of IL-1 β , ROS and senescent markers but lower phagocytic activity and pro-inflammatory cytokine production⁶⁶. Barrett et al. also showed an increased expression of IFN-1 signaling via DNA recognition pathway, cGAS in aged brains along with an increase in the phosphorylation of *Stat1* which is an IFN-I effector molecule⁶⁷. The evidence points towards a complex picture of age interacting with injury as a stimulus for inflammation related degenerative/repair processes.

Alzheimer's disease is a neurodegenerative disorder which is the 6th leading cause of death in the US. Its symptoms are marked by an onset and progressive decline in behavioral and cognitive functions like memory, language comprehension and processing, attention, reasoning and judgement⁶⁸. The risk for Alzheimer's disease (AD) has long been known to be associated with the incidence of TBI as studies have repeatedly shown a very strong correlation between the two⁶⁹⁻⁷¹. Consequently, both diseases share pathologies, especially when considering the long-term effects of TBI on the brain. BBB breakdown in TBI is known to lead to both ischemic damage, leading to hypoperfusion and vascular dysfunction, and A β accumulation, which is a prominent feature of AD^{72,73}. Metabolic acidosis in TBI can be another contributor towards A β accumulation⁷⁴. The role of A β oligomers in the activation of mitochondrial pathways of endothelial cell stress and death

has been well characterized^{75,76}. A β can also bind to microglial receptors like *Marco* (Macrophage Receptor With Collagenous Structure), *Cd36*, *Rage* (advanced glycosylation end product-specific receptor), *Tlr2*, *Tlr4*, *Cmklr1* (Chemerin Chemokine-Like Receptor 1) and *Piezo1*^{77,78} (Piezo Type Mechanosensitive Ion Channel Component 1) or be engulfed by TAM receptor tyrosine kinases (*Axl* and *Mertk*)⁷⁹ to increase its uptake or induce a pro-inflammatory response⁴¹. Hyperphosphorylated Tau accumulation, another hallmark of AD pathology is also observed in patients after diffuse axonal injury as microtubule networks within axons are disrupted^{80,81}. A recent study shows that AD like neuronal tau-acetylation is induced post TBI in mouse cerebral cortex and hippocampus, correlating the accumulation of tau with injury intensity. Blocking of this process led to rescue from neurodegeneration and neurobehavioral impairment^{82,83}. Microglia can be stimulated by both phosphorylated and non-phosphorylated tau via separate pathways^{84,85}. Variant genes which have been shown to be risk-conferring have been found to be upregulated in microglia in this study as well as previous studies, for example, *ApoE*⁴¹ (Apolipoprotein E), *Trem2*⁸⁶ (Triggering Receptor Expressed On Myeloid Cells 2), *Clu*⁸⁷ (Clusterin), *Cd33*⁸⁸, *Inpp5d*⁸⁸ (Inositol Polyphosphate-5-Phosphatase D), *Cr1*⁸⁹ (Complement C3b/C4b Receptor 1).

1.4 Microglia: Functions and Subtypes

Microglia are highly dynamic cells that are the main resident immune cells of the brain. They get activated in the presence of stimuli like pathogens, injury, stroke or aging and are also responsible for clearing cell debris and toxic substances as well as refinement of synaptic networks, advancement of developmental apoptosis, and supporting of neuronal survival by secretion of growth factors⁹⁰. When TBI occurs, microglia are one of the first

cells to respond and reach the site of injury to begin immediate damage control by modifying their morphology initiating inflammatory cascades leading to the production of cytokines. They detect DAMPs released by surrounding cells via various pattern recognition receptors that allow them to sense and respond to the local environment.

Without any stimulus in normal conditions, microglia remain in the “quiescent” or “resting” or “homeostatic” state expressing genes like CX3C motif chemokine receptor 1 (*Cx3cr1*), involved in synaptic pruning, microglial migration and blocking neuronal excitotoxicity⁹¹⁻⁹³; Purinergic receptor P2Y12 (*P2ry12*), for metabolite sensing, protrusion extension, maintaining regulatory junctions between microglia and neurons and has also been shown to control CA1 neuron excitability and fear in mice⁹⁴⁻⁹⁶; Sialic acid binding Ig-like lectin H (*Siglech*), involved in patrolling and phagocytic activity; Siglec-3 or *rage*, which is an inhibitor of phagocytic activity and several others. The term “resting” is now regarded as a misnomer as these microglia are actually quite active (ceaselessly motile) even without any stimulus as they are constantly surveilling, clearing cellular debris, pruning and remodeling synapses, looking for any harmful infiltration by foreign bodies or toxic chemicals⁹⁷. The consensus on the exact profile and function of activated microglia is divided. An aggressive form of microglia, known as the “M1 pro-inflammatory” microglia, are activated as a response to stimuli triggering inflammation and in general are neurotoxic, releasing pro-inflammatory factors like MHC II molecules, which make them similar to perivascular macrophages in expression⁹⁸. They also contribute to NO synthesis which mediates neuronal cell death^{98,99}. C-C chemokine receptor 2 (*Ccr2*) is also expressed in these cells to bind with astrocytic C-C chemokine ligand 2 (*Ccl2*) for further recruitment of pro-inflammatory microglia¹⁰⁰. Surface markers like *Cd16*, *Cd32*, *Cd86*, *Cd40* and

Cd74 can also be observed leading to enhanced production of pro-inflammatory cytokines like IL-1, IL-6, IL-12, IL-17, IL-18, IL-23, Tnf α and IFN γ . The opposite profile of this phenotype is observed in the “M2 anti-inflammatory” microglia whose function is stop inflammation and promote neuroprotection and homeostasis. They express Arginase 1 (*Arg1*) which is needed for making polyamines active in wound healing and tissue remodeling and also inhibits iNOS/NO production¹⁰¹. *Ym1* or Chitinase-like 3 is also expressed in the presence of anti-inflammatory cytokines like IL-4 and IL-13; its role is to prevent the degradation of extracellular matrix components^{98,102}. However, strong arguments against this classification system have been made with evidence pointing towards a more mixed phenotype shown by microglia in various inflammation inducing states like infection, aging, injury and stroke⁹⁰.

What's the “DAM” problem?

With the advent of single-cell sequencing, transcriptional heterogeneity of tissues has been made discernable. Recent publications employing this method have shown a new state with different names in different models. Phenotypes similar to this phenotype have been called the “Disease-associated microglia” (found in AD 5xFAD mouse model)¹⁰³, “Microglial neurodegenerative phenotype” (AD, Amyotrophic Lateral Sclerosis and Multiple Sclerosis mouse model)¹⁰⁴, “axon tract-associated microglia” (injury and development)¹⁰⁵ and “proliferative-region-associated microglia” (postnatal mice)¹⁰⁶. They have some overlap in gene expression but are not all similar in their transcriptional signature, suggesting some overlapping and differential functionality specific to the context. The characteristic features of this population include a downregulation of homeostatic genes like *P2ry12*, *Tmem119*, *Cx3cr1*, *Siglech* among various others. Some key genes which get upregulated are

Apolipoprotein E (*ApoE*), Osteopontin 1 (*Spp1*), Transmembrane glycoprotein NMB (*Gpnmb*), Integrin subunit alpha X (*Itgax*), Leukocyte immunoglobulin-like receptor subfamily B member 4A (*Lilrb4a*) which enrich pathways of endocytosis, regulation of immune response and lysosomal/phagocytic pathways. Triggering Receptor Expressed On Myeloid Cells 2 (*Trem2*) is a gene considered to play a crucial role in the activation of microglia mediating cell migration, proliferation and survival¹⁰⁷. The original “DAM” paper attributes the activation of microglia in a 2 step process which involves an initial upregulation of *Trem2*, β_2 microglobulin (*B2m*), TYRO protein tyrosine kinase-binding protein (*Tyrobp*) and a later upregulation of *Lpl*, *Cst7*, *Axl* and *Itgax*¹⁰⁸. A further subdivision of DAMs have been suggested with some having a more pro-inflammatory profile with genes like *Tlr2*, *Ptgs2*, *Cd44* and *Il1b* and other having an anti-inflammatory profile with genes like *Igf1*, *ApoE* and *Myo1e*¹⁰⁹. Wang et al. in a recent publication showed that *Trem2* was dependent on spleen associated tyrosine kinase (*Syk*) based pathway to induce DAM microglia which promote engulfment of A β plaques while a Hematopoietic Cell Signal Transducer (*Dap10*) based pathway induces an *ApoE* expressing prodromal stage¹¹⁰. Some have argued that DAM are present in all individuals at all stages with an increase in number as aging or other inflammation triggering events happen while others have proposed a stricter activation-based presence specific to stimuli only¹¹¹. Single cell studies in aged mice without any external stimulus has also revealed similar clusters. Hammond et al. found a cluster (entitled “OA2”) with increased cell number and upregulation of chemokines *Ccl3* and *Ccl4* with *Il1b* suggesting a pro-inflammatory profile while another cluster, “OA3” was found to be enriched interferon response genes like *Ifitm3*, *Rtp4*, and *Oasl2*¹⁰⁵. Frigero et al. also were able to show that “activated response

microglia” (ARM) were part of the normal aging process as well, with females showing a faster progression towards a decline in the homeostatic state microglia to ARM microglia, which interestingly corresponds with reportedly higher incidence of AD in females. These microglia were enriched in MHC class II genes (*H2-Ab1*, *H2-Aa*, and *Cd74*) and tissue repair genes (*Spp1*, *Gpnmb* and *Dkk2*)¹¹². In pathological models of neurodegeneration, microglia have been shown to play a complex role, instigating both beneficial and harmful effects. An age attenuated function of microglia is the phagocytosis of A β plaques to prevent the spread of more toxic soluble amyloid molecules in the brain^{113–115}. On the other hand, microglia have been shown to contribute to synaptic loss when exposed to soluble A β oligomers in early AD mediated by complement component C1q and complement receptor 3¹¹⁶. In other studies with TBI models, it has been shown that microglia contribute to neuronal damage post TBI, which is rescued upon microglial depletion causing upregulation of genes associated with dopamine signaling, long-term potentiation, calcium signaling and synaptogenesis^{117,118}. Overall, the field is in a flux of exactly how this once obscure phenotype contributes to the pathology of neurodegeneration. The prospect of finding a therapeutic target, either to propagate or diminish this cell type to ameliorate the disease is tantalizing. My study aims to resolve some of the repair vs degenerative processes occurring with respect to both aging and TBI in microglia with the hopes of identifying potential targets for inhibition or activation.

The hippocampus has a complex architecture with sub-regions and various cell types performing unique and specific functions¹¹⁹. Single nucleus Ribonucleic acid sequencing (snRNA-Seq) is a new technique which gives researchers the opportunity to explore how TBI perturbs gene expression and define the pathological cell states seen in TBI, in a cell

type specific manner according to their transcriptional profiles. Coupled with single nucleus Assay for Transposase-Accessible Chromatin (snATAC-Seq), the regulatory features driving these changes in expression can be pointed out and give direction to future therapies as potential targets. Compared to single cell sequencing (scRNA-Seq and scATAC-Seq), single nucleus sequencing methods give a number of advantages, especially considering how hard to dissociate cells like neuronal populations. Elimination of the protease digestion / heating step makes the dissociation protocol faster, reducing the chance of aberrant transcription. It has been shown that snRNA-Seq achieves better sensitivity and classification of cell types¹²⁰. Spurious gene expression arising from ribosomes is also minimized since they are localized to the cytoplasm when they get fully mature. This especially helps in capturing transcripts of transcription factors since they would not be translated by immature ribosomes during disassociation, thus helping in identifying regulatory elements controlling gene expression. snRNA-seq also helps take a snapshot of the nuclear transcriptome, transcripts associated with neuronal activity that may be expressed nascently can be captured^{120,121}.

My master's thesis focuses on the analysis of snRNA-seq and snATAC-seq data from hippocampal tissue in a mouse model of TBI, comparing the effects of brain injury in young vs. aged mice. To my knowledge, this is the first study on rodent models of TBI using a multi-modal single nucleus approach employing both snRNA-seq and snATAC-seq. This study was conducted with the hopes of defining and characterizing the transcriptional and regulatory landscape in the context of TBI and aging.

2. Methods

2.1 Animals

This study was performed using 3-month-old and 18-month-old male C57BL/6J mice. Mice were housed in the animal care facility at the University of Maryland School of Medicine under a 12 h light/dark cycle, with ad libitum access to food and water. All surgical procedures were performed in accordance with protocols approved by the Institutional Animal Care and Use Committee at the University of Maryland School of Medicine.

2.2 Experimental design

18-month-old and 3-month-old C57BL/6J mice (n=4 per group) were subjected to either controlled cortical injury (CCI) or Sham surgery. A custom designed CCI device was used by the Stoica lab which consisted of a microprocessor controlled pneumatic impactor with a 3.5mm tip. Briefly, mice were anesthetized with isoflurane evaporated in a gas mixture containing 70% N₂O and 30% O₂ and administered through a nose mask (induction at 4% and maintenance at 2%). A 10mm midline incision was made over the skull, the skin and fascia were reflected, and a 4mm craniotomy was made on the central aspect of the left parietal bone. The impounder tip of the injury device was then extended to its full stroke distance (44 mm), positioned to the surface of the exposed dura, and reset to impact the cortical surface. Moderate-level CCI was induced using an impactor velocity of 6 m/s and deformation depth of 2mm. Sham animals underwent the same procedure as TBI mice except for the craniotomy and impact. At 28 days post injury, mice were anesthetized (100

mg/kg sodium pentobarbital, I.P.) and transcardially perfused with ice-cold 0.9% saline (100 ml), the ipsilateral brain tissue was rapidly dissected and flash-frozen^{122,123}.

2.3 Nucleus isolation, snRNA-seq, and snATAC-seq

Single-Nucleus RNA Sequencing: Nuclei were isolated from frozen brain tissue following a published protocol with slight modifications¹²⁴. Briefly, frozen brain tissue was mechanically disaggregated using disposable homogenizer and by pipetting up and down in chilled extraction buffer consisting of Poly(1-vinylpyrrolidone-co-vinyl acetate) (Sigma #190845), 0.1% TritonX-100, and 1% bovine serum albumin (BSA) in dissociation buffer (DB; 82 mM Na₂SO₄, 30mM K₂SO₄, 10mM Glucose, 2.5mM MgCl₂, 10mM Hepes pH7.4, and RNase inhibitor [Protector, Roche]). Homogenates containing nuclei were resuspended in DB and filtered with 70 um and 40 um strainers. To separate nuclei from debris, the nuclei suspension was mixed in a 25% (final) iodixanol layer over a 27% iodixanol cushion, followed by centrifugation (13000g x 20min, 4° C), then nuclei were washed twice in DB. Nuclei were counted using a MoxiGoII (Orflo) cytometer, and the concentration was adjusted to 365 nuclei/ul in phosphate buffered saline with 2% BSA. 17,000 nuclei were loaded in each well of a Chromium Controller (10x Genomics). Sequencing libraries were prepared using NextGEM 3' Gene Expression reagents (10x Genomics), following manufacturer's instructions and sequenced on HiSeq4000 (batches 1 and 3) and NovaSeq6000 (batch 2) sequencers.

Single-nucleus ATAC sequencing: Cellular nuclei were isolated from frozen brain tissue following the Chromium Single Cell ATAC Demonstrated Protocol¹²⁵. Briefly, frozen samples were triturated in a disposable homogenizer (Biomasher, Takara) with 0.1X Lysis Buffer. Lysates were diluted with 0.5ml wash buffer and filtered with 70 um and 40 um

strainers (Pluriselect). Nuclei were centrifuged at 500g x5min and resuspended in diluted nuclei buffer at 3,000 nuclei/ul. Each sample was processed individually to this stage, then nuclei from a male and female donor (Table S1) were pooled to target 10,000 nuclei in total. Tn5 transposition and snATAC-seq library construction were performed using the 10x Genomics ATAC kit (v1), following manufacturer's instructions, and sequenced on a NovaSeq6000 sequencer.

2.4 snRNA-seq Data Processing and Quality Control

The raw sequencing reads were processed using Cell Ranger v5.0 (10x Genomics)¹²⁶. The cellranger mkfastq pipeline was used to demultiplex the FASTQ base call files. The outputs were used to run cellranger count which was used to align the sequencing reads to the mouse reference transcriptome (mm10) using STAR, which aligns the reads to the genome in a splice-aware manner. This pipeline filters out the UMIs with invalid barcodes and those with MAPQ < 255 (mapping quality). This score is a representation of a read being confidently mapped to a single exonic loci, in spite of also being aligned to other non-exonic loci. Intergenic reads are also filtered out although we chose to include the intronic reads for our analysis. Confidently mapped exonic and intronic reads were then aligned to annotated transcripts ignoring all anti-sense reads. After barcode correction by matching all the barcodes against a barcode whitelist, all reads are grouped by barcode, corrected UMIs and gene annotation. To call cell barcodes (or cells), Cell Ranger uses the EmptyDrops algorithm (ref) which better identifies low-RNA containing cells, especially when such populations are mixed with high RNA-containing populations. Cell Ranger also performs a secondary analysis which includes PCA, and then passes the PCA-reduced data

to UMAP (uniform manifold approximate projection) and tSNE. It also employs a graph-based clustering algorithm followed by Louvain Modularity Optimization.

2.5 snATAC-seq Data Processing and Quality Control

The raw base call files were processed by Cell Ranger ATAC v2.1¹²⁷ through the cellranger-atac mkfastq pipeline generating FASTQ files. cellranger-atac count was then run which performs filtering, alignment, counting, identification of transposase cut sites, accessible chromatin peak detection, cell calling, generation of the count matrix, dimensionality reduction, clustering and differential accessibility analysis. First, Cell Ranger ATAC detects the location of the 10x barcode and picks the location that maximizes the fraction of valid barcodes. Error correction is performed to resolve for sequencing errors. To error correct invalid barcodes which are not on the list, Cell Ranger ATAC tries to find all valid barcodes within one mismatch of the observed invalid sequence, then scores them on the basis of the abundance of that barcode in the read data and quality value of the incorrect bases. The invalid barcodes are only corrected if there is a greater 90% probability that that barcode is the real barcode. For trimming adapter and primer oligo sequence before reference alignment, Cell Ranger ATAC uses an algorithm similar to the cutadapt tool. A modified version of the BWA-MEM algorithm is used to align the reads to the mouse reference (mm10) genome. Since barcoded fragments representing template molecules are amplified during the library preparation process resulting in multiple read pairs from the same original template, Cell Ranger ATAC selects one of the read pairs filters out the rest checking if MAPQ is greater than 30 on both reads, isn't mitochondrial, not chimerically mapped and maps to a gene-containing contig. To call peaks, actual signal coming from open chromatin must be distinguished from random

transposase activity generating background noise. For this, Cell Ranger ATAC first determines a global peak threshold followed by local refinements since both signal and noise can vary across datasets and locally across the genome. Each candidate peak is then padded by 5 Kb on either side to include local background context. Local maxima are identified, and putative peaks are generated by extending the local maxima to the total prominence of the maxima. Each putative peak is then filtered on the basis of signal-to-noise ratio. A Bayesian posterior probability estimate is used by Cell Ranger ATAC to exclude peaks that don't have at least 95% confidence that the signal-to-noise ratio is above 1.5. The final step is to examine all fragments within a peak, if one cut of the fragment is outside and one is inside then the peak is padded to fully contain more of those fragments. The next step of cell calling is associating the barcodes found in the library to the cells in the sample. Cell Ranger ATAC firstly identifies barcodes that have a fraction of fragments overlapping the called peaks lower than the fraction of genome in peaks. These are filtered out along with a doublet filtering algorithm which filters multiple barcodes associated with the same cell. Cell calling is then performed which subtracts a fixed count (depth dependent) from all barcodes which is the number of fragments per barcode, assuming a contamination rate of 0.02. The barcodes that correspond to real cells vs non-cells are separated using an odds ratio limit of 100000. Further analysis by Cell Ranger ATAC was carried out with default methods – Latent Semantic Analysis (LSA) and t-SNE for clustering, dimensionality reduction and visualization.

I also ran the aggr pipeline which merges all the fragments from each sample into one aggregated file. The default Depth Normalization method was used which equalizes the average read depth per cell between groups before merging. Cell Ranger ATAC also

corrects for batch effects based on a mutual nearest neighbors (MNNs) algorithm. MNNs (pairs of similar cells) are detected for every pair of batches and the difference in chromatin accessibility between cells in a MNN pair gives an estimate of the batch effect. A batch effect score is produced which is calculated by how many of the 100 nearest-neighbor cells belong to the same batch and then are normalized by the number expected when there would have been no batch effect. The average of this normalized score in a random subset of all cells (10%) is the reported batch effect score.

I took the barcodes from each fragment file (file with position sorted start and end position of each fragment observed in a cell) of each sample and matched it against the aggregated fragment file from the aggr run to make a separate batch-corrected fragment file for each sample.

2.6 scRNA-seq Clustering and Cell Annotation

The outputs from Cell Ranger for all 16 samples was then read into R environment using Seurat¹²⁸ and then normalized within each sample using Seurat's default "LogNormalize" method which normalizes the gene expression counts for each cell by the total expression and then multiplies by a scaling factor of 10,000. For each sample, genes which exhibit high cell-to-cell variability were determined using Seurat's FindVariableFeatures() function with defaults which applies variance-stabilizing transformation. Anchors for all the Seurat objects for each sample were then produced using Seurat's FindIntegrationAnchorsFunction() which identifies anchors to be used later for data integration from each sample. Anchors are pairs of cells from each dataset that are each other's mutual nearest neighbors. Each anchor is then assigned a score based on the k.score (parameter equal to 30) anchors within its own and its pair's dataset. The anchor set is then

integrated using the `IntegrateData()` function which performs a pairwise integration in an iterative manner. In this step, distance between two datasets is calculated as the total number of cells in the smaller dataset divided by the total number of anchors between the two datasets. The distance matrix for all sample pairs is then clustered to determine a guide tree. The output of the function is a Seurat object with the original count matrix as well as an “integrated” matrix with batch corrected counts. Using the integrated matrix, `ScaleData()` function is called to apply linear transformation as is needed before performing Principal Component Analysis. By default, Seurat only uses the variable features determined in a previous step as input. `FindNeighbors()` is then run which uses the first 30 principal components (default) to construct a cellular KNN graph based on the Euclidean distance in PCA space and then edge weights between the cells are refined based on Jaccard similarity. The cells were then iteratively clustered into clusters by applying the Louvain algorithm. The resolution parameter determines the granularity expected when grouping cells together and we used a value of 0.2. The same PCs as calculated before were then used as input for generating a two-dimensional visualization of the cells grouped by cluster using Uniform Manifold Approximation Projection (UMAP). The marker genes for each cluster were calculated through the `FindAllMarkers()` function which uses a wilcoxon rank sum test to calculate the upregulated genes in each cellular cluster compared to all other clusters. Marker genes for each cluster were annotated manually using an interactive web application – dropviz.org and the Allen Mouse Whole Cortex and Hippocampus (10x Chromium v3) dataset as a reference for hippocampal cell types^{119,129}. The Saunders et al. (DropViz) dataset was primarily used for annotation while the Allen dataset was used for finer annotation of GABAergic neuronal subtypes, since the resolution of clustering

yielded more subtypes of inhibitory neurons than profiled in the Saunders et al. dataset. This process was repeated after removing clusters of mixed or systemic origin and then reintegrating (starting from the producing anchors step) and reclustering the cells to get clean, doublet free global clusters with cells expected in the hippocampus.

After obtaining a clear global separation of cellular clusters, cells identified as microglia were selected and the whole Seurat pipeline as described above, starting from splitting the Seurat object into 16 objects by sample, normalizing and reintegrating them to finding clusters (here, we found the optimal value for the resolution parameter to be 0.3) and looking at marker genes was repeated. Here also, we repeated this process 2-3 times each time removing clusters which were clearly showing marker genes of two or more than two cell types (neuronal, astrocytic and/or oligodendrocytic), giving us a final Seurat object with 4 microglial clusters, systemic B-cells and T-cells and parenchymal macrophages.

2.7 Differential Gene Expression Testing

For differential gene expression testing, I took the raw genes x cells counts matrix from each cell type and used it with edgeR¹³⁰ to test for differentially expressed genes across conditions using 6 total contrasts. First, I filtered the matrix to only have the genes which have at least 3% expression across all cells. This matrix is then read as a list-based object called DGEList which is required by edgeR. I applied a grouping factor in three ways – grouping all cells by whether they came from injured mice (TBI and Sham), by age (18-month-old and 3-month-old) and by experimental group (18-month-old TBI or Sham mice or 3-month-old TBI or Sham mice). Normalization factors were calculated by using the calcNormFactors() function to account for genes which are highly expressed in some samples which can leave other genes undersampled for the analysis. A design matrix was

constructed to describe the treatment condition for the subsequent Generalized Linear Model (GLM) approach I used for estimating dispersion. `estimateDisp()` is used to estimate the dispersion for all genes using the Cox-Reid profile adjusted likelihood method (since in our case we have more than 1 factor). Quasi-likelihood F test was used to perform differential testing using 6 contrasts – TBI vs Sham, 18-month-old vs 3-month-old, TBI vs Sham in 18-month-old mice and 3-month-old mice, and 18-month-old vs 3-month-old in TBI induced and Sham treated mice. The differentially expressed genes were combined in a single matrix containing p-values, false discovery rates and log fold changes across all contrasts.

For microglia, only the microglial cells – cells from cluster M1, M2, M3 and M4 were used for this pipeline.

2.8 Pseudotime Ordering Using Monocle

To study the trajectory of microglial cells going from one state to another, I used the raw counts matrix of all microglia and used it in Monocle 2¹³¹ to create a `CellDataSet` (`cds`) object using the `newCellDataSet()` function. Since I was using transcript counts, I used a negative binomial model for the `expressionFamily` parameter. Data was normalized using `estimateSizeFactors()` and dispersion was calculated using `estimateDispersions()`. The `detectGenes()` function was used to set a minimum threshold for gene expression which counts how many cells express each feature above a minimum threshold. The threshold level was set at 0.1 (default). Genes which were being expressed in at least 50 cells were retained. A few cells with very low or very high transcript recovery were also filtered out. To cluster the cells and reduce dimensionality, Monocle uses tSNE and an unsupervised clustering model. The top 85 marker genes for each cluster were then ordered according to

the expected trajectory and set into the cds object using `setOrderingFilter`. I used Monocle's implementation of Reverse Graph Embedding in the next step to reduce data dimensionality. The final step is ordering the cells in pseudotime using the `orderCells()` function which uses a machine learning approach to fit the best "tree" (a structure with one end being the "root" and other end(s) being the "leaves"). The parameter "reverse" was set to TRUE. The plots for the cell trajectories were called using `plot_cell_trajectory()`.

To see what genes were being expressed during the branching of microglia from M1/M2 state to M3 and M4 state, I used Branched Expression Analysis Modeling (BEAM) which is a statistical approach in the Monocle 2 package. It compares two models with a likelihood ratio test for branch dependent expression. The full model is a product of the branch a cell is assigned to and smoothed pseudotime. This was visualized through a special type of heatmap through the `plot_gene_branched_heatmap()` function. The plots for individual genes showing their expression through the two trajectories were generated through `plot_genes_branched_pseudotime()` function.

2.9 snATAC-seq Clustering and Analysis Using ArchR

For downstream clustering and analysis, ArchR v1.0.2¹³² was used with mm10 (BSgenome.Mmusculus.UCSC.mm10) genome for all steps of the analysis. ArchR reads data in the format of Arrow files which are HDF5-format based files, updated by ArchR as further analyses are performed. These arrow files are not actually read into the R environment but held into memory as addresses bound by a single analytical framework – ArchRProject. I ran `createArrowFiles()` with default parameters which created Arrow files for each sample along with a "TileMatrix" having counts of insertion sites for every 500 bp bin of the genome. Predicted gene expression scores are stored in the

“GeneScoreMatrix” which are based on weighting insertion counts in tiles nearby a gene promoter. This step also performs quality control. All cells with lesser than 1000 fragments are filtered out. The signal-to-background ratio or the transcription start site (TSS) score is calculated as the ratio of peak of enrichment centered at the TSS (expected to be universally enriched) relative to the flanking regions of the TSS (+/- 1900 to 2000 bp). A ratio of less than 4 excludes the cell from the analysis. `addDoubletScores()` function was used to infer the scores predicting which cell is actually a “doublet” (single barcode, 2 cells) and add it to the Arrow files. After creating an `ArchRProject` which is an R object connecting all the Arrow files together, the doublets were filtered out with the default filter ratio of 1.5 (maximum ratio of predicted doublets as a factor of the total number of cells). ArchR uses iterative Latent Semantic Indexing (LSI) for dimensionality reduction. In this approach an initial LSI transformation is performed on the most accessible tiles and the clusters which are of lower resolution and not confounded are identified. Variable peaks across the clusters are identified and used for LSI again. The number of iterations were set to 2 (default). Harmony was used within the ArchR framework to correct for batch effect differences using `addHarmony()` function specifying the reduced dimensions from the previous run of the iterative LSI to be used. The same graph clustering approach used in Seurat¹²⁸ was applied to cluster all the cells using `addClusters()` function with a resolution of 0.2. to visualize the clusters in a reduced dimension space, `addUMAP()` was run on the Harmony output. To annotate the clusters, marker features were identified based on gene scores calculated by ArchR. ArchR calculates gene scores based on the local accessibility of the gene region including the promoter and the gene body. To include distal regulatory elements, ArchR identifies the subset of tiles within the default 500bp gene window and

do not cross another gene region. The gene scores are depth-normalized to a default value of 10,000. The list of marker features was obtained by running the `getMarkerFeatures()` function in which each cell group is compared to its own background cell group to determine if the cell group in question has higher accessibility. Annotation was done with the help of the same tool as was used for the snRNA-seq experiment. This was repeated in a similar way as selected marker features from each cluster were overlaid on the UMAP plot for global cell clusters using the `plotEmbedding()` function. Given the sparsity of snATAC-seq data, I also imputed the gene scores to smooth the signal across nearby cells using `addImputeWeights()` function which uses MAGIC¹³³, an algorithm for denoising high-dimensional data. I integrated the snATAC-seq and snRNA-seq data within the framework of ArchR which uses the `FindTransferAnchors()` function from Seurat, parallelized to make it more computationally efficient. Integration was performed in 2 steps – an agnostic, unconstrained version was performed first which aligns all the cells in each dataset to the other dataset. To improve the quality of this integration, a biased, constrained integration was performed in which I inputted the annotation of cell types and integrated each cell type in one dataset to the corresponding cell type in the other one. The combined matrix of cells from both datasets was added to the Arrow files using the `addGeneIntegrationMatrix()` function. Before calling peaks and identifying marker peaks, I made pseudo-bulk replicates within ArchR to achieve appropriate statistical significance since snATAC-seq data can be very sparse and is binary. ArchR does this in a way that for each cell cluster, there are sufficient cells from a single sample to maintain sample heterogeneity and biological variation. The maximum replicates per cluster was chosen to be 5 (default) and the maximum cells per replicate per cluster would be 500 with a

minimum 40 cells per replicate per cluster (default). Peak calling in ArchR was done by executing `addReproduciblePeakSet()`. In ArchR, peaks are called through MACS2¹³⁴. The peaks are then first ranked by their significance and any peaks overlapping with the significant peaks are removed which is repeated until no more peaks exist. Using the same `getMarkerFeatures()` function, I identified the marker peaks.

To identify differentially accessible peaks across TBI and age, the “PeakMatrix” which contains insertion counts per cell per peak was used with edgeR using the same framework as used for the snRNA-seq differential gene expression analysis.

2.10 Gene Regulatory Network (GRN)

Firstly, a binarized matrix of annotated motifs is created in ArchR across all peaks using the JASPAR2020 database using the `addMotifAnnotations()` function. This binarized matrix is used to make a base gene regulatory network in which the presence of a motif in each peak is numerically indicated. I separately annotated all the peaks to genes with ChIPSeeker using the annotation package for mm10 mouse genome. The transcription start site range was defined as +2000bp to -2000bp. ArchR uses the approach utilized by Cicero to create low-overlapping aggregates of single cells prior to analysis involving correlation of features. Aggregates with greater than 80% overlap with any other aggregate are filtered out to reduce bias. Co-accessibility scores were calculated using the `addCoaAccessibility()` function in ArchR. A base GRN is constructed having all the motif annotations with peaks, transcription factor (TF) motifs, target genes along with co-accessibility scores. This data frame is then integrated with gene expression counts. The counts are smoothed by log₂ transformation. Then, a list of regulators of each target gene (all the genes in the gene expression matrix) is constructed with the transcription factor for each of those targets

matched with the latter. Any target gene having less than 2 regulators is filtered out. GENIE3¹³⁵ is then implemented for each target gene having more than 2 regulators and a list of target genes, regulators and their weight scores. The top 50,000 TF-gene links were selected to look at “hub” TFs with the strongest relationships.

An enrichment analysis is done by running a Fisher’s exact test separately on the upregulated and downregulated genes found through the differential gene expression analysis by edgeR as described in previous sections. The enrichment analysis is also repeated separately for activating TFs and repressing TFs defined by correlating the expression of the TF with the target gene in the snRNA-seq data (positive correlation meaning activating and negative correlation meaning repressing).

3. RESULTS

3.1 A single-cell gene expression and chromatin accessibility atlas for the aging mouse hippocampus and its sensitivity to brain injury

We performed 10x Genomics single-nucleus RNA sequencing (snRNA-seq) to characterize the effects of traumatic brain injury (TBI) in the hippocampus of young (3-month-old) vs. aged (18-month-old) mice (n=4 mice per condition; Fig. 1A). Initial data processing identified 136,265 cells. After filtering of low-quality cells, we studied the transcriptomes of 87,791 cells. Clustering of these cells revealed 15 major cell types, which we annotated based on established markers (Fig.1B and 1C; Supplementary Table 1). Cell type proportions were similar across the 16 samples with several notable exceptions. Specifically, microglia and choroid plexus were more abundant in mice that experienced TBI. Microglia were slightly more in aged mice as well. Other populations like astrocytes showed higher proportions in aged Sham treated or young TBI-induced mice while oligodendrocytes generally showed higher numbers in aged mice compared to young mice. Dentate granule cells also showed a high proportion coming from aged Sham-treated mice with low numbers in 3-month-old TBI mice. The neuronal population coming from the subiculum classified as “Neuron_subiculum_Slc17a6” showed a drastic effect where more than half of all such neurons came from young TBI-induced mice while Sham mice had a much lower population with aged TBI mice showing a slight increase in the number. The combined cluster of endothelial, mural and fibroblast cells again showed a similar pattern. CA1 neurons were relatively lesser in population in the TBI-induced mice, with a very slight change with respect to age (Fig.1D). Overall, there seems to be cell type specific

effects of age on both TBI and Sham treated mice with a general trend of increased cell numbers seen with either age or TBI or both with a few exceptions.

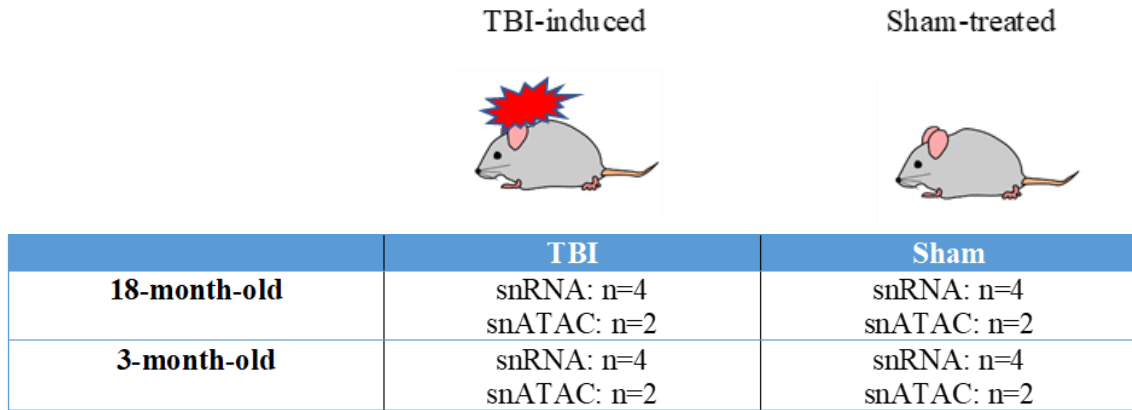


Figure 1A: Experimental design showing the 4 groups with n=4 mice each; show ATAC too.

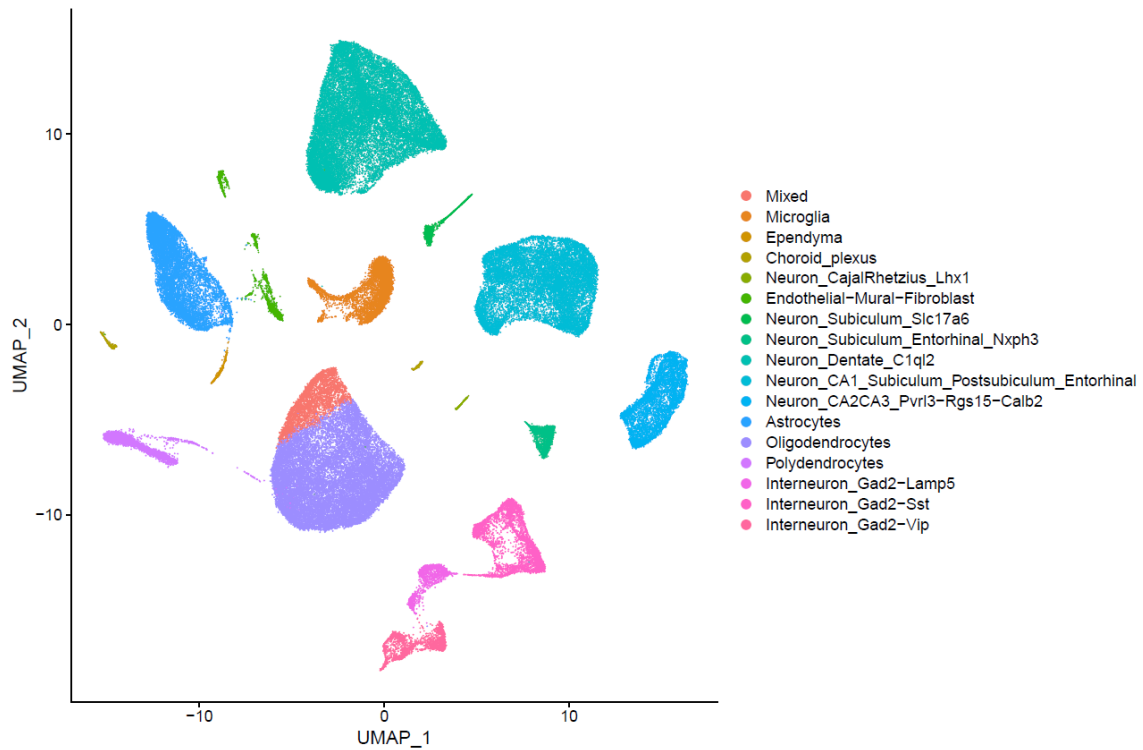


Figure 1B: UMAP consisting of global clusters observed across all samples after clustering in Seurat.

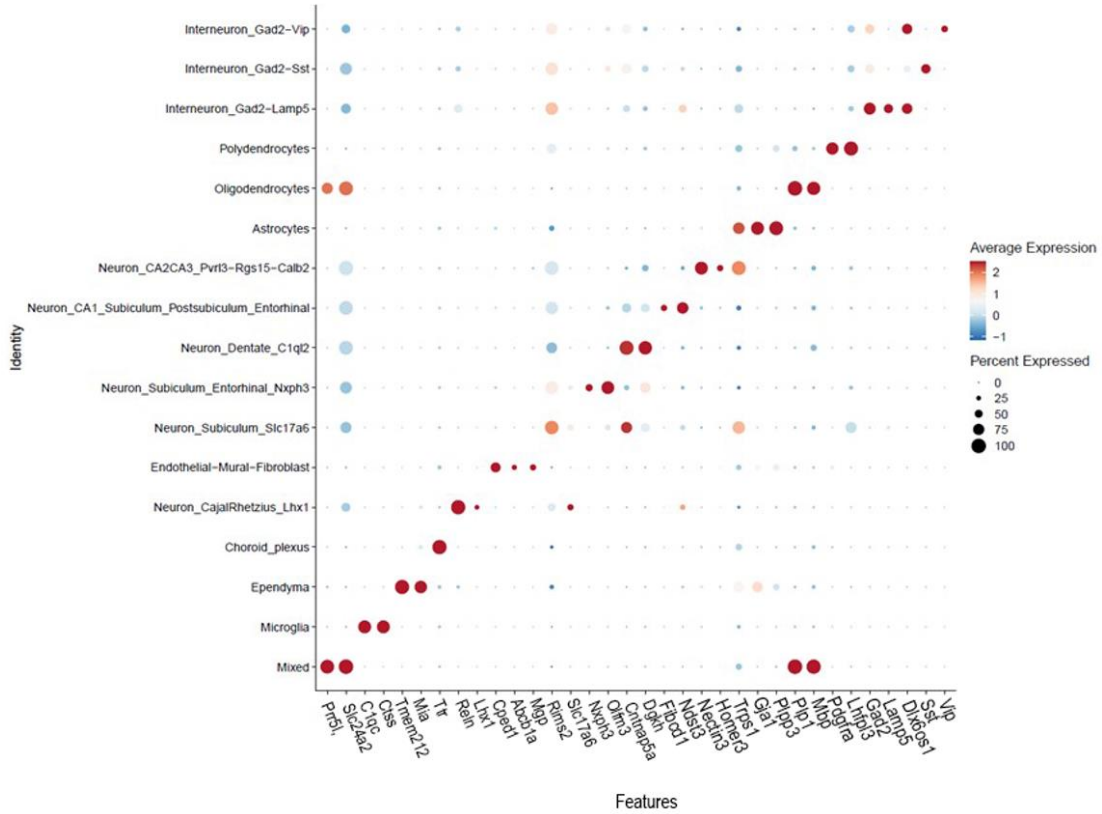


Figure 1C. Dotplot of all cell-type specific markers used, representing cell type specific expression for each cell type observed. The “mixed” cluster shows markers of both oligodendrocytes and microglia

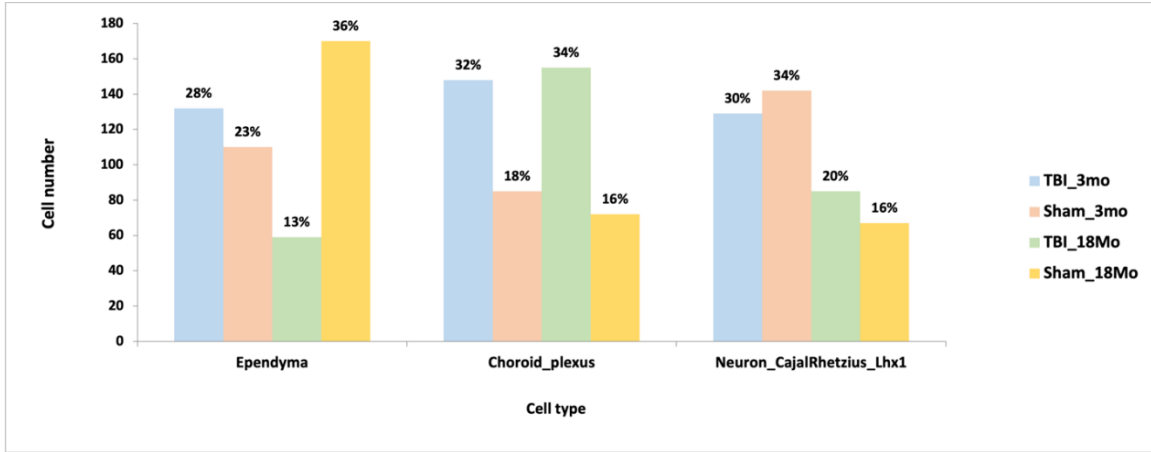
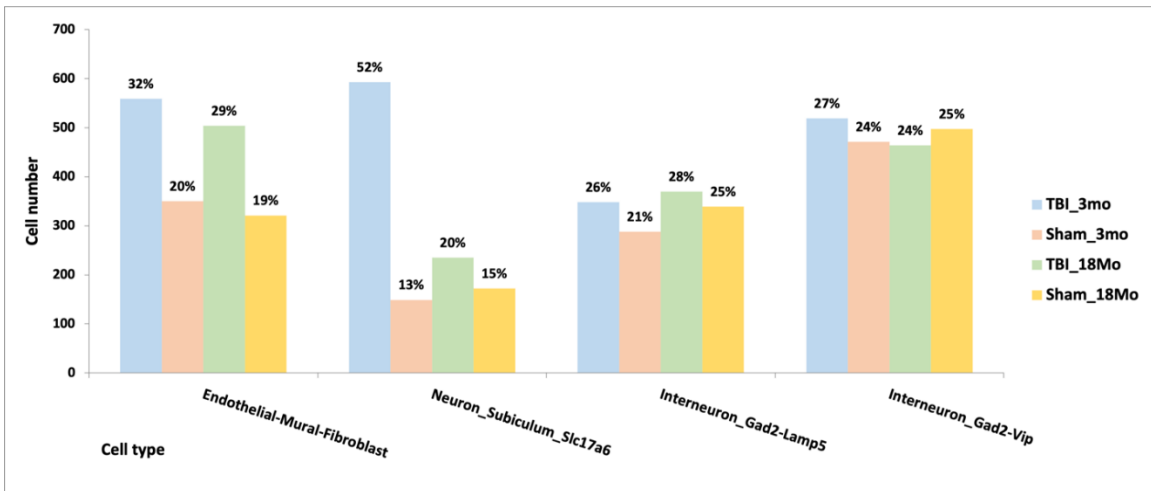


Figure 1D. Bar graphs representing number of nuclei per group per cell-type. The percentages are representative of the composition of the specific cell type population per group.

Figure 1D continued..



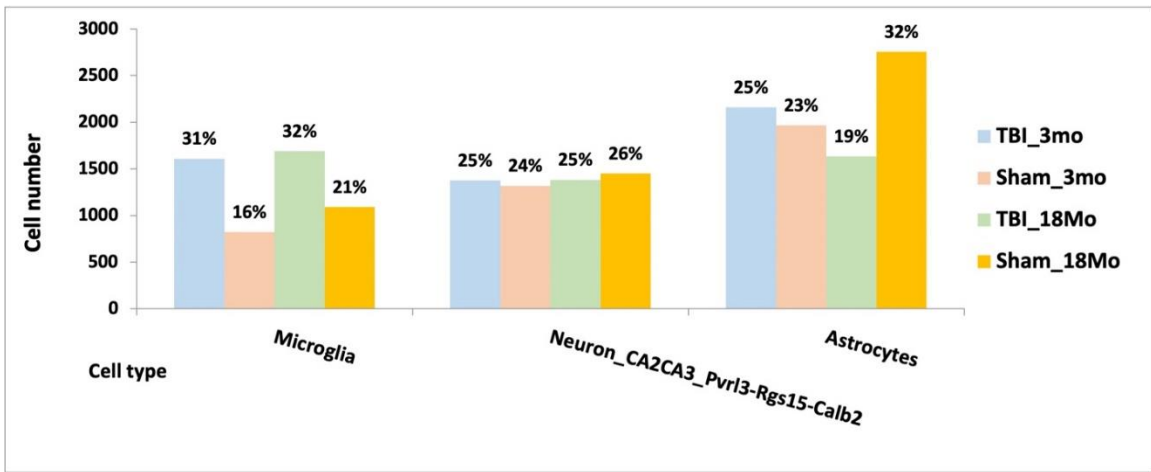
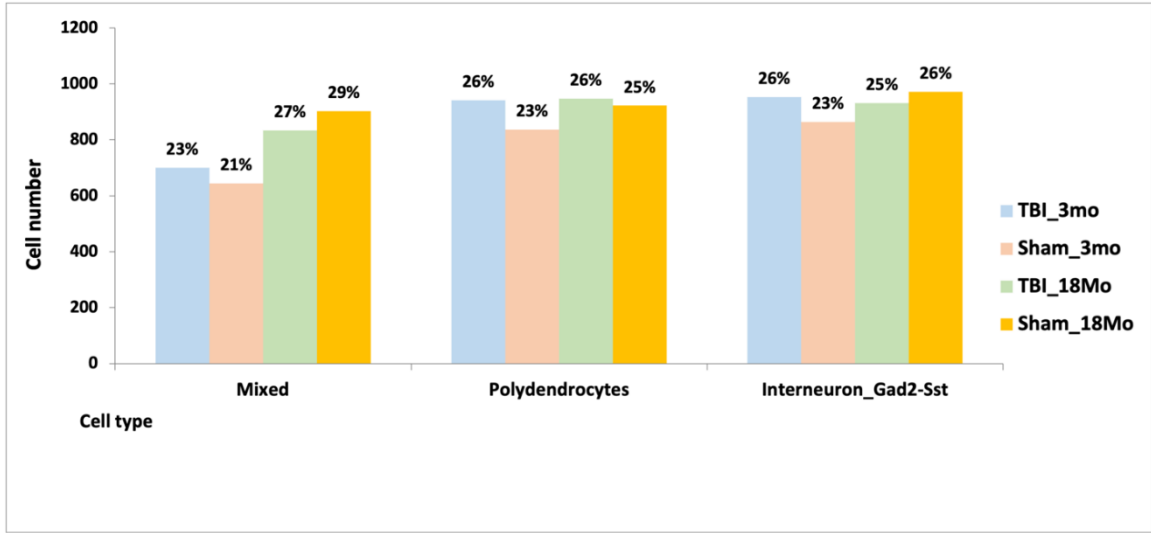
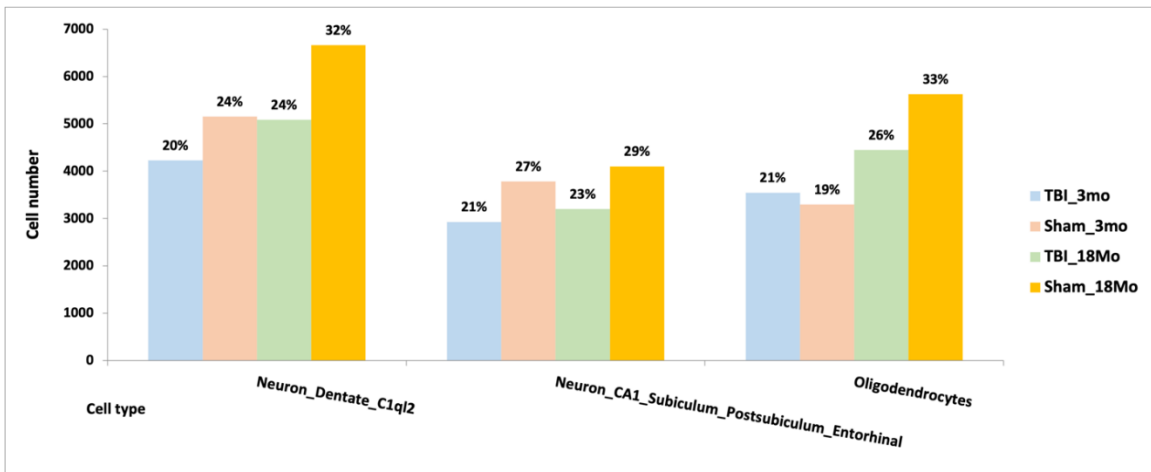


Figure 1D continued..



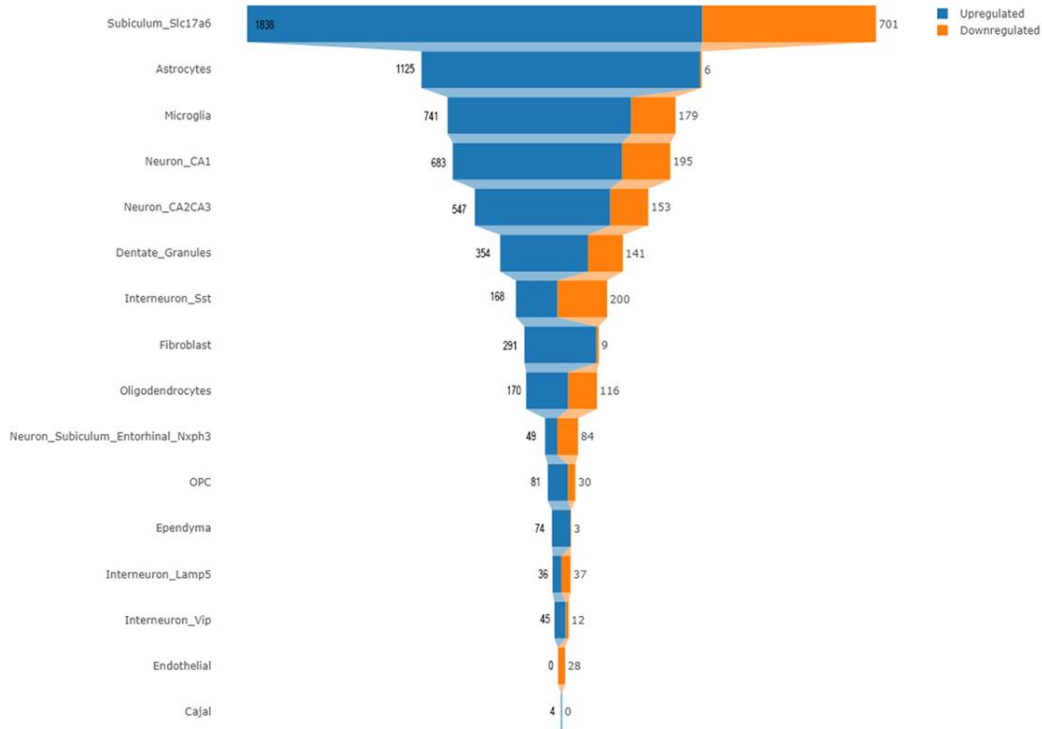


Figure 1E. Number of significantly upregulated and downregulated DEGs observed in each celltype [FDR < 0.01, $|\log_2FC| > 0.2$].

For the snATAC-seq part of the study, a similar experimental model was used as the one used for snRNA-seq. Using 10x Genomics Chromium v3, 8 hippocampi were sequenced, n=2 in each of the 4 groups as shown in Fig.1A. Cell Ranger ATAC was used to pre-process the FASTQ files to generate position sorted bam files, filtered matrices of peak regions and fragment files. The output was entered into ArchR v1.0.2 where quality control and batch effect correction was performed. A UMAP representing the clusters of cell types of the final 67,398 cells is shown in Fig. 2A. The annotation of the 13 cell types inferred from the data was done on the basis of marker genes calculated from gene scores, which are fundamentally a prediction of the expression of a gene based on the chromatin

accessibility of regulatory elements proximal to the gene (Fig. 2B-2M and Supplementary Table 2). Cell type proportions by experimental group also reflected a similar trend as the trends shown by snRNA-seq data – there was a general trend of mice with TBI having more cells than Sham treated cells (Fig. 2N). The only exception to this trend were dentate granule cells which showed lower cells in the 3-month-old TBI group than its Sham counterpart.

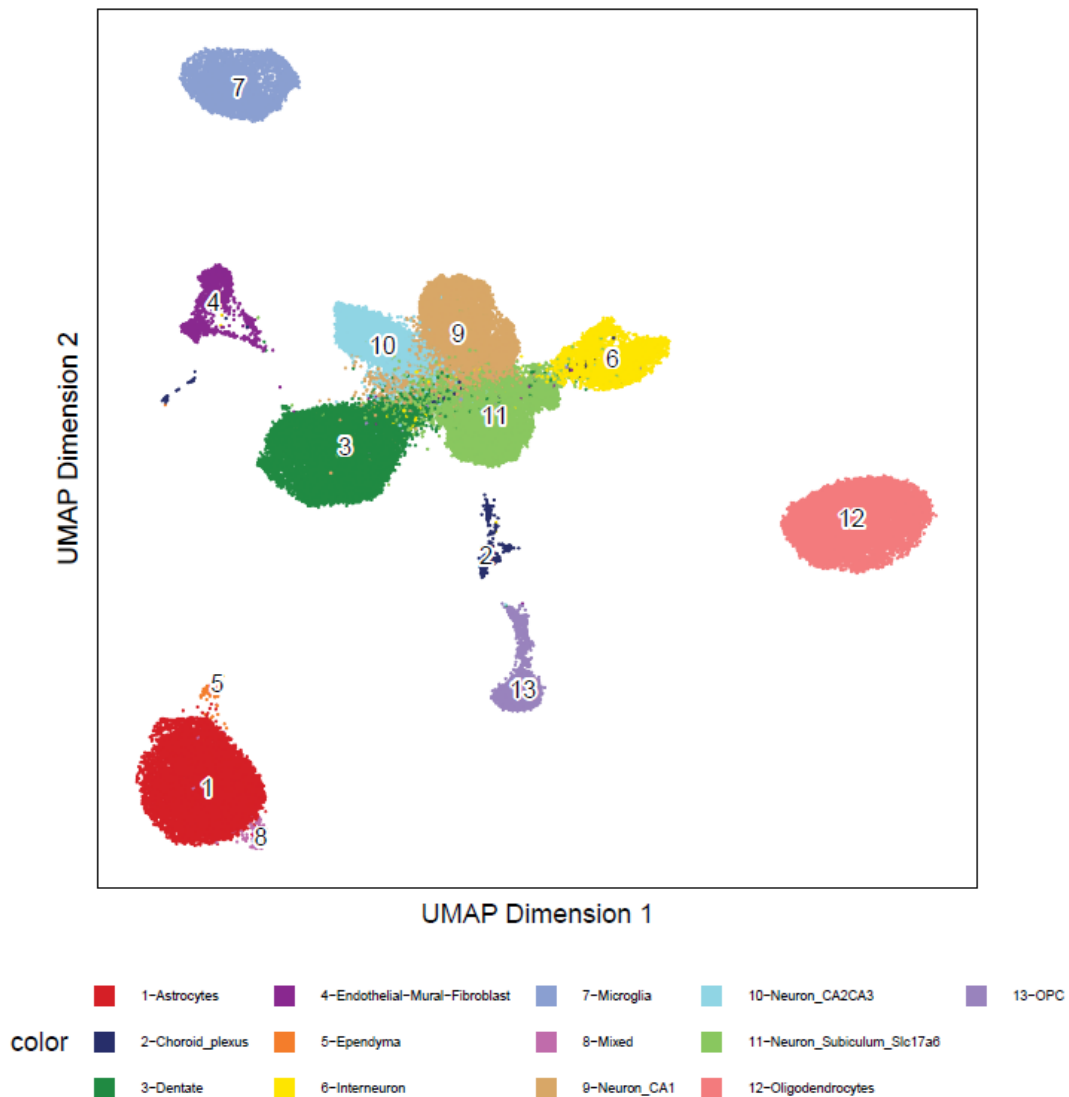


Figure 2A. UMAP showing all global snATAC-seq clusters obtained after clustering with ArchR.

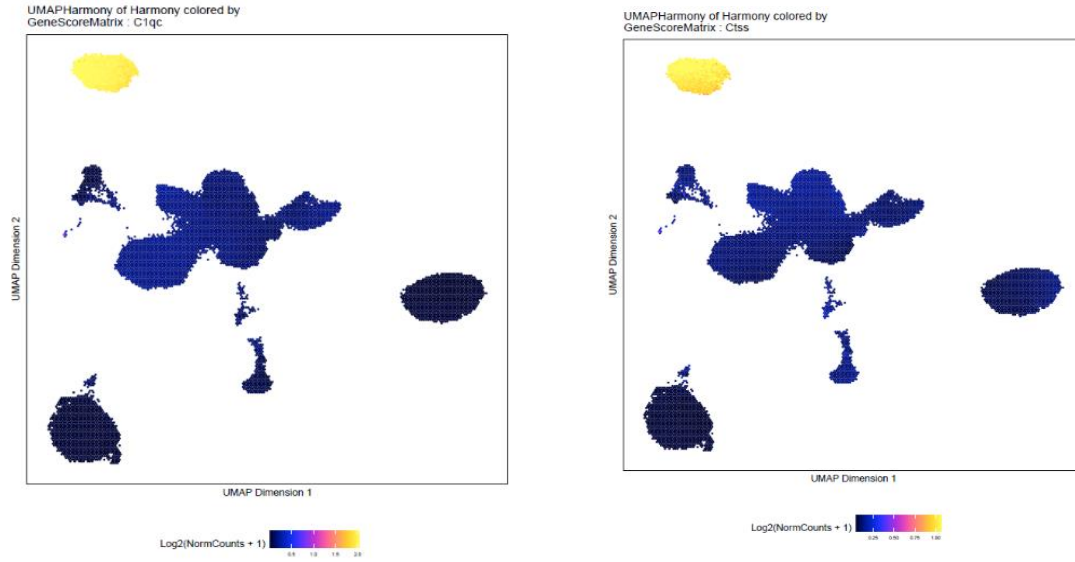


Figure 2B. Visualization of marker gene activity scores of microglia on global UMAP embedding.

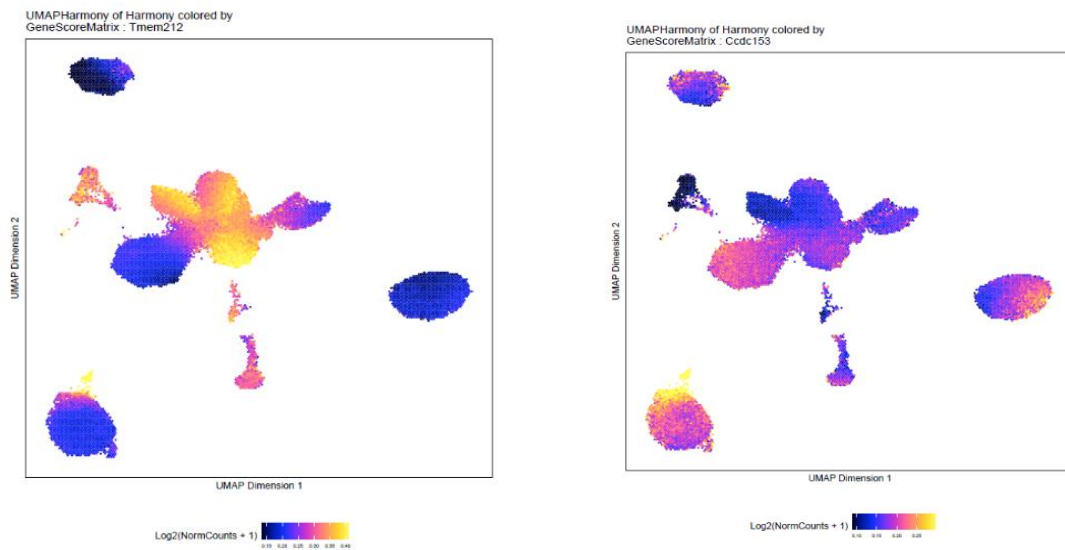


Figure 2C. Visualization of marker gene activity scores of ependyma cells on global UMAP embedding.

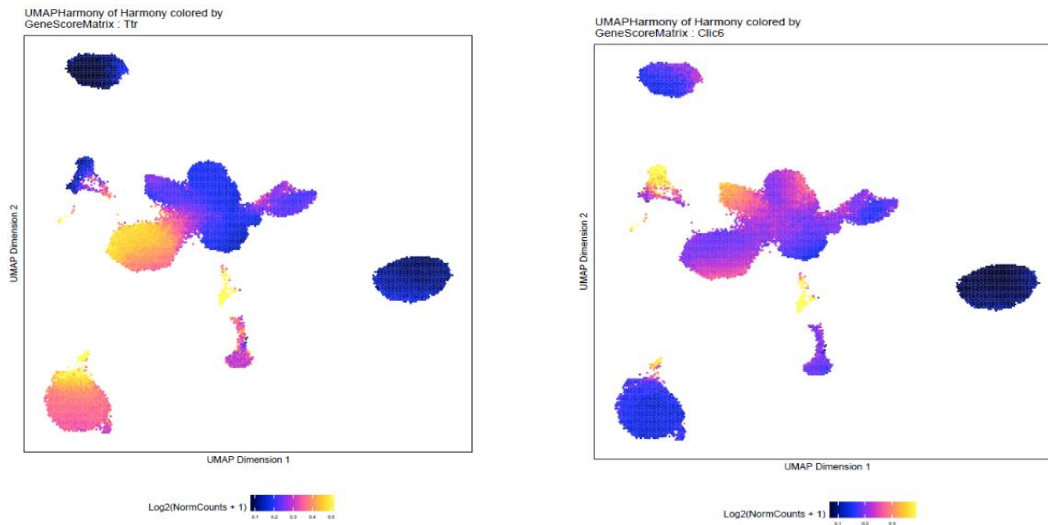


Figure 2D. Visualization of marker gene activity scores of choroid plexus cells on global UMAP embedding.

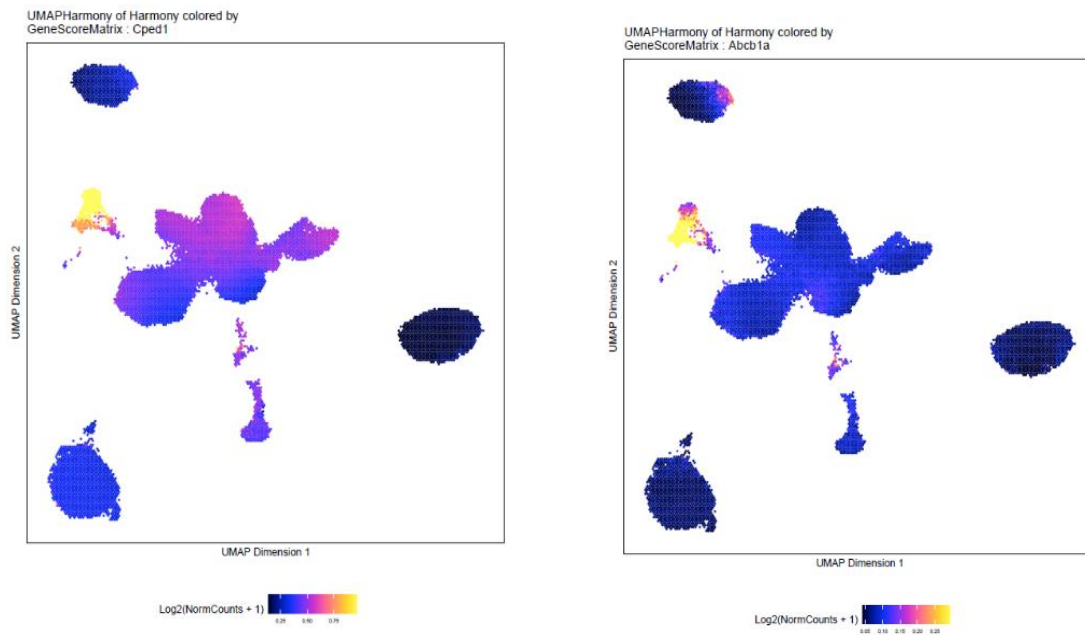


Figure 2E. Visualization of marker gene activity scores of combined cluster of endothelial, mural and fibroblast cells on global UMAP embedding.

Figure 2E continued

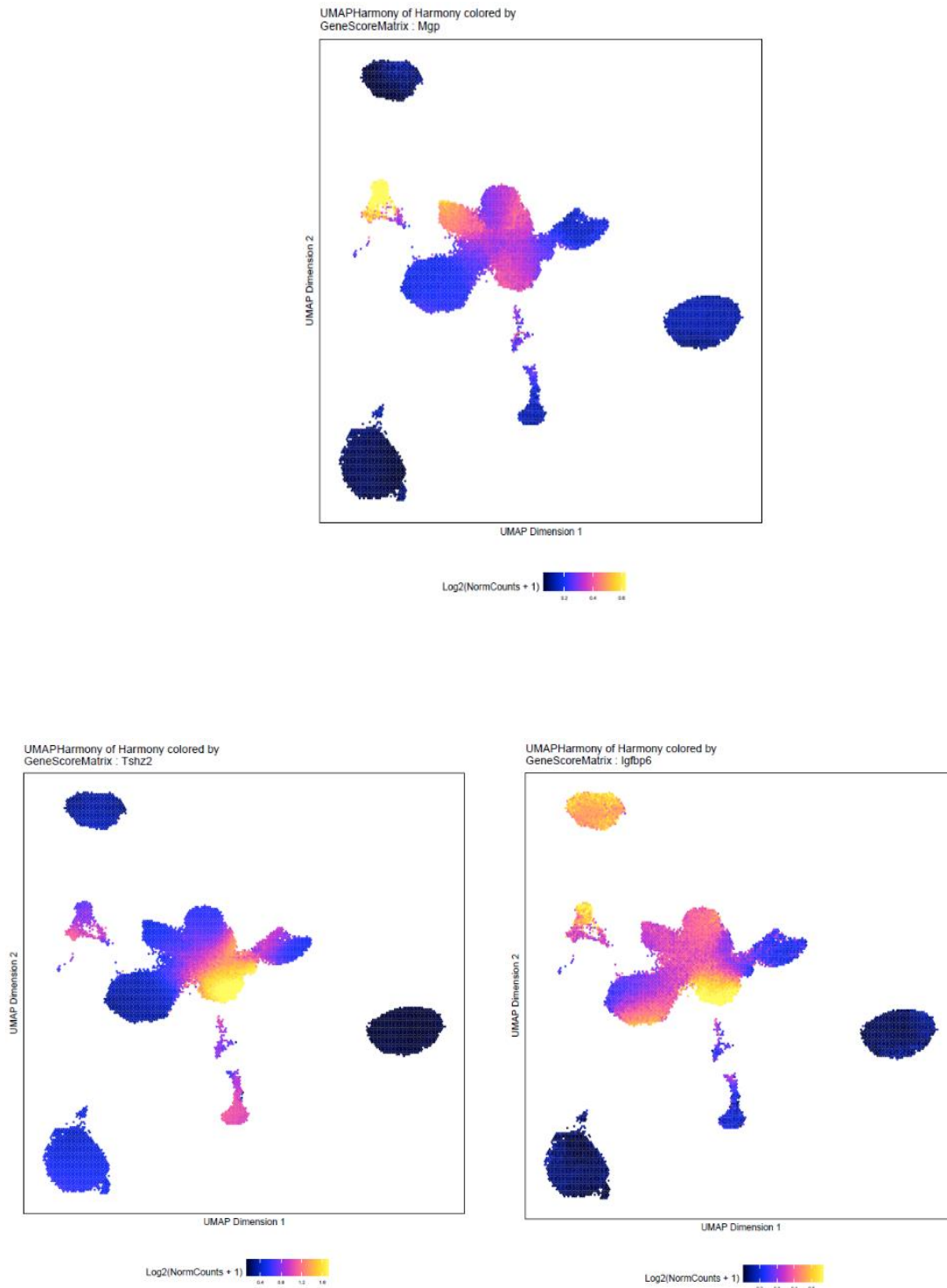


Figure 2F. Visualization of marker gene activity scores of Neuron_Subiculum_Slc17a6 cells on global UMAP embedding.

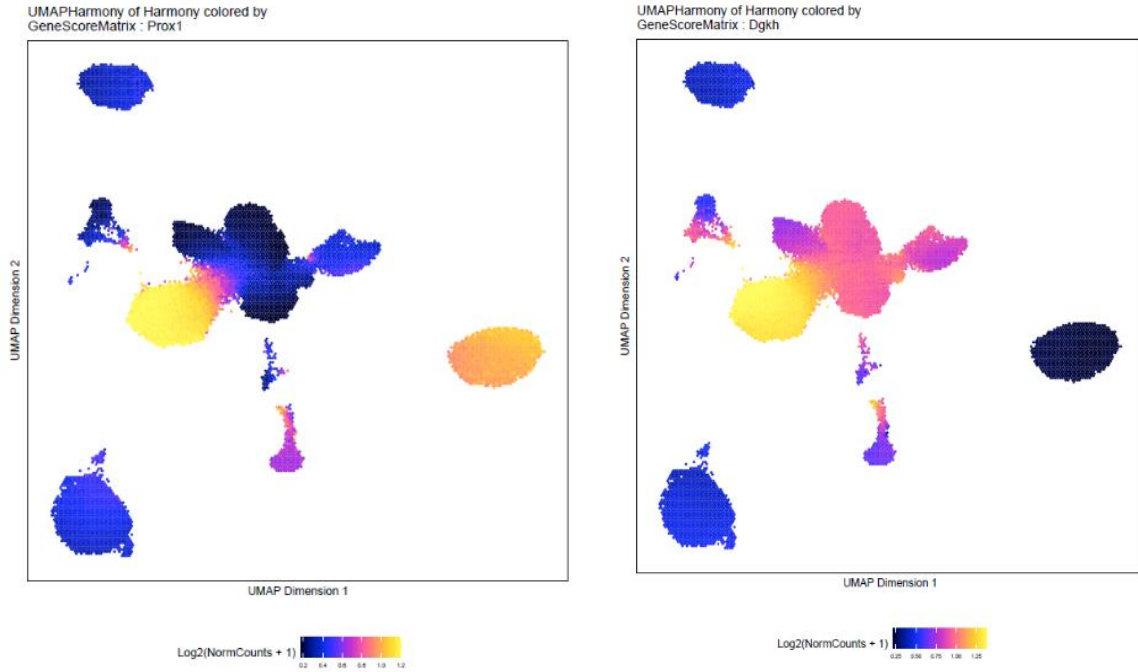


Figure 2G. Visualization of marker gene activity scores of Neuron_Dentate_C1q12 cells on global UMAP embedding.

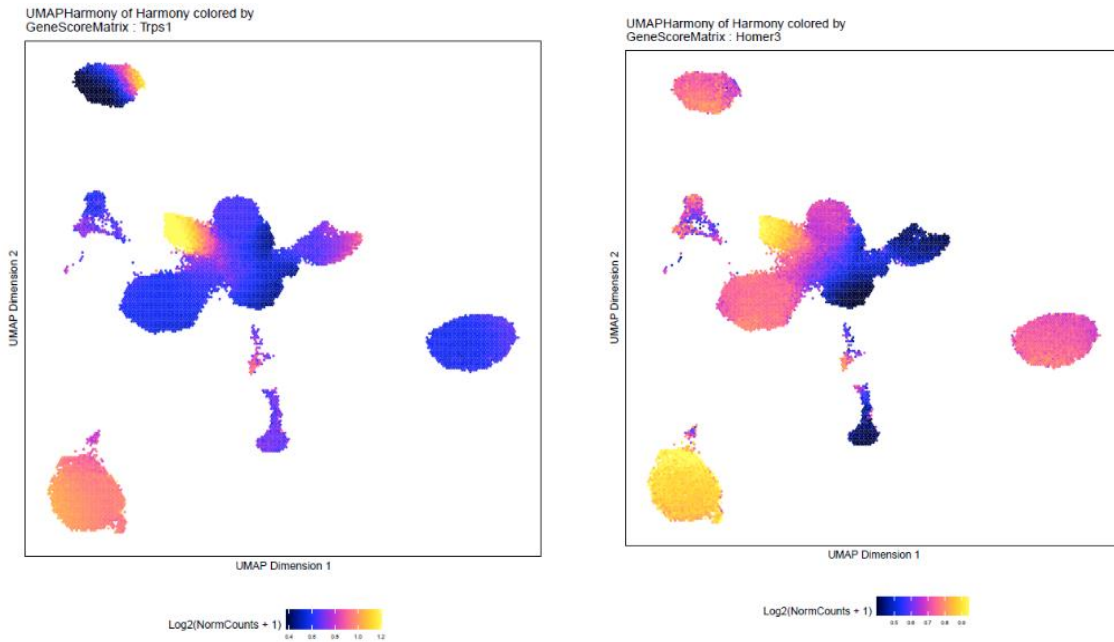


Figure 2H. Visualization of marker gene activity scores of Neuron_CA2CA3_Pvr13-Rgs15-Calb2 cells on global UMAP embedding.

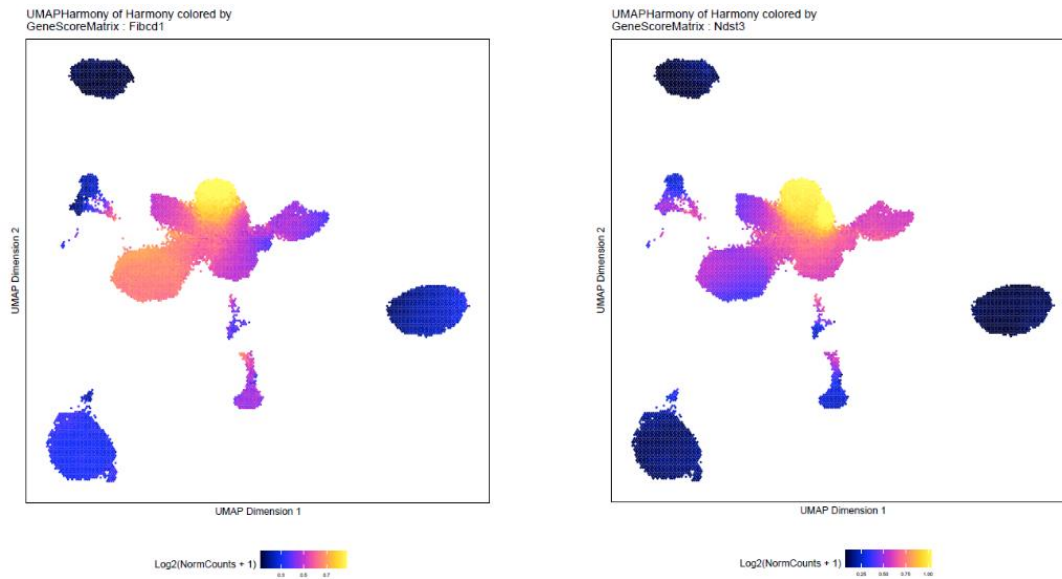


Figure 2I. Visualization of marker gene activity scores of Neuron_CA1_Subiculum_Postsubiculum cells on global UMAP embedding.

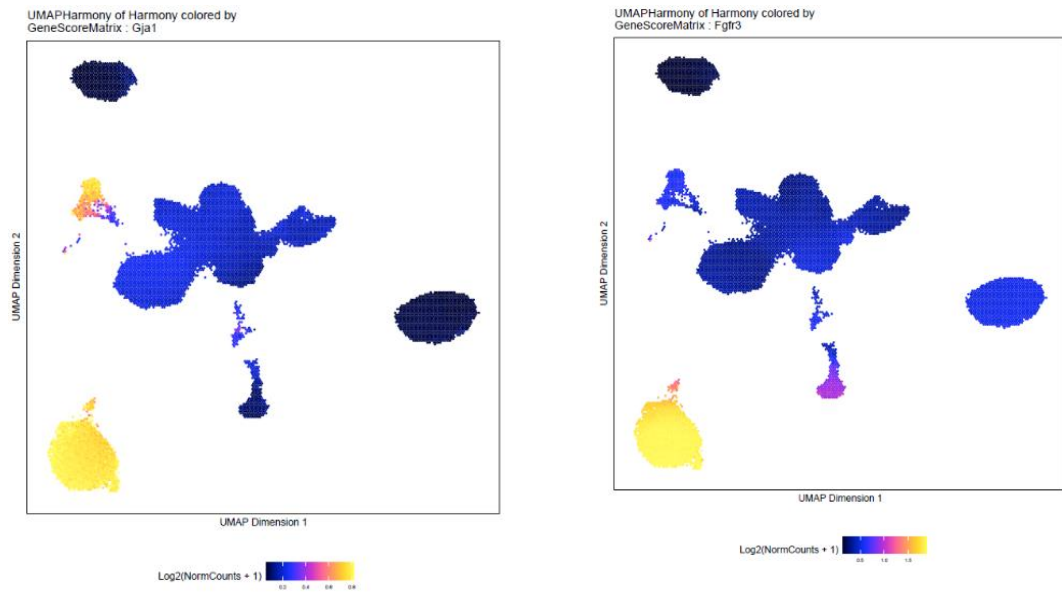


Figure 2J. Visualization of marker gene activity scores of astrocytes on global UMAP embedding.

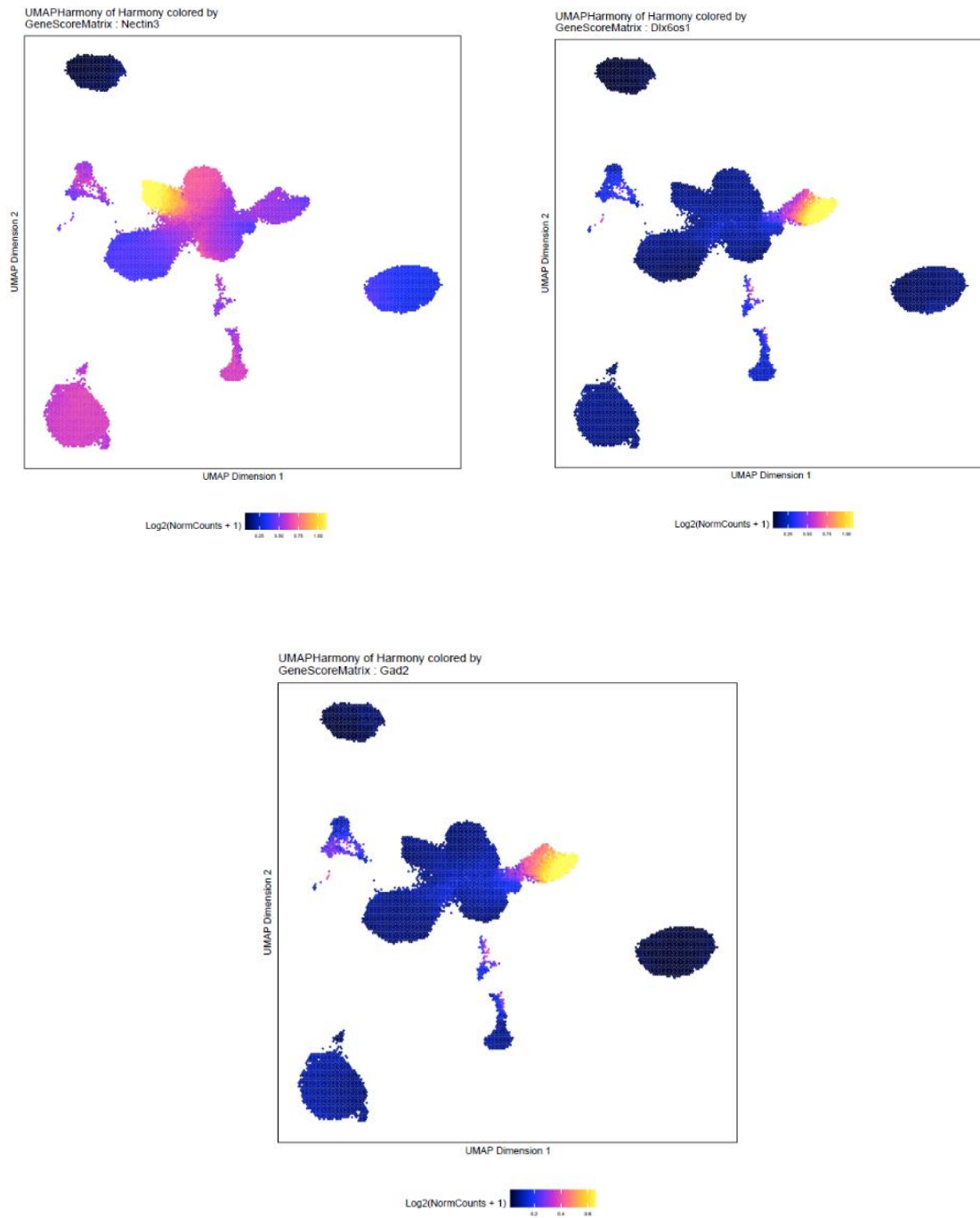


Figure 2K. Visualization of marker gene activity scores of interneuron cells on global UMAP embedding.

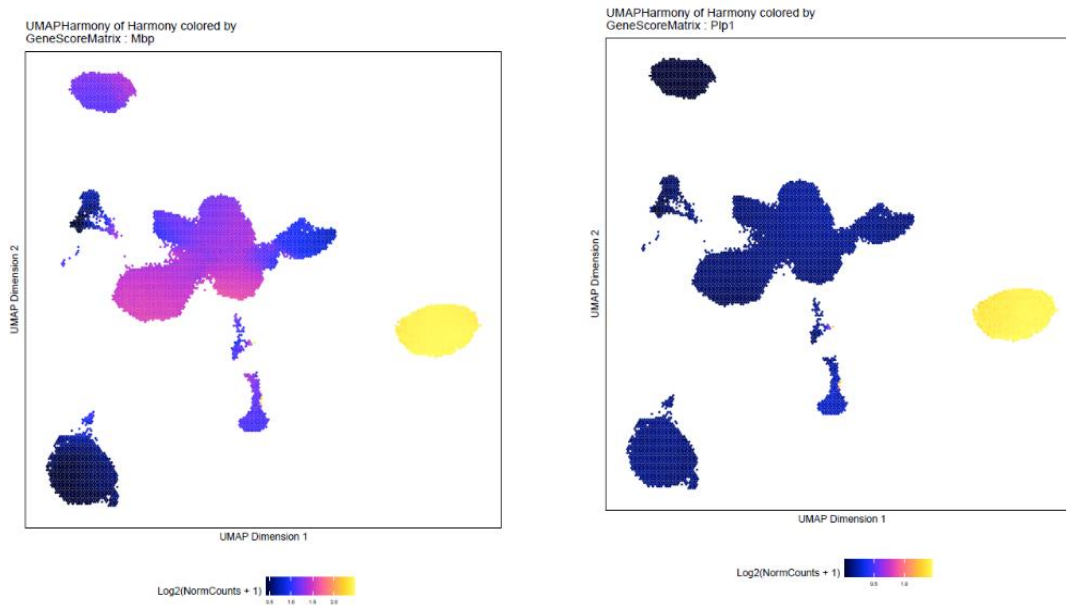


Figure 2L. Visualization of marker gene activity scores of oligodendrocytes on global UMAP embedding.

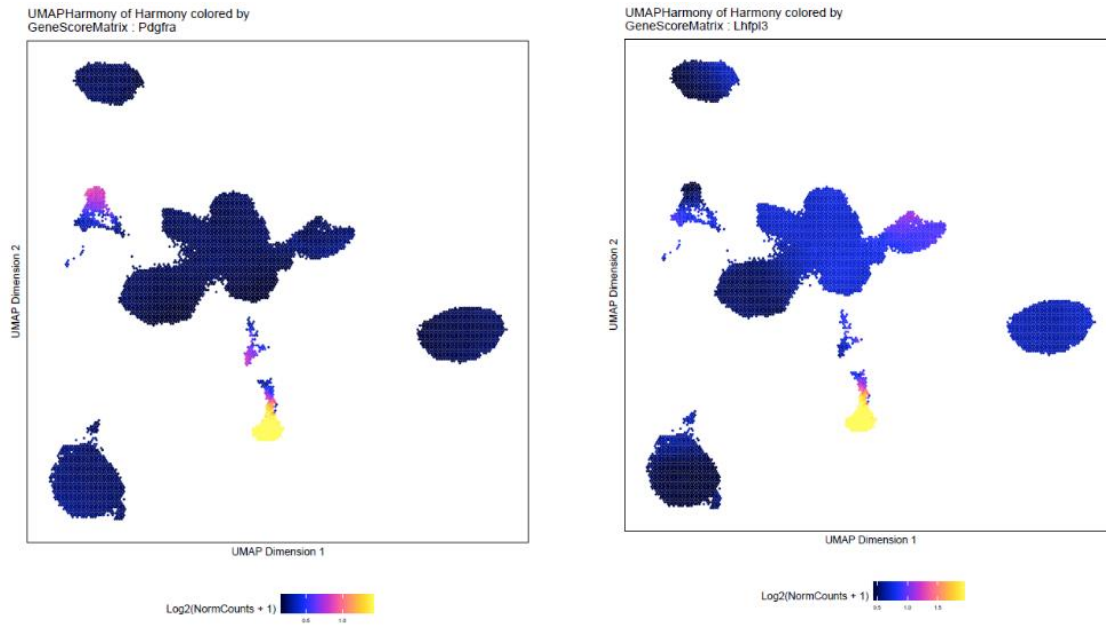


Figure 2M. Visualization of marker gene activity scores of OPC (oligodendrocyte progenitor cells) on global UMAP embedding.

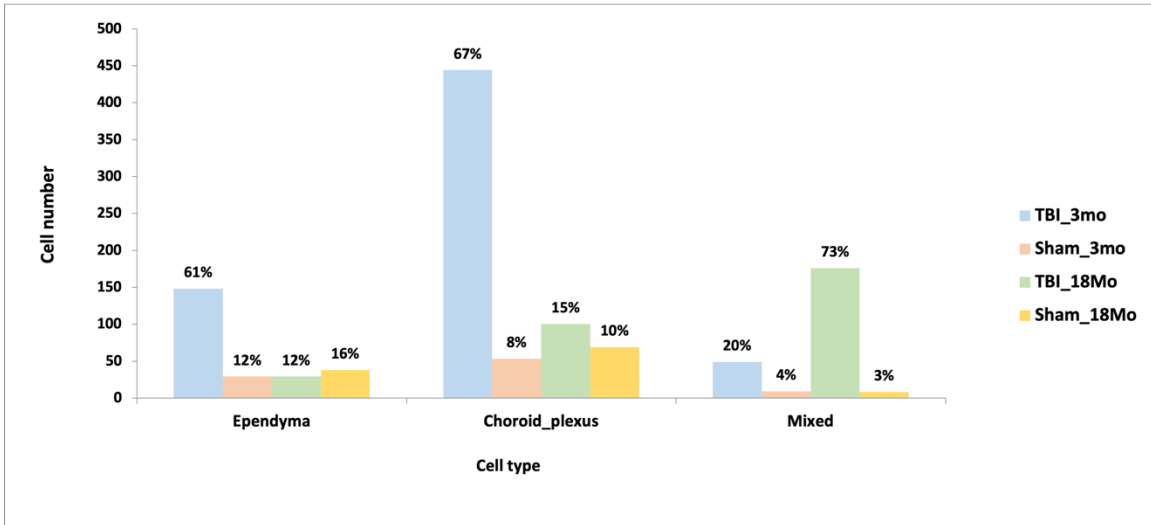
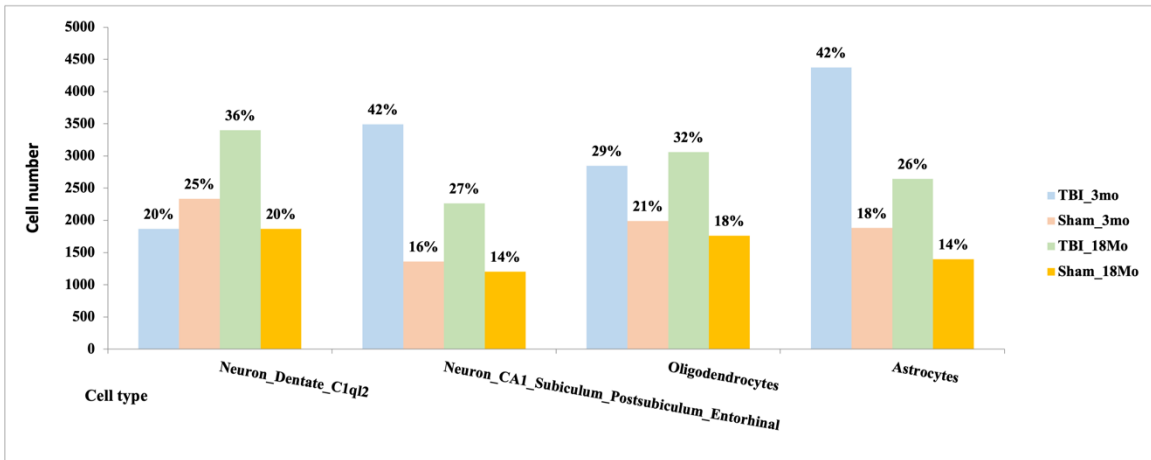
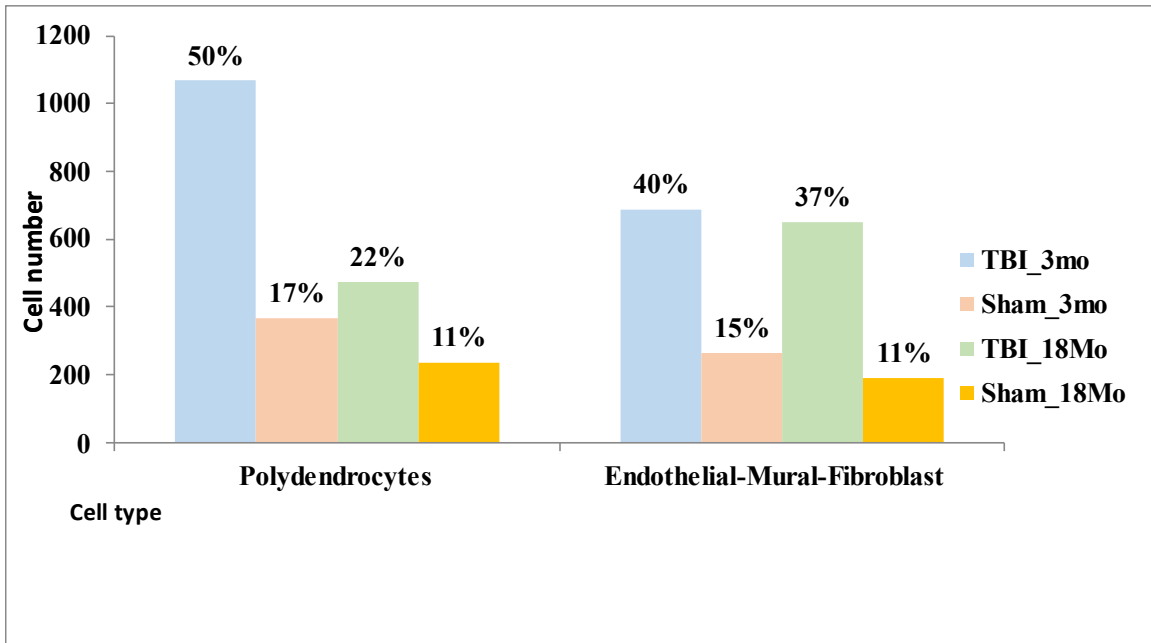
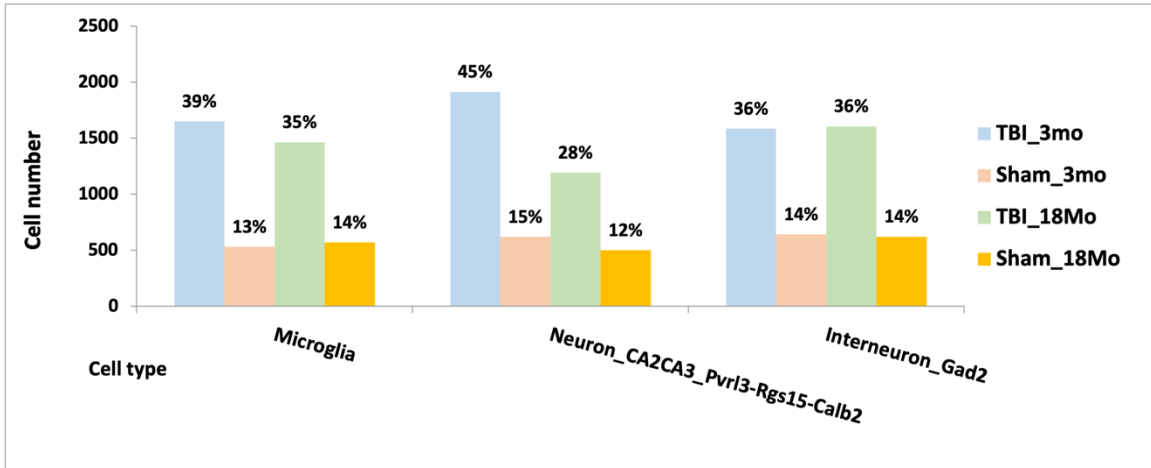


Figure 2N. Bar graphs representing number of nuclei per group per cell-type. The percentages are representative of the composition of the specific cell type population per group.

Figure 2N continued



3.2 Functional heterogeneity of microglia in the context of inflammation and aging

Microglia subtype classification

Our next objective was to characterize the microglial response to TBI, hypothesizing that TBI would induce inflammation and degeneration associated changes. We re-clustered the immune cells from all samples and identified 7 sub-clusters, including four microglial states and three peripheral immune cell populations, B cells, T cells and macrophages (Fig. 3A). The cluster labeled M1 showed a marker signature of genes expressed in homeostatic microglia (*Csmd3*, *Siglech*, *P2ry12*)¹¹¹. M2 cluster showed a very similar profile with homeostatic genes like *Ctss*, *Cst3*, *Hexb*, *Selplg* but also *Trem2*, *Cd81* and *Tyrobp* (Supplementary Table 3), molecules which are known to lead to an activated state¹³⁶. The marker genes of M3 cluster showed a similar expression profile as has been characterized before in other single-cell studies. This subtype has been called “disease-associated microglia (DAM)”¹⁰³ or the “microglial neurodegenerative phenotype (MGnD)”¹⁰⁴ or “activated response microglia (ARM)”¹¹² in different studies. In our study, the top marker genes for this cluster included *Spp1*, *Apoe*, *Gpnmb*, *Cacna1a* among others. The M4 cluster showed a “classical” pro-inflammatory signature, previously characterized as the “M1 pro-inflammatory” microglia with marker genes like MHC class II genes (*H2-Eb1*, *H2-Ab1*, *H2-Aa1*), *Cd74*, *Ccr2* among others^{98,137}. The top marker genes for each cluster are visualized in Fig. 3B.

Differential Gene Expression analysis

Differential gene expression testing of all microglial cells (not including T cells, B cells and macrophages) was done through edgeR with various contrasts to reveal condition and

age specific transcriptomic changes (Supplementary Table 3). The number of significant DEGs contrasting all mice with TBI against Sham-treated mice was high in microglia with 741 upregulated DEGs and 179 downregulated DEGs (Fig. 1E). The top upregulated DEGs were also markers of M3 and M4 clusters like *Spp1* (tissue remodeling and phagocytosis)^{106,138,139}, *Lyz2* (lysosomal activity), *Gpnmb* (mTOR based regulation through inflammation)¹⁴⁰, *H2-D1* (class I MHC protein) and *Cd74* (class II MHC protein and cell survival)¹⁴¹. among others. The downregulated genes were a host of genes found expressed during homeostatic conditions which included the PKC family of genes, *Khdrbs3*, a splicing transcript shown to be downregulated in the microglia of the hippocampus of APP mice model of AD¹⁴², core homeostatic genes like *Numb*, *Selplg*, *Siglech*¹¹¹ as well as several ribosomal and Cox genes. Most of the downregulation was driven by differences in the Sham-treated and TBI-induced cells in the M1 and M2 cluster. I also contrasted all 18-month-old mice against all 3-month-old mice and performed a Pearson's product moment correlation between the genes differentially expressed in TBI and those in aging. I found the two gene lists to be highly correlated with a p-value of 1.97e-12 and correlation coefficient (r^2) of 0.6. To see if aging had any specific effect on differential gene expression in the context of TBI, I compared the genes differentially expressed in TBI-induced microglia vs Sham microglia within all 18-month-old and within all 3-month-old mice (Fig. 3C). A good number of genes (312) were commonly differentially expressed in both 18-month-old and 3-month-old mice in the context of TBI. These primarily consisted of canonical markers of microglial activation like *ApoE*, *Spp1*, *Cd74*, *Lyz2* and *H2-D1*^{103,105,106}. About 139 genes were specific to 3-month-old mice when the injured mice were contrasted with the control mice. Ferritin Heavy Chain 1 (*Fth1*) was one of the top

genes by false discovery rate (FDR = 8.84×10^{-9}) in that list, and interestingly showed significant downregulation (FDR < 0.01) in 18-month-old mice when contrasting TBI against Sham. *Fth1* has been previously shown to be a feature of activated microglia participating in iron loading and has shown to surface in other single-cell studies as a feature of microglia reacting to a neurodegenerative stimulus^{103,143}. Other genes like *Olfrl111*¹⁴⁴ and *Prdx1*¹⁴⁵ which have been shown to be expressed in various neurodegenerative models of mice were also uniquely upregulated in the 3-month-old mice induced with TBI, although, ST6 beta-galactoside alpha-2,6-sialyltransferase 1 (*St6gal1*) which has been shown to be downregulated in LPS model of inflammation for microglia, was upregulated¹⁴⁶. A list of all the DEGs in 18-month-old mice with TBI compared to Sham mice, not present in the DEGs for 3-month-old mice in the same context gave a list of 691 genes, a considerable difference from the 139 genes specific to 3-month-old mice (Fig. 3D). Markers of microglial activation and proinflammation like *Lgals3bp*^{103,147}, *Fgf13*¹⁴⁸, *Hk2*¹⁴⁹, *Stat1* were at the top of the list, although *Stat1*, which is a known driver of microglia mediated inflammation¹⁵⁰. *Stat1* was also almost within the adjusted p-value cut-off we had used to define significant differential expression in 3-month-old mice as well. Contrasting 18-month-old with 3-month-old mice within all TBI mice and Sham mice (Fig. 3E), we first explored commonly upregulated genes between the two contrasts to isolate the effects of just aging (FDR < 0.01, $|\log_2FC| > 0.1$). This gave 43 genes including upregulation of *Lrmda*, a little known gene shown to be upregulated in *Lrrk2*-knockout mice (PD mouse model) when compared to wild type¹⁵¹ and which has also been suggested as a microglial marker^{152,153}. Zöller et al. performed a study using immunohistochemistry, fluorescence activated cell sorting (FACS) and RNA isolation to identify genes in aged

mouse cortex. *Ildr2* (expressed in inflamed tissue inhibiting T-cell activity)¹⁵⁴ and *Arhgap15* were both shown to be upregulated as they have in our data as well¹⁵⁵. Members of the Rho-GTPase family and *Sp100* have been previously associated with aging-related effects^{155,156} while *Cd84* and *Ccl12* are genes that have been shown to be active during microglial repopulation in mice after treatment with a *Csf1r* inhibitor¹⁵⁷. Downregulated genes were mostly genes associated with a homeostatic state (*Cst3*, *Numb*, *Siglech*, *Csf1r*) as was expected. 72 genes were specific to aging in mice of the control group. Interestingly, *Fth1* was seen here again as what was down in 18-month-old mice with TBI was up in Sham-treated, aged mice when compared to young, Sham-treated mice. Along with some ribosomal proteins, *Cd63*, *Cst7* and *Cd9*, genes upregulated in “stage II DAM microglia” were also up in control group, aged mice^{103,108}. *Fbrs11*, a gene expressed in human AD microglia of the frontal cortex was also seen¹⁵⁸. Downregulation of some homeostatic genes including *Rnase4*, *Hexb*, *Cx3cr1* and *Tgfbr1*¹⁵⁹ was seen but some genes implicated in microglial inflammatory response were also downregulated including long non-coding RNA *Malat1*¹⁶⁰, pro-inflammatory marker *Cd74*⁹⁸ and *Pld4*¹⁶¹ (associated with phagocytic action of microglia). 184 DEGs were specific to TBI mice when comparing 18-month-old vs 3-month-old mice. The top genes were as expected -markers of inflammation which included MHC class I genes (*H2-D1*, *H2-K1*), *Cd74*, *B2m*, *Ctss*, *Lgals3bp* and *Stat1*. The downregulated genes were mostly a host of ribosomal and Cox- genes along with DAM marker *Aldoc*; *Calm1*, a potassium channel regulator^{162,163} and *Sptbn1*, a housekeeping gene¹⁶⁴.

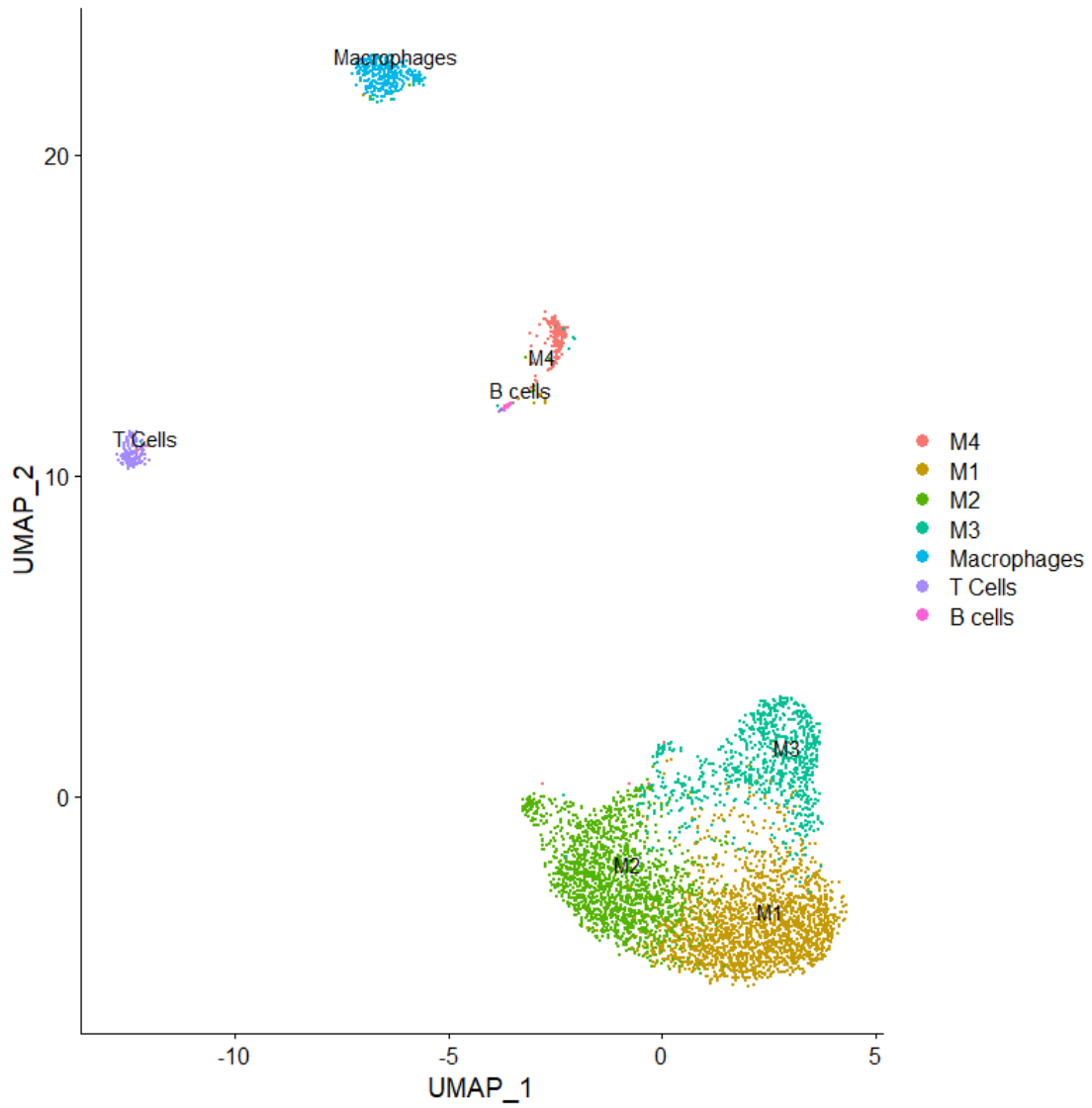


Figure 3A. UMAP of microglial cells from the snRNA-seq experiment showing microglia and parenchymal immune cell populations.

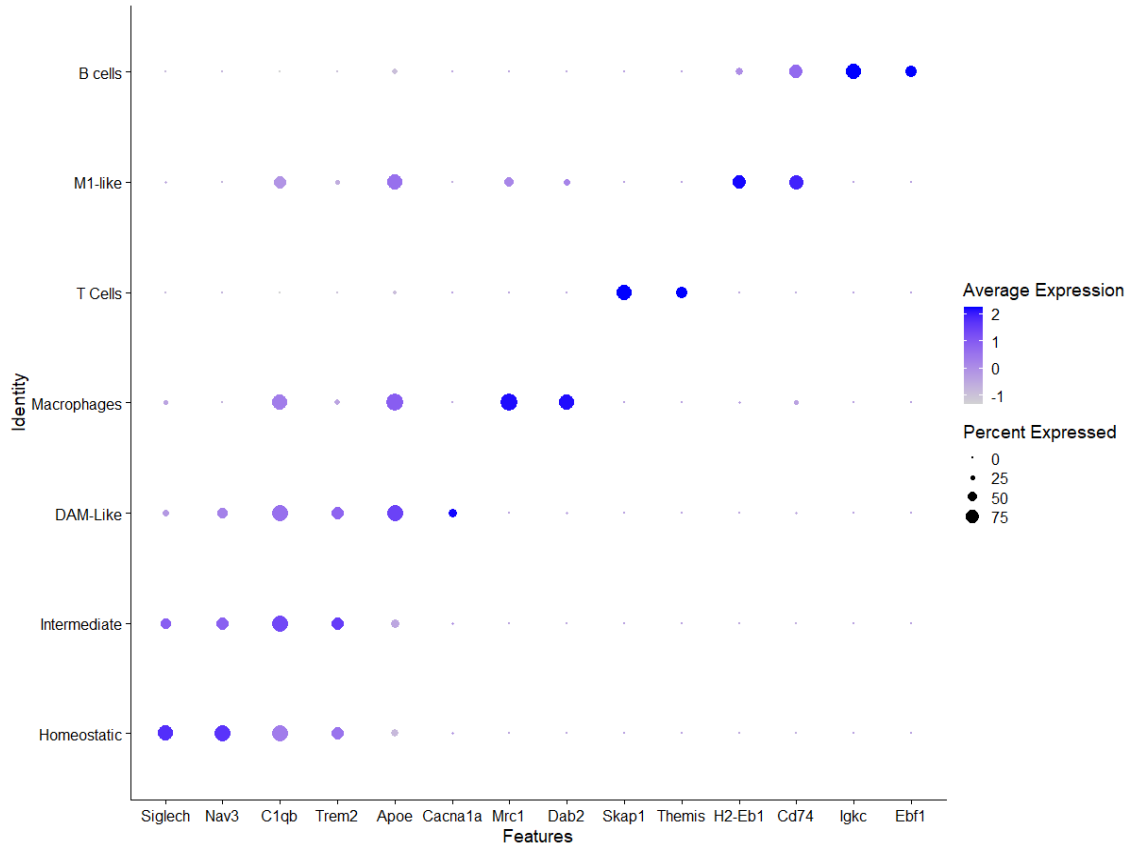


Figure 3B. Dotplot of marker genes observed for the subtypes of microglia.

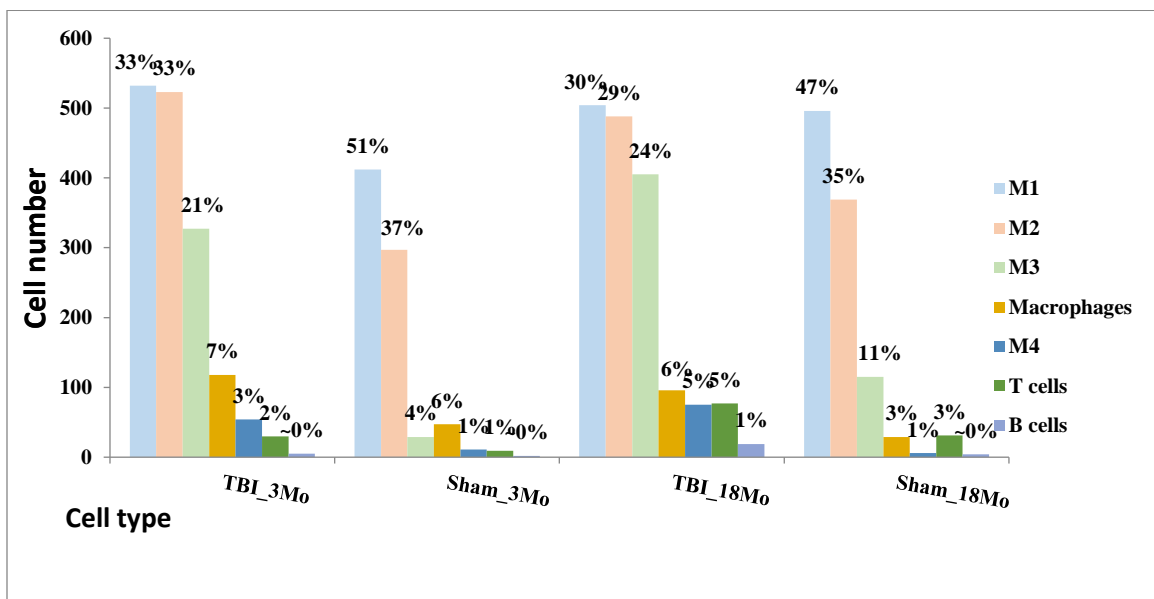


Figure 3C. Cell numbers of immune cell clusters

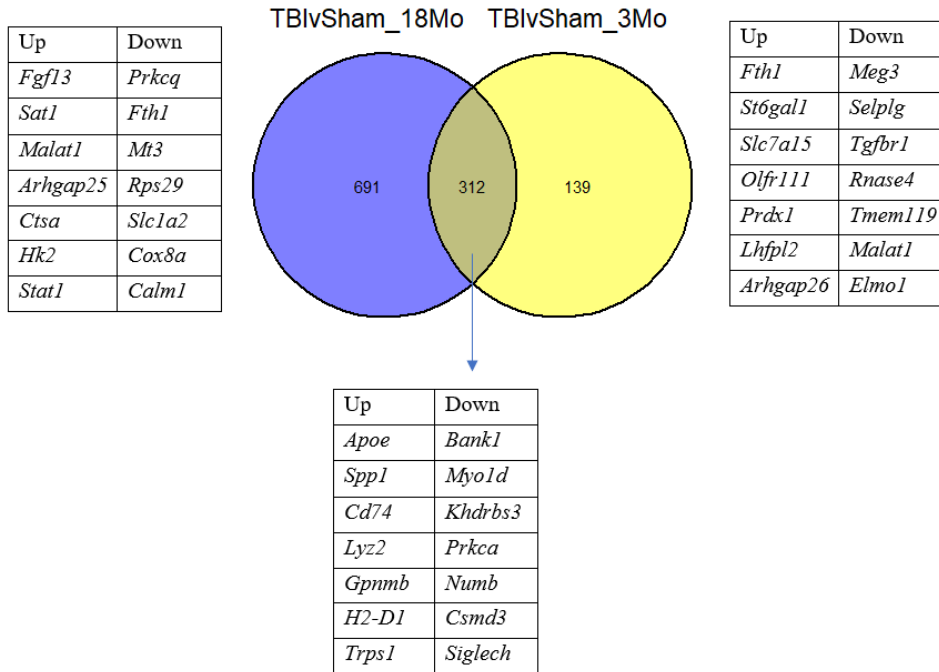


Figure 3D. Venn diagram depicting the number of differentially expressed genes in 18-month-old and 3-month-old mice contrasting TBI against Sham.

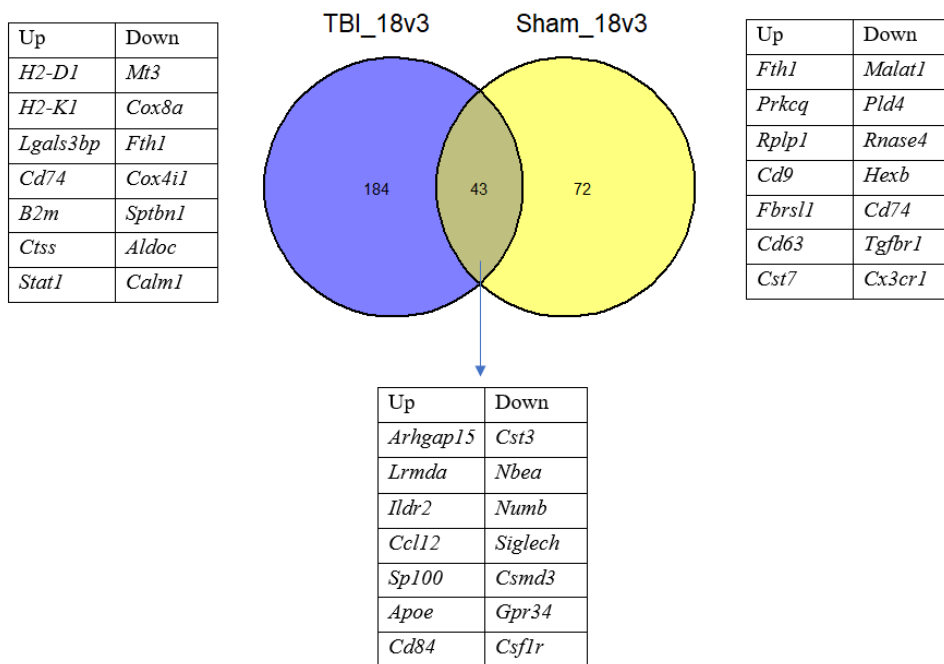


Figure 3E. Venn diagram depicting the number of differentially expressed genes in TBI and Sham mice contrasting 18-month-old against 3-month-old.

In a similar way, we explored differential accessibility from peaks obtained through ArchR's implementation of MACS2. The differential accessibility was calculated using edgeR with the same contrasts using the peak matrix of peaks by cells with peaks annotated through ChIPSeeker. Contrasting just TBI mice with Sham mice gave a list of 21,566 peaks (FDR < 0.01) with 9556 unique annotations. The top annotated peak was *Pde1b*, a distal intergenic peak, which is a known positive regulator of pro-inflammatory response of microglia^{165,166} and a negative regulator of spatial and contextual memory in hippocampus¹⁶⁷. *Cfc1*, a distal intergenic peak was also present which is a member of the epidermal growth factor-Cripto/FRL-1/Cryptic (EGF-CFC) family not implicated in TBI before. *Kdm7a*, a histone-demethylase related gene previously shown to be upregulated in an in vitro microglial model of subarachnoid hemorrhage¹⁶⁸, was also upregulated with a distal peak. Contrasting age, 30,370 peaks were differentially accessible in 18-month-old vs 3-month-old mice. (Fig. 4A). Seeing the differential accessibility specific to age, the DAPs specific to 18-month-old mice by FDR were; *Ncor2*, distal intergenic annotation implicated before in microglial regulation of inflammatory activity and a positive regulator of cognitive function¹⁶⁹⁻¹⁷¹; *Nckap11*, an intronic annotation which is a known participant in the microglial pathogen phagocytosis pathway^{172,173}, among others. *Dnm2* was also found, with both distal intergenic and intronic annotation, a microRNA deregulated in a number of neuropathies¹⁷⁶; *Frdm4a* (distal intergenic), an AD-associated GWAS gene and a regulator of Tau secretion¹⁷⁷; *Sell1*, a highly active gene in malignant gliomas¹⁷⁸ among others. The DAPs specific to 3-month-old mice were a promoter peak annotated to *Tlhc2*, a gene associated with DOOR syndrome which involves intellectual disability¹⁷⁴; *Timm21* (distal intergenic), implicated in being involved in a sex-specific effect of targeting protein

to mitochondria¹⁷⁵; *Ifitm2*, a gene which is a known marker of DAM microglia from previous studies¹⁰³ among others. Age and group specific cross-sectional contrasts also revealed a pattern of more dramatic changes in 18-month-old mice across TBI than 3-month-old mice (Fig. 4B) and also more prominent changes across age in TBI mice than Sham mice (Fig. 4C).

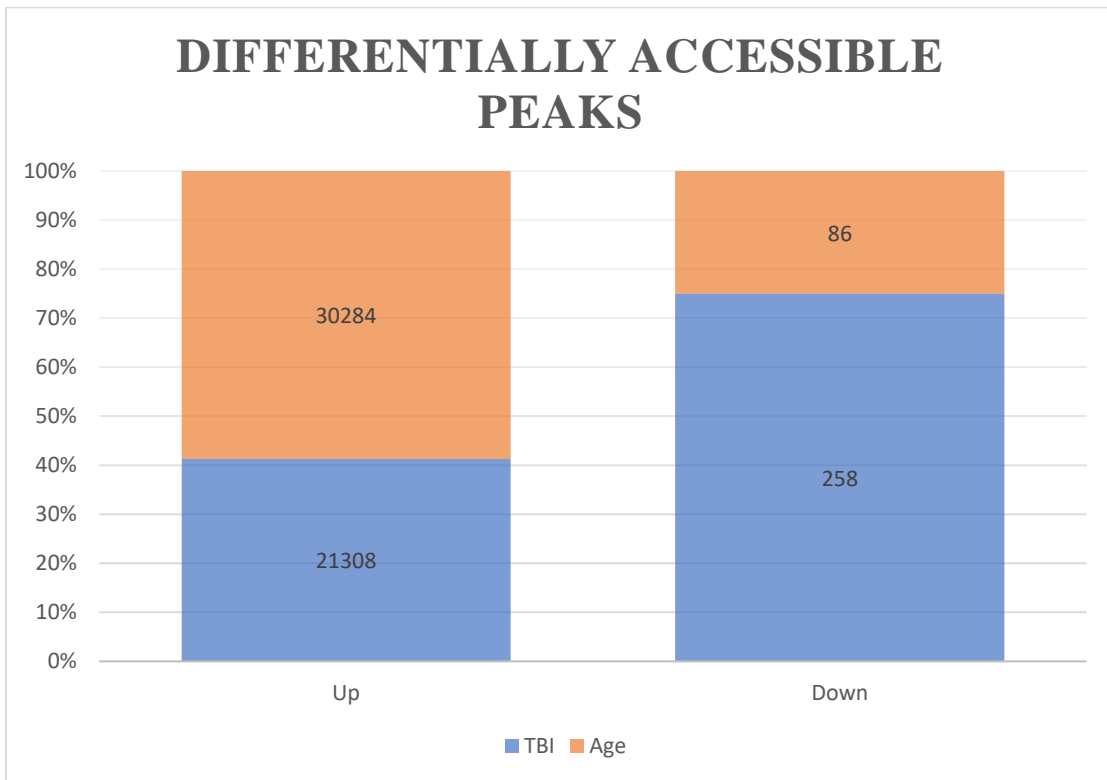


Figure 4A. Number and percentage of differentially accessible peaks by condition and age in microglia

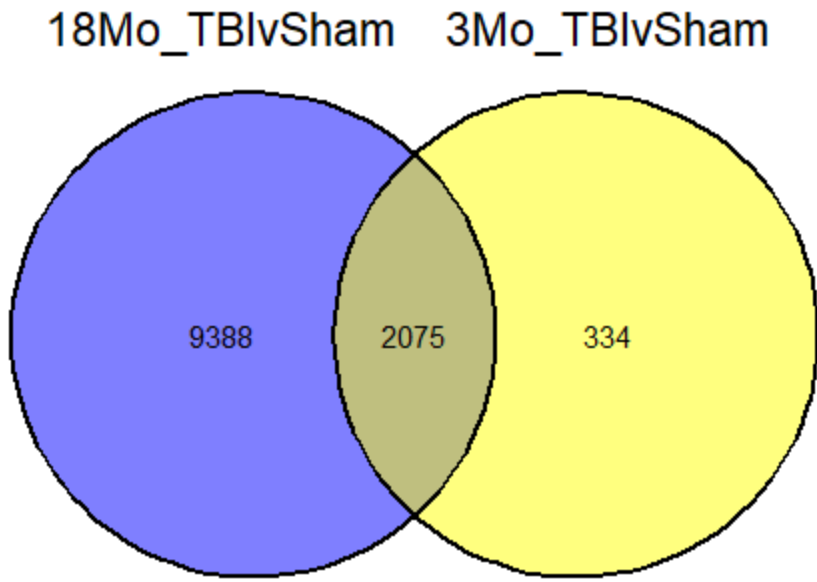


Figure 4B. Venn diagram showing number of DAPs common and unique to 18-month-old and 3-month-old mice in the context of TBI

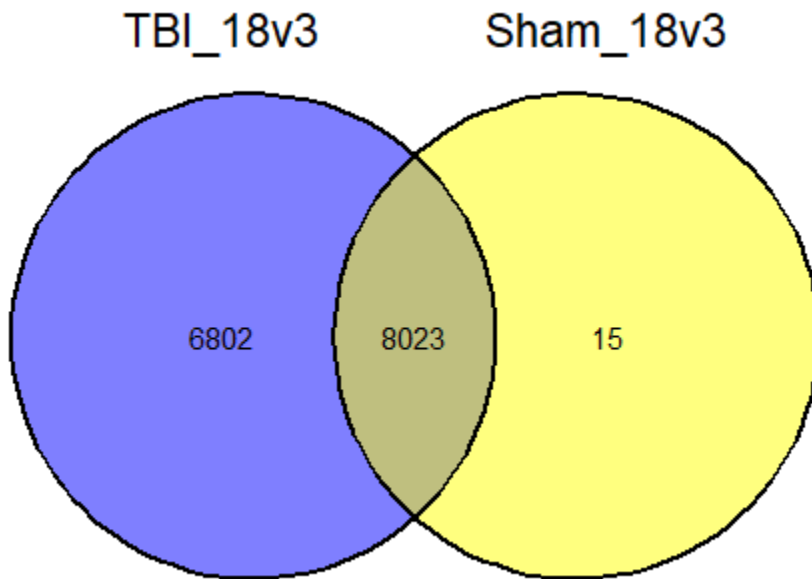
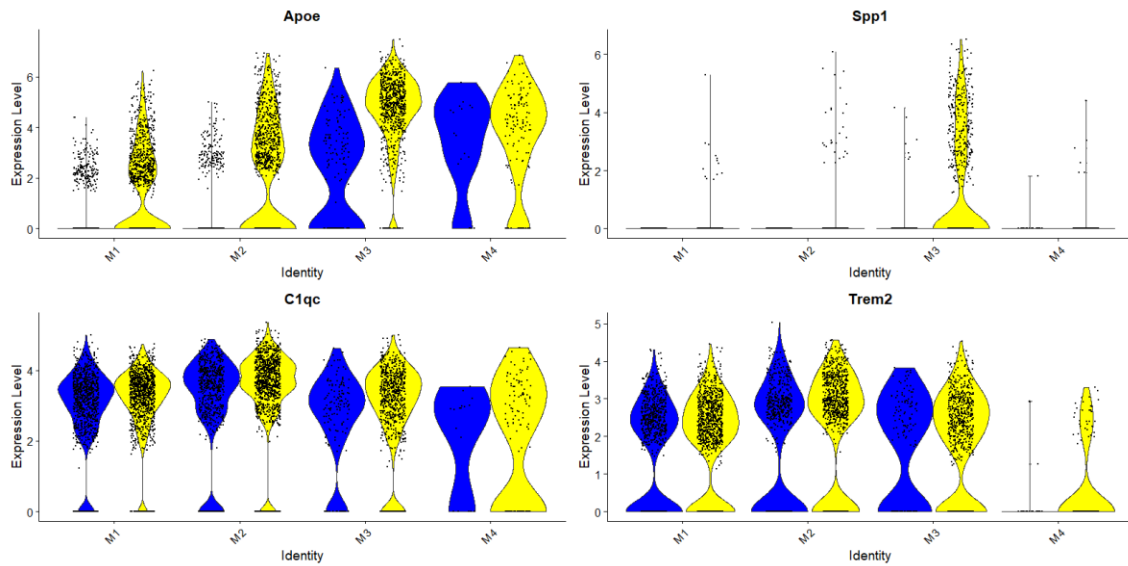


Figure 4C. Venn diagram showing number of DAPs common and unique to TBI-induced and Sham-treated mice in the context of aging

Looking at subtype-type specific gene expression changes, also showed some striking effects (examples given in Fig. 5A). Contrasting TBI vs Sham in M1 cells gave a list of 376 significantly differentially expressed genes (FDR <0.01). Although, most of the genes differentially expressed had a relatively low log fold change, *ApoE* was the at the top of the list with a >2 log fold change. Most of these changes are most likely driven by the M1 state in TBI mice more probable to be in a primed state towards M3 and M4. The list also consisted of Complement component C1q subunit genes, *Trem2*, *H2-D1* among others. The same analysis in M2 cluster gave a list of the 112 genes having half of which were the same genes as in M1 but with higher log fold changes and half were other genes not significant in M1. This half consisting of new genes being downregulated from the change from M1 to M2 with the same contrast were mostly downregulated genes like *Fth1*, *Ttr*, *Malat1*, Ribosomal proteins, *Mt3*, Cox genes among others. The M3 and M4 clusters had low counts of microglial cells in the Sham cluster and the overall global microglial changes driven in the context of TBI were driven by these 2 clusters mostly so that gave us very similar results to our previous lists, as was expected. Looking at the cluster-specific effects of age, we contrasted 18-month-old mice against 3-month-old mice with TBI and Sham respectively and then compared the two lists (examples of genes showing effect in gene expression shown in Fig. 5B). This gave us 24 genes for M1 microglia which were significantly differentially expressed in TBI mice but not in Sham mice which included *Arhgap15*, *H2-D1*, *Mt3*, *B2m*, a phagocytic gene; *Cd244a* which was once described to be exclusive to natural killer and T cells but has been found in microglia as well in recent studies^{179,180}, among others. The same analysis in the M2 cluster gave us 26 genes with some overlap from the M1 cluster like *H2-D1* and *B2m* and others like some Cox and

ribosomal genes, *H2-K1*, *Olf111* and *Aldoc*. For M3 and M4, we contrasted all 18-month-old mice with 3-month-old mice as the proportion of microglia in Sham mice was very low anyway. For M3 microglia, this returned a list of 24 genes with the top ones being *Mamdc2*, a highly upregulated gene in microglia of AD and neurotropic infection mice models¹⁸¹; *Mmp12*, a facilitator of migration of inflammatory reactions by cleaving inflammatory cytokines and chemokines¹⁸² and, *Arhgap15* among others. For M4, this returned only 6 genes with mostly chemokine ligands – *Cxcl9*, *Ccl12* and *Ccl8* along with *Ttr*, *Apod* and



Plxdc2.

Figure 5A. Violin plots of the cluster wise gene expression of genes differentially upregulated in TBI. The yellow plots on the right for each cluster show its expression in TBI mice while the blue plots on the left of each cluster show its expression in Sham mice.

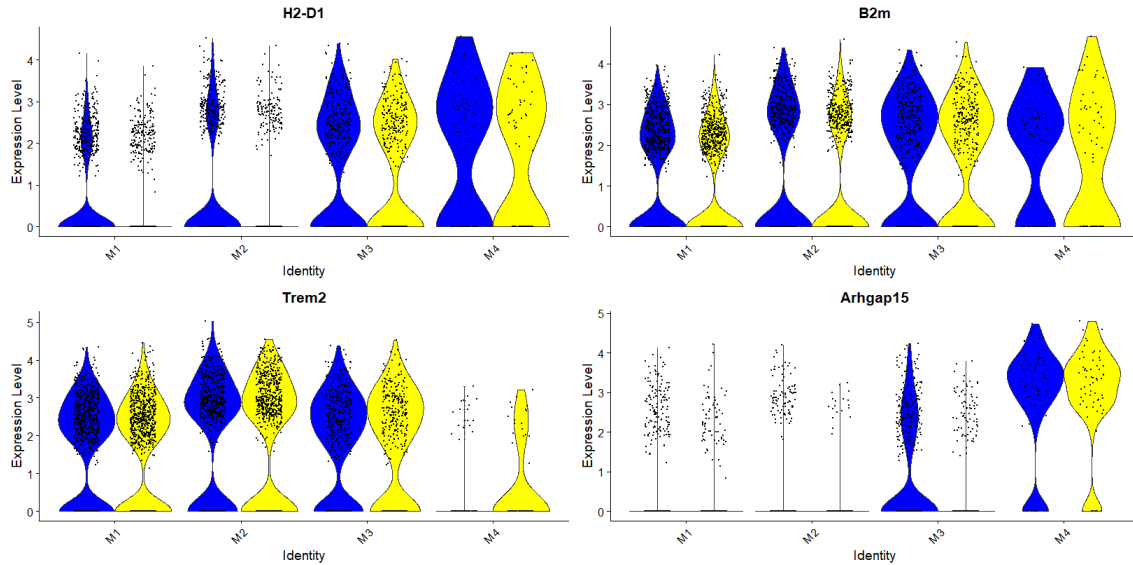


Figure 5B. Violin plots of the cluster wise gene expression of genes differentially upregulated with age. The yellow plots on the right for each cluster show its expression in 3-month-old mice while the blue plots on the left of each cluster show its expression in 18-month-old mice

3.3 Pseudotime trajectory construction and analysis

I used Monocle¹³¹ to track the trajectory of microglial activation through various subtypes. When using just Monocle2 with the raw counts matrix from the snRNA-seq microglia (M1, M2, M3 and M4), the trajectory showed an initial starting point consisting of mostly M1 and some M2 cells as well, with the trajectory slowly graduating to have more M2 cells and then diverging into two separate trajectories – one branch having primarily M3 microglial cells and the other branch having all the M4 cells clustered along the end. (Fig. 6A and 6B)

I also looked at genes that change in expression with pseudotime using Branched Expression Analysis Modelling (BEAM) (Fig. 6C). Simultaneously looking at changes in gene expression in each experimental group, *Clqa*, which shows upregulated expression

in M2, showed downregulation in M4 but maintained similar levels of expression in M3. This gene did not show any significant difference with respect to age but a clear upregulation when comparing TBI mice against control mice. *Trem2*, another marker of the M2 cluster which shows clear upregulation in M2, showed downregulation in both pathological phenotypes – M3 and M4. Interestingly, when looking at M2 specific DEGs, contrasting all 18-month-old mice in the context of TBI, revealed no differential expression while there was significant differential expression in young mice subjected to TBI. *Cacna1a*, a P/Q-type voltage gated Ca^{2+} channel, mutations in which cause a cluster of neurodegenerative disorders¹⁸³ and which was also found upregulated in prefrontal cortex microglia in a mice model of alcohol dependence¹⁸⁴, showed significant upregulation in 3-month-old M3 microglia in the context of TBI but non-significant in M3 microglia of 18-month old mice. *Myo1e*, a phagocytosis-related gene in microglia which has been shown upregulated in an anti-inflammatory subset of DAM-like microglia also showed M3-specific upregulation in TBI-induced mice although did not reveal any significant differences with age. *Myo5a*, another gene associated with lysosomal activity and intracellular trafficking showed concurrent upregulation in both M3 and M4 microglia, showed significant upregulation in 18-month-old mice but not in 3-month-old mice when comparing TBI against Sham (Fig 6D, 6E and 6F).

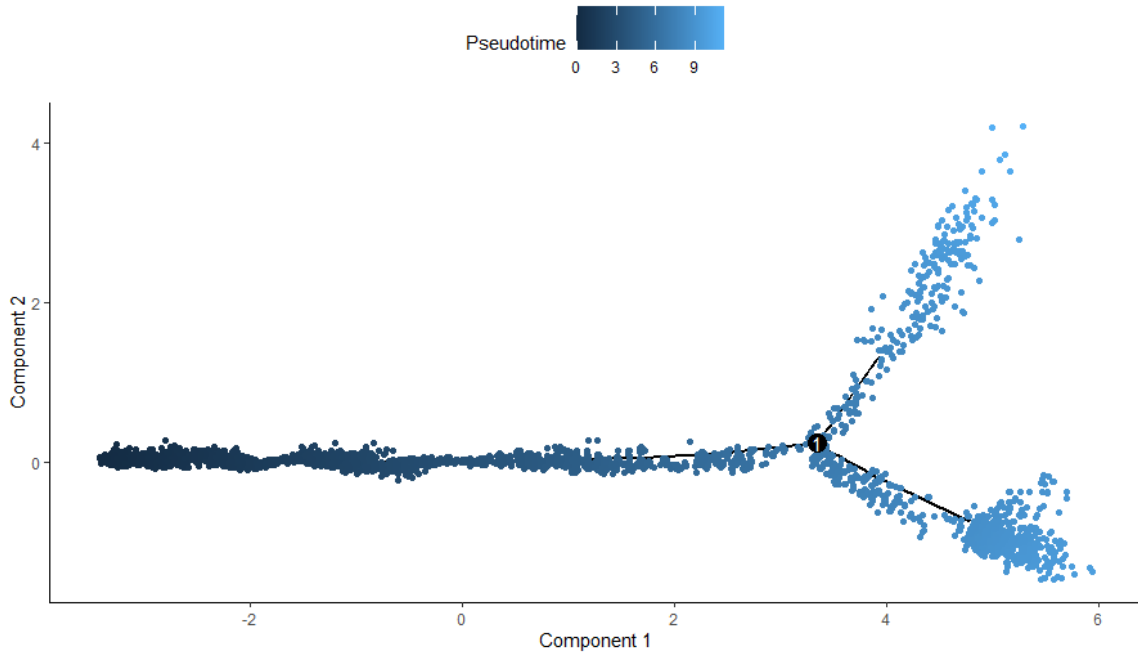


Figure 6A. Cells arranged along a trajectory showing pseudotime.

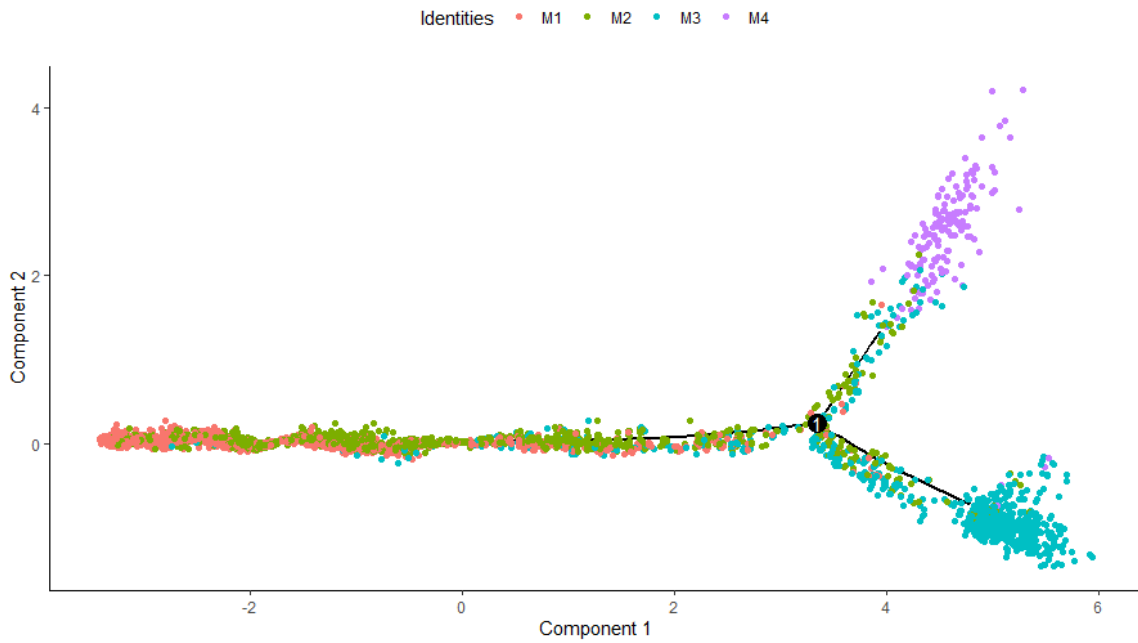


Figure 6B. Cells arranged along a trajectory showing the arrangement of different clusters of microglia along the branches.

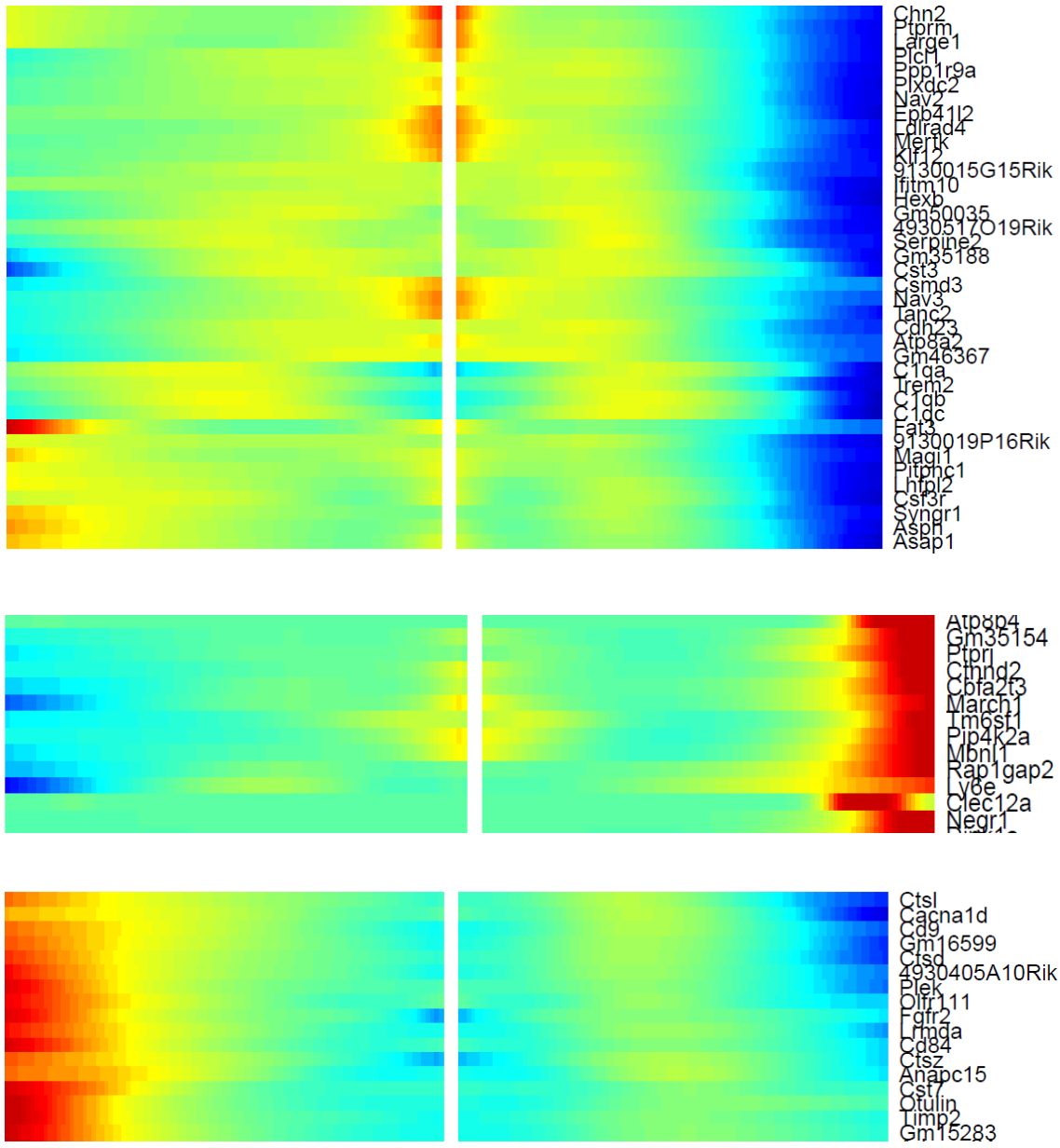


Figure 6C. Important areas of the heatmap generated from BEAM analysis. The branch from the middle to the left shows the expression pattern of genes in M3 microglia while the branch going from the middle to the right is showing the same for M4 microglia

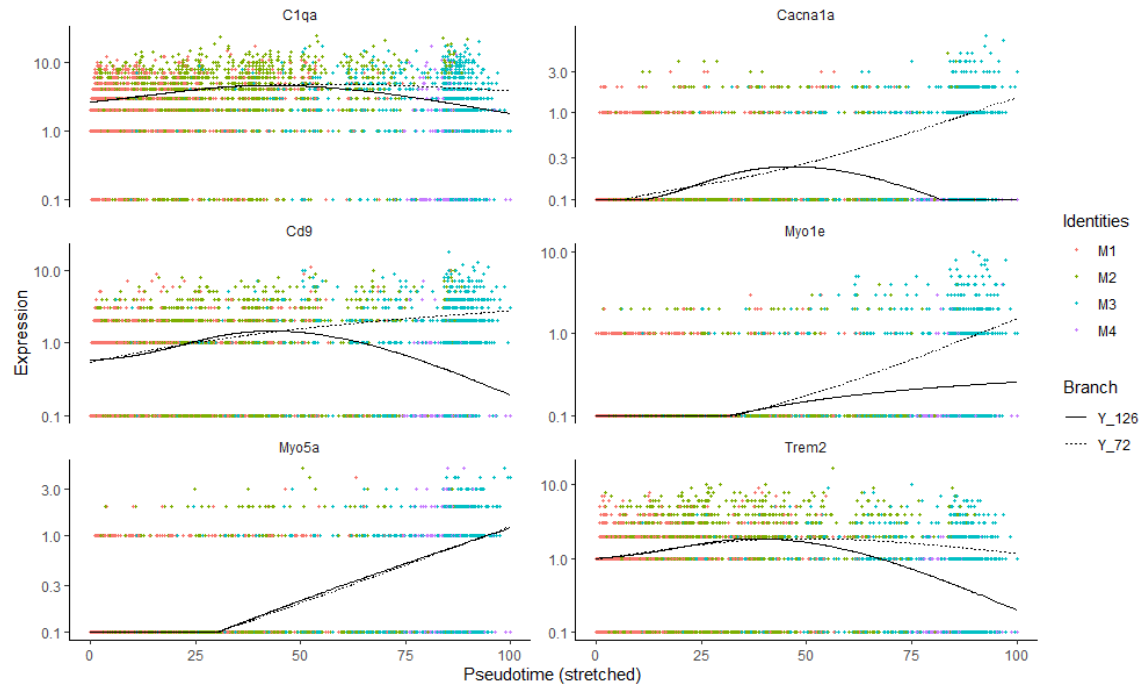


Figure 6D. Plots showing the pattern of expression along the branches of the trajectory. The dotted line shows the trajectory branching into a cluster of M3 cells and the solid line shows the branch with M4 cells clustered at the end

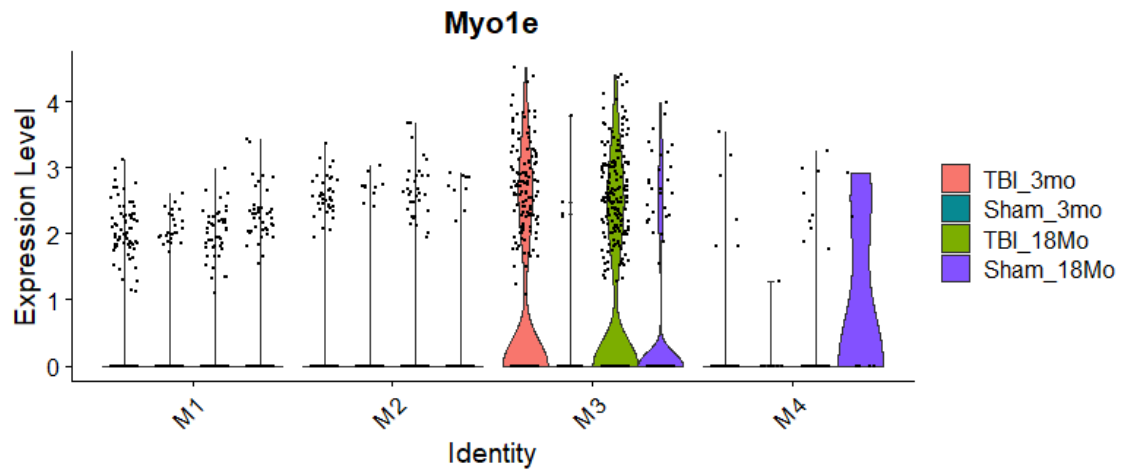


Figure 6E. Expression pattern of genes in each experimental group that show change with pseudotime

Figure 6E continued

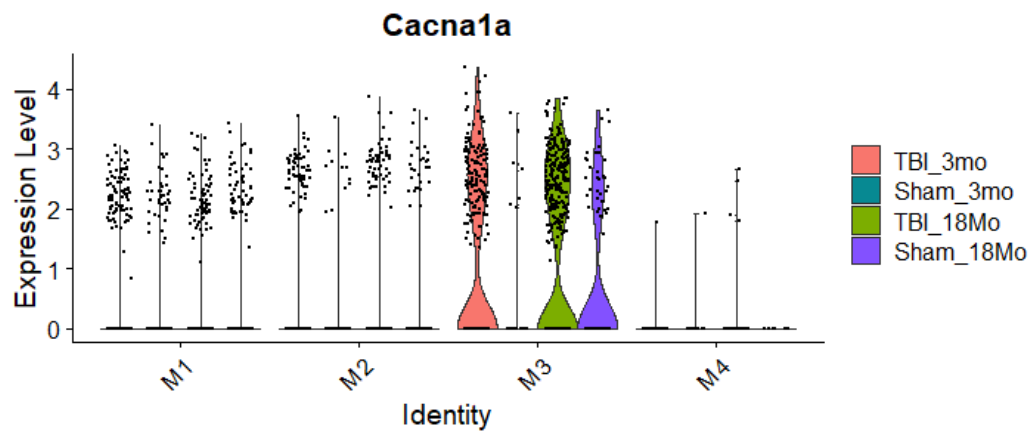
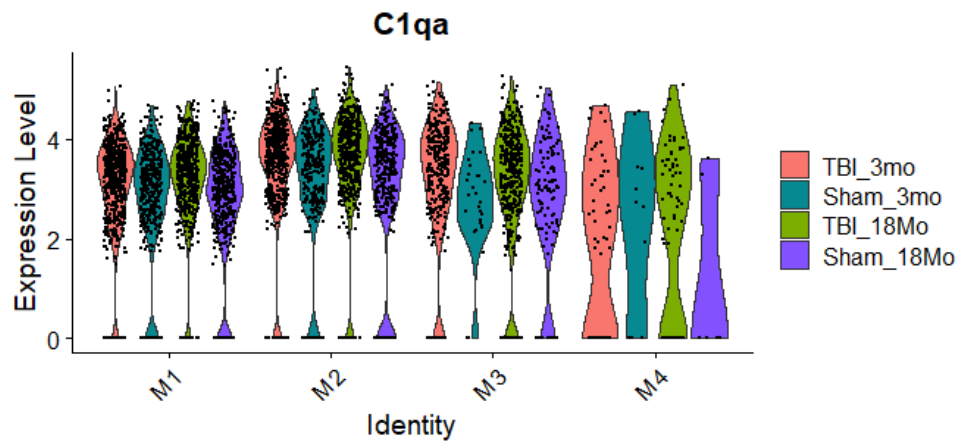
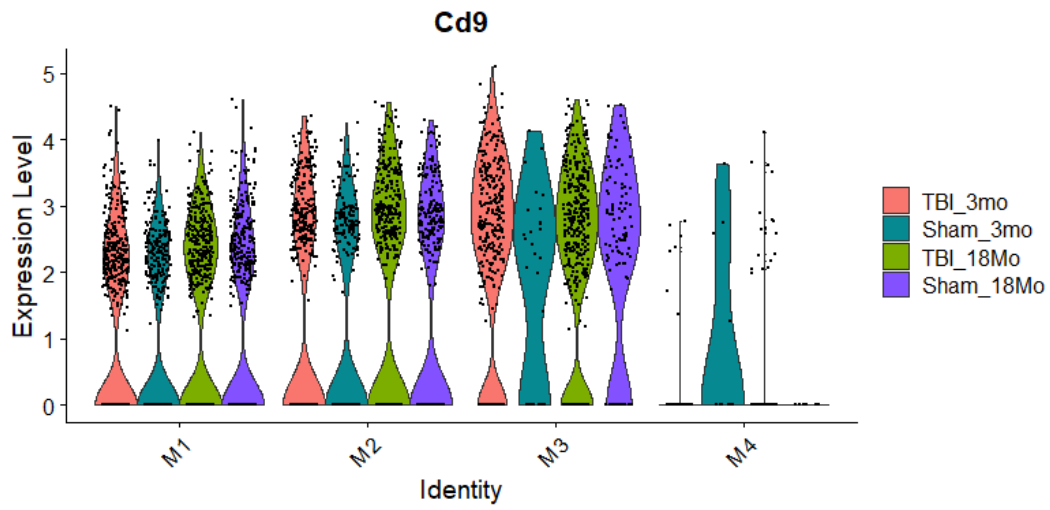
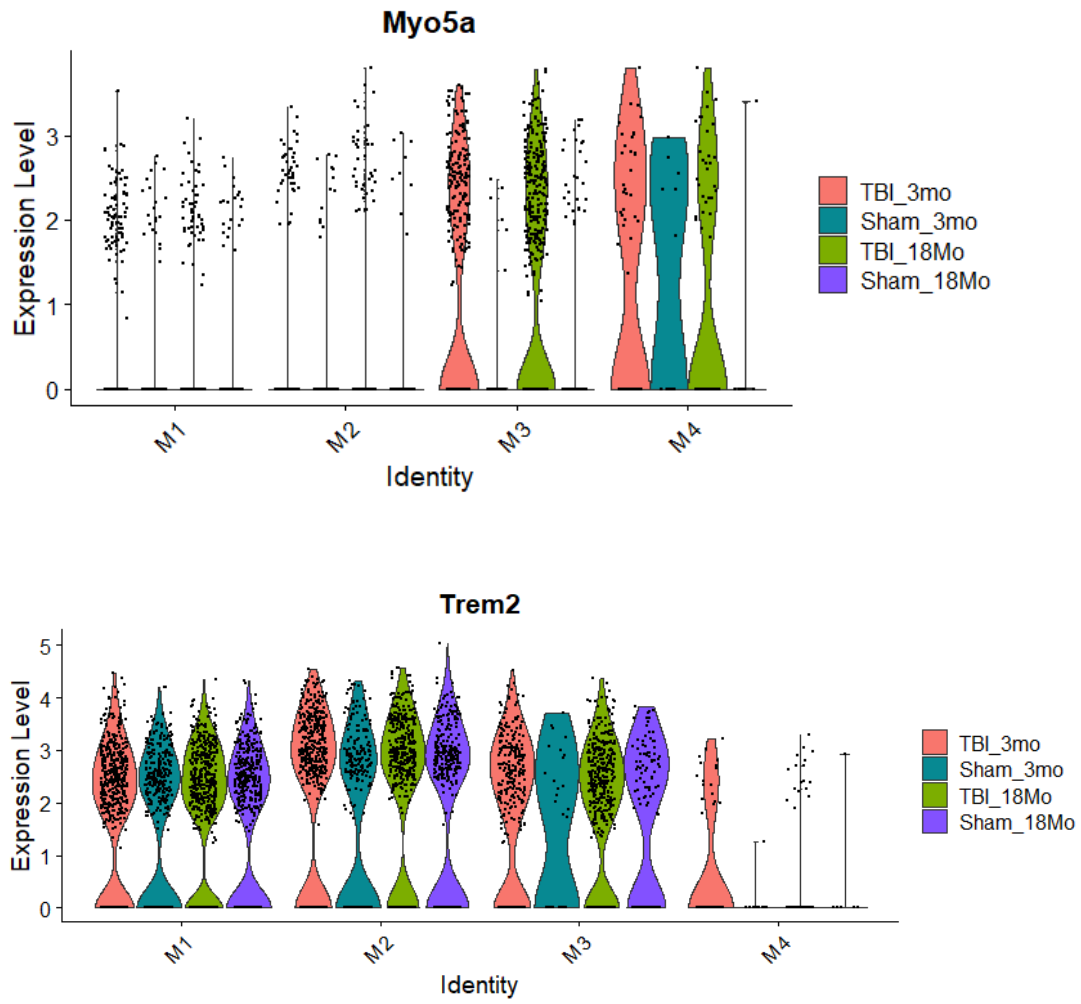


Figure 6E continued



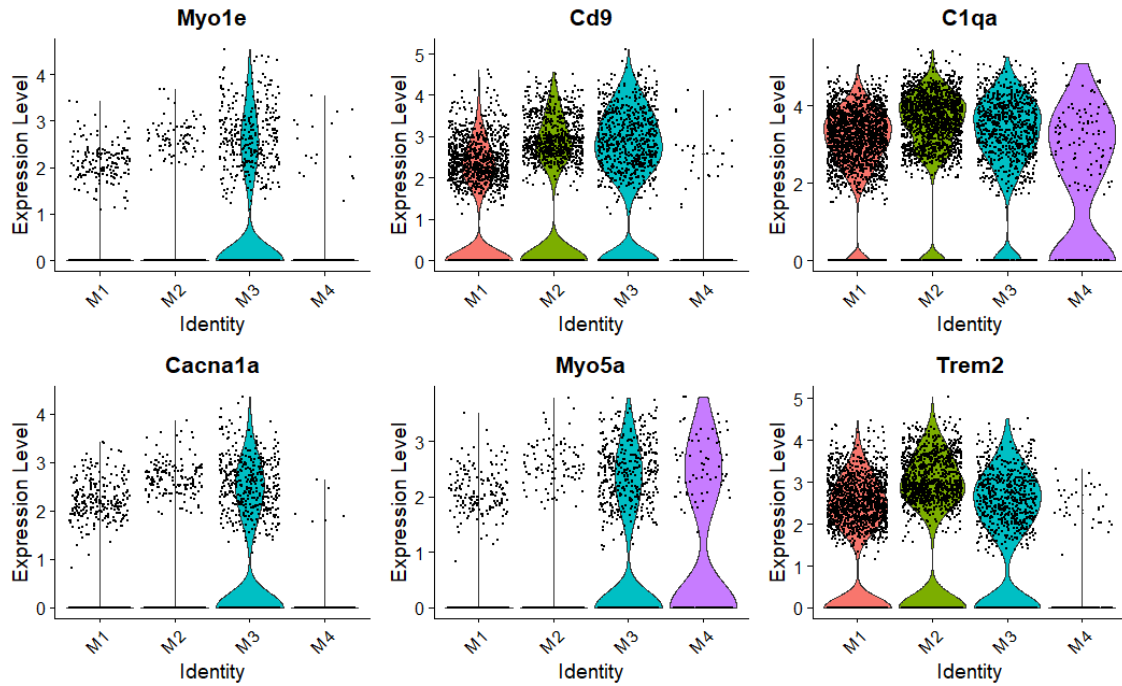


Figure 6F. Expression pattern of genes in each cluster that show change with pseudotime

3.4 Integration of snRNA-seq and snATAC-seq data

Using the cell barcodes from ArchR's characterization of global cell types, the cells were subsetted out of the raw fragments file from cellranger-atac aggr output and integrated with raw counts matrix of the microglia from the snRNA-seq experiment using LIGER. After cleanup, I clustered the combined cells into separate subtypes which returned 3 clusters with microglial cells and 2 of T-cells and B-cells, respectively (Fig. 7A). The cells from snRNA-seq and snATAC-seq converged homogenously across the clusters (Fig. 7B).

We reconstructed a gene regulatory network model leveraging data from both snRNA-seq and snATAC-seq experiments using GENIE3. For this, peaks were annotated to genes using ChIPSeeker. Then, peak specific transcription factor motif annotations were used from ArchR's implementation of ChromVAR and combined into a dataframe having

peaks, motif and gene annotations along with co-accessibility scores. Expression data from the snRNA-seq was smoothed before integrating with the data from the snATAC-seq experiment. The top 50,000 links from the GENIE3 output were subsetted and an enrichment analysis of the targets was performed against the differentially expressed genes in TBI against Sham. This gave a list of 19 transcription factors that were either activating or repressing with top ones being *Nfe2l2*, a well-known transcription factor being involved in neuroprotective processes after inflammatory stimuli^{185,186}. The genes most strongly correlated to be activated by *Nfe2l2* consisted of genes expressed more in M3 cluster relative to the other clusters, for ex. *Ifi207*, *Lyz2*, *Fmnl2*, *Lilrb4a*, and *Spp1* among others. Repressing targets of *Nfe2l2* were *Cst3*, *Malat1*, *Csmd3*, *Selplg* and *Ly6e*. *Runx1* was another transcription factor found in this list well characterized to be involved in microglial activation, proliferation and anti-inflammatory to pro-inflammatory conversion^{187–189}. Some target genes of this factor *Celf2*, a known regulator of *Trem2* expression, *Gab2*, *Mitf*, *Lrmda* and Rho-GTPase activating proteins which were differentially expressed in different age-based contrasts. *Tcf12*, a transcription factor found upregulated in microglia of high-grade human glioma samples¹⁹⁰. Activating activity was associated with targets like *Slc9a9*, a gene associated with autism, *Inpp4b*, *Myo5a* and *Exoc4* among others. Negative regulatory activity was targeted towards genes like *Cst3*, *Malat1*, C1 complement genes, *Hexb*, *Slc2a5* and others (Bonferroni corrected p-value < 0.05) (Supplementary Table 3). Expression levels of the regulatory factors described above are showed in Fig. 7C.

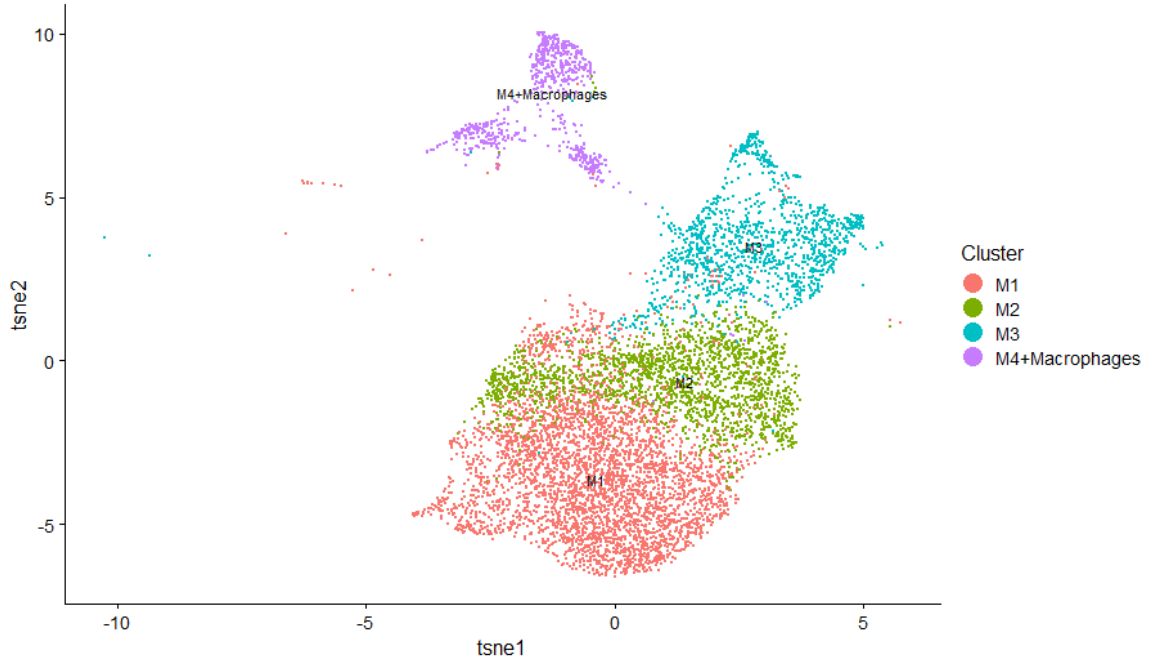


Figure 7A: Clusters of microglia annotated according to the same annotation as the one used for snRNA-seq represented here in a 2D space through a UMAP plot

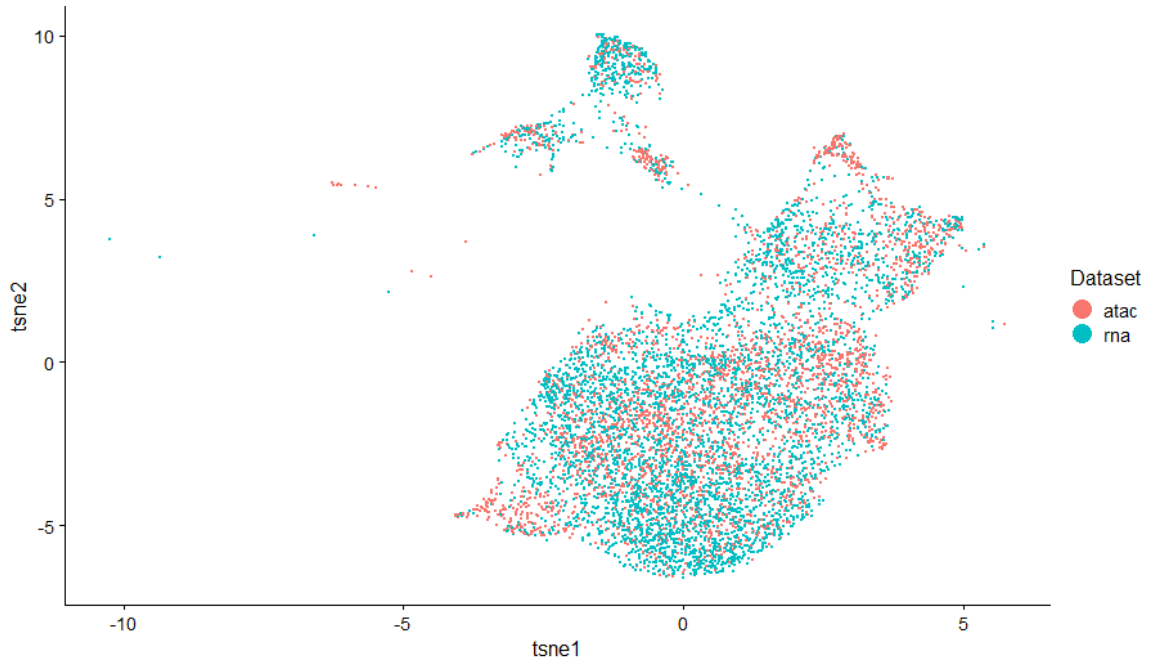


Figure 7B. UMAP plot showing convergence of cells from snATAC and snRNA-seq across clusters

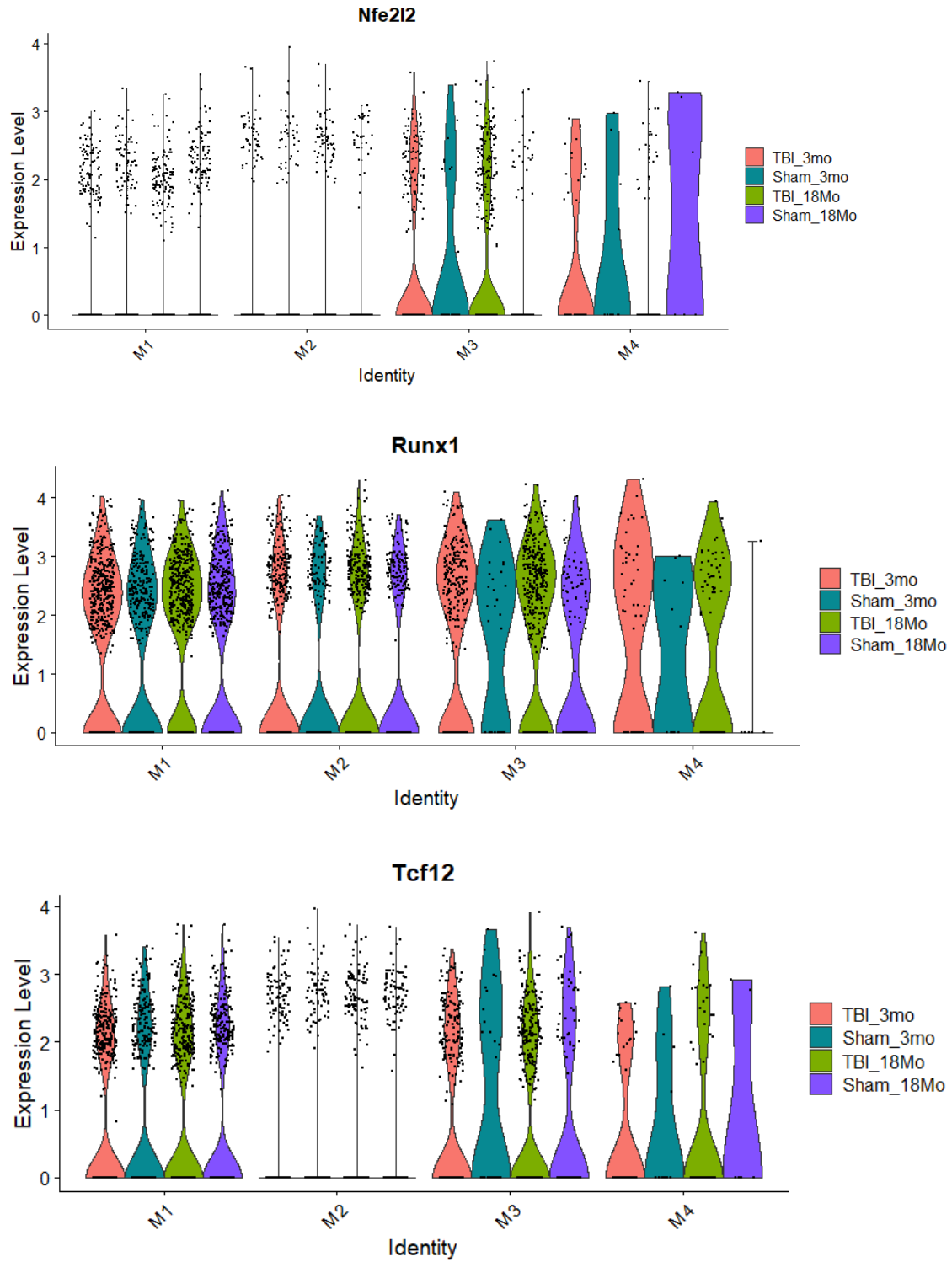
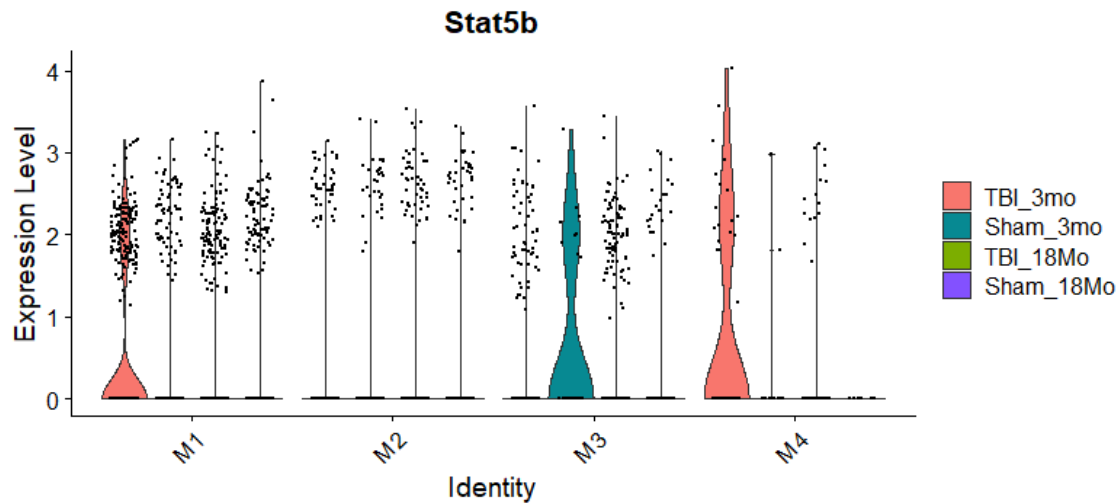


Figure 7C. Gene expression patterns of major regulatory factors observed in the GRN

Figure 7C continued



4. DISCUSSION

In the present study, we have profiled an atlas of cell types present in mice hippocampus using both snRNA-seq and snATAC-seq. We were able to identify 16 cell types using just the snRNA-seq and 13 cell types using the snATAC-seq data. Population numbers showed patterns indicative of phenotypic function. Microglial cells clearly increased in number in a pathological state – showing a 72% increase on exposure to TBI while aged mice showed an increase of 14% in cell numbers in the snRNA-seq dataset. Oligodendrocytes on the other hand, showed a bigger increase in numbers with age, which is consistent with what is known in the field¹⁹¹. CA1 neurons showed a 22% decline with the induction of TBI and an 8% increase with age. Other clusters like astrocytes showed a mixed response as well showing a 20% decrease in TBI but a 6% decrease with aging. While these numbers do not pre-empt a definite conclusion, it is indicative of an exacerbated immune response in injury and aging.

Looking more closely at microglia, we were able to confirm the presence of a unique microglial population of cells in response to TBI with an expression profile very similar to previously characterized DAM microglia/MGnD microglia. This population is distinct from the classical “pro-inflammatory M1” microglia which were also observed in our dataset. Differential gene expression analysis showed a strong effect of TBI increasing the expression of many genes associated with a strong immune response in the brain. We also saw multiple ways in which aging itself had an effect and how it changed the transcriptional response with respect to injury. Overall, we observed a high correlation between the genes differentially expressed in TBI and aging (p-value $\ll 0.001$, $r^2 = 0.6$). *Fth1*, a gene encoding the heavy subunit of Ferritin, which is a protein expressed in microglia is responsible for iron metabolism in the brain. Although it has been shown in a previous study of marmosets that aged brains (hippocampal tissue) have lower ferritin positive microglia may preclude neurodegeneration as a result of increased RNA oxidation, iron accumulation and dystrophic, but “M2 anti-inflammatory” like profile¹⁹², our study showed an increased expression of *Fth1* in aged control mice but a strong decrease in expression if the mice were induced with TBI, contrasting aged mice with young mice, meaning an increased expression in young mice induced with TBI. Ferritin has also been shown to be expressed in DAM microglia. This shows a complex pathology involving the iron metabolism pathway, showing that an anti-inflammatory but dystrophic phenotype is induced in 3-month-old mice but not in 18-month-old mice which might be correlated with poorer repair processes in aged mice induced with TBI. This is also most likely a function of early DAM-like microglia, with the M2 cluster showing the highest expression of *Fth1*, followed by M3 cluster.

While we observed an expected downregulation of known markers of “homeostatic” microglia in both contexts of TBI and aging, there were some specific response genes upregulated uniquely in either case. For example, *Lgals3bp*, the binding protein for Galectin-3 a protein that binds to β -galactoside residues previously found to be expressed in reactive microglia^{104,193} was found upregulated specifically in TBI-induced, aged mice in our study. Both Galectin-3 (*Lgals3*) and *Lgals3bp* were marker genes in the M3 cluster and the former is also a *Trem2* ligand¹⁹⁴. Interestingly, *Trem2*, a very important receptor surfacing in multiple studies was not found to be differentially expressed with age but only on the induction of TBI. *Cd74*, a class II MHC molecule has been shown to be a marker for “M1 pro-inflammatory” microglia (cluster M4 in our study). Other than antigen presentation, *Cd74* is also a receptor binding site for macrophage inhibition inhibitory factor (MIF), through which immunochemotactic of microglia is promoted triggering inflammatory responses¹⁹⁵. This gene was found to be specifically upregulated in TBI exposed mice when comparing aged mice with young but downregulated in control group when comparing with the same contrasts.

We explored cluster-specific differential gene expression, expecting to find cell types driving this differential response in young and aged mice. The M2 cluster is particularly of interest as it shows upregulation of C1q genes, *Trem2*, *H2-D1*, *Cd81* and *Hexb* and a slight downregulation of some homeostatic genes like *Csmd3*, *Siglech* and *Nav3*. The 18-month-old mice did not express *Trem2* differentially in this cluster when comparing expression in TBI mice with Sham mice. The transcriptional profile of this cluster seems to match with a cluster identified in another study using an AD mouse model (cluster 8)¹⁹⁶. This cluster is proposed by us to be an intermediate cluster of cells between M1 microglia with the

homeostatic signature and the DAM/MGnD-like M3 microglia, given its simultaneous downregulation and upregulation of genes associated with homeostatic function of microglia and a slightly similar profile with “stage I DAM microglia”. M3 microglia showed a more drastic shift in expression with clear downregulation of most homeostatic genes and an upregulation of several immune response/repair/inflammation associated genes like *Spp1*, *ApoE*, *Gpnmb*, *Cst7*, *Lpl* among others. This transcriptional profile has been characterized in multiple mouse models in multiple single-cell/nucleus studies. What was of particular interest here is to see the difference with respect to age in this cluster to see its response in aged vs young mice. 2 genes came at the top being strongly downregulated – *Mamdc2* and *Mmp12*. *Mamdc2* is a gene very recently shown to regulate immune response to viral infections¹⁹⁷. It has also been shown in single cell studies using AD and aging have found downregulation of *Mamdc2*¹⁹⁸. We also noted that even though *Mamdc2* was strongly downregulated when comparing with respect to age, it was actually upregulated in TBI mice. Contrasting M3 cells of TBI mice with Sham mice of just the 18-month-old mice actually still showed upregulation of *Mamdc2* but changing the contrast to 18-month-old vs 3-month-old in just the TBI mice again showed a very strong downregulation suggesting that both 3-month-old and 18-month-old mice had some expression of *Mamdc2*, but the 3-month-old mice upped the expression of this gene on exposure to TBI. Research has shown that *Mmp12* might be upregulated in the brain during normal aging, which was confirmed with the few DAM cells in Sham-treated mice showing an increased expression with respect to age. This is flipped completely in the opposite direction when mice are induced with TBI. It has been suggested that aging associated neuroinflammation is enhanced because of *Mmp12* by facilitating the recruitment of Bone

Marrow microglia¹⁹⁹. This gene has not yet been explored in the context of neurodegenerative diseases and is a novel potential target showing a complex interaction with external stimuli and age. Further investigation may yield results, although it is worth mentioning that both of these transcripts were detected at very low levels in our single-nucleus sequencing assays. M4 cells were not detected in enough numbers to show a significant difference.

Hub TFs which were the strongest activators or repressors of differentially expressed genes were revealed by constructing the gene regulatory network. *Nfe2l2*, was also differentially expressed in the context of TBI in 18-month-old mice but not in 3-month-old mice. We suggest that this transcription factor might be responsible for the exaggerated response seen in older populations and might be considered as a part of a targeted therapy. *Runx1*, also showed upregulation in TBI microglia although in a celltype specific manner with significant effects being seen in M1 and M3 phenotype. This transcription factor might be responsible for the exaggerated downregulation of homeostatic signature seen in older mice as we observed significant values in both 18-month-old and 3-month-old mice with slightly higher fold change in 18-month-old mice within M1 microglia. Only 18-month-old mice showed an upregulation of *Runx1* in the M3 cluster. *Stat5b* on the other hand showed upregulation in 3-month-old mice in the context of TBI in M1 microglia only, suggesting a role in neuroinflammatory response in young mice.

Further analysis, especially using the snATAC-seq data looking into cell-type specific differential accessibility, motif footprinting and looking beyond the hub TFs from the gene regulatory network will be conducted. We expect to gain a deeper understanding of the regulators of gene expression seen in the snRNA-seq data. Future studies may also include

capture of the transcriptome and the epigenome at the single cell level at different time points post-injury to confirm the trajectory of microglial function across different age groups.

REFERENCES

1. GBD 2016 Traumatic Brain Injury and Spinal Cord Injury Collaborators. Global, regional, and national burden of traumatic brain injury and spinal cord injury, 1990-2016: a systematic analysis for the Global Burden of Disease Study 2016. *Lancet Neurol.* 2019;18(1):56-87. doi:10.1016/S1474-4422(18)30415-0
2. Dijk JTJM van, Dijkman MD, Ophuis RH, Ruiters GCW de, Peul WC, Polinder S. In-hospital costs after severe traumatic brain injury: A systematic review and quality assessment. *PLoS ONE.* 2019;14(5). doi:10.1371/journal.pone.0216743
3. Surveillance Report of Traumatic Brain Injury-related Emergency Department Visits, Hospitalizations, and Deaths. :24.
4. Ozga JE, Povroznik JM, Engler-Chiurazzi EB, Haar CV. Executive (dys)function after traumatic brain injury: special considerations for behavioral pharmacology. *Behav Pharmacol.* 2018;29(7):617. doi:10.1097/FBP.0000000000000430
5. Plassman BL, Havlik RJ, Steffens DC, et al. Documented head injury in early adulthood and risk of Alzheimer's disease and other dementias. *Neurology.* 2000;55(8):1158-1166. doi:10.1212/wnl.55.8.1158
6. Zgaljardic DJ, Seale GS, Schaefer LA, Temple RO, Foreman J, Elliott TR. Psychiatric Disease and Post-Acute Traumatic Brain Injury. *J Neurotrauma.* 2015;32(23):1911-1925. doi:10.1089/neu.2014.3569
7. Skandsen T, Kvistad KA, Solheim O, Strand IH, Folvik M, Vik A. Prevalence and impact of diffuse axonal injury in patients with moderate and severe head injury: a cohort study of early magnetic resonance imaging findings and 1-year outcome: Clinical article. *J Neurosurg.* 2010;113(3):556-563. doi:10.3171/2009.9.JNS09626

8. Schmidt OI, Infanger M, Heyde CE, Ertel W, Stahel PF. The Role of Neuroinflammation in Traumatic Brain Injury. *Eur J Trauma*. 2004;30(3):135-149. doi:10.1007/s00068-004-1394-9
9. Ng SY, Lee AYW. Traumatic Brain Injuries: Pathophysiology and Potential Therapeutic Targets. *Front Cell Neurosci*. 2019;13. Accessed January 29, 2022. <https://www.frontiersin.org/article/10.3389/fncel.2019.00528>
10. Saatman KE, Duhaime AC, Bullock R, Maas AIR, Valadka A, Manley GT. Classification of Traumatic Brain Injury for Targeted Therapies. *J Neurotrauma*. 2008;25(7):719-738. doi:10.1089/neu.2008.0586
11. Maas AIR, Peul W, Thomé C. Surgical decompression in acute spinal cord injury: earlier is better. *Lancet Neurol*. 2021;20(2):84-86. doi:10.1016/S1474-4422(20)30478-6
12. Chesnut RM, Marshall LF, Klauber MR, et al. The role of secondary brain injury in determining outcome from severe head injury. *J Trauma*. 1993;34(2):216-222. doi:10.1097/00005373-199302000-00006
13. Dash HH, Chavali S. Management of traumatic brain injury patients. *Korean J Anesthesiol*. 2018;71(1):12-21. doi:10.4097/kjae.2018.71.1.12
14. Girgis F, Pace J, Sweet J, Miller JP. Hippocampal Neurophysiologic Changes after Mild Traumatic Brain Injury and Potential Neuromodulation Treatment Approaches. *Front Syst Neurosci*. 2016;10. Accessed January 21, 2022. <https://www.frontiersin.org/article/10.3389/fnsys.2016.00008>
15. Dorsett CR, McGuire JL, DePasquale EAK, Gardner AE, Floyd CL, McCullumsmith RE. Glutamate Neurotransmission in Rodent Models of Traumatic Brain Injury. *J Neurotrauma*. 2017;34(2):263-272. doi:10.1089/neu.2015.4373
16. D'Ambrosio R, Maris DO, Grady MS, Winn HR, Janigro D. Impaired K⁺ Homeostasis and Altered Electrophysiological Properties of Post-Traumatic Hippocampal Glia. *J Neurosci*. 1999;19(18):8152-8162. doi:10.1523/JNEUROSCI.19-18-08152.1999
17. Hablitz JJ, Langmoen IA. Excitation of hippocampal pyramidal cells by glutamate in the guinea-pig and rat. *J Physiol*. 1982;325:317-331.
18. Arundine M, Tymianski M. Molecular mechanisms of calcium-dependent neurodegeneration in excitotoxicity. *Cell Calcium*. 2003;34(4-5):325-337. doi:10.1016/s0143-4160(03)00141-6
19. Bains M, Hall ED. Antioxidant therapies in traumatic brain and spinal cord injury. *Biochim Biophys Acta*. 2012;1822(5):675-684. doi:10.1016/j.bbadis.2011.10.017

20. Verweij BH, Muizelaar JP, Vinas FC, Peterson PL, Xiong Y, Lee CP. Impaired cerebral mitochondrial function after traumatic brain injury in humans. *J Neurosurg.* 2000;93(5):815-820. doi:10.3171/jns.2000.93.5.0815
21. Tymianski M, Charlton M, Carlen P, Tator C. Source specificity of early calcium neurotoxicity in cultured embryonic spinal neurons. *J Neurosci.* 1993;13(5):2085-2104. doi:10.1523/JNEUROSCI.13-05-02085.1993
22. Faden AI, Demediuk P, Panter SS, Vink R. The Role of Excitatory Amino Acids and NMDA Receptors in Traumatic Brain Injury. *Science.* Published online May 19, 1989. doi:10.1126/science.2567056
23. Smith JS, Fulop ZL, Levinsohn SA, Darrell RS, Stein DG. Effects of the Novel NMDA Receptor Antagonist Gacyclidine on Recovery From Medial Frontal Cortex Contusion Injury in Rats. *Neural Plast.* NaN/NaN/NaN;7:73-91. doi:10.1155/NP.2000.73
24. The Effects of Memantine on Glutamic Receptor–Associated Nitrosative Stress in a Traumatic Brain Injury Rat Model - ClinicalKey. Accessed November 7, 2022. <https://www.clinicalkey.com/#!/content/playContent/1-s2.0-S1878875018301839?returnurl=https:%2F%2Flinkinghub.elsevier.com%2Fretrieve%2Fpii%2FS1878875018301839%3Fshowall%3Dtrue&referrer=https:%2F%2Fwww.frontiersin.org%2F>
25. Sönmez A, Sayın O, Gürgen SG, Çalışır M. Neuroprotective effects of MK-801 against traumatic brain injury in immature rats. *Neurosci Lett.* 2015;597:137-142. doi:10.1016/j.neulet.2015.05.001
26. Thomas TC, Hinzman JM, Gerhardt GA, Lifshitz J. Hypersensitive Glutamate Signaling Correlates with the Development of Late-Onset Behavioral Morbidity in Diffuse Brain-Injured Circuitry. *J Neurotrauma.* 2012;29(2):187-200. doi:10.1089/neu.2011.2091
27. Chamard E, Lasseigne M, Henry L, et al. Neurometabolic and microstructural alterations following a sports-related concussion in female athletes. *Brain Inj.* 2013;27(9):1038-1046. doi:10.3109/02699052.2013.794968
28. Kierans AS, Kirov II, Gonen O, et al. Myoinositol and glutamate complex neurometabolite abnormality after mild traumatic brain injury. *Neurology.* 2014;82(6):521-528. doi:10.1212/WNL.000000000000105
29. Abe K, Saito H. Possible linkage between glutamate transporter and mitogen-activated protein kinase cascade in cultured rat cortical astrocytes. *J Neurochem.* 2001;76(1):217-223. doi:10.1046/j.1471-4159.2001.00062.x
30. The concentrations and distributions of three C-terminal variants of the GLT1 (EAAT2; slc1a2) glutamate transporter protein in rat brain tissue suggest differential regulation - ClinicalKey. Accessed November 7, 2022. <https://www.clinicalkey.com/#!/content/playContent/1-s2.0->

S0306452209003947?returnurl=https:%2F%2Flinkinghub.elsevier.com%2Fretrieve%2Fpii%2FS0306452209003947%3Fshowall%3Dtrue&referrer=https:%2F%2Fen.wikipedia.org%2F

31. Levenson J, Weeber E, Selcher JC, Kategaya LS, Sweatt JD, Eskin A. Long-term potentiation and contextual fear conditioning increase neuronal glutamate uptake. *Nat Neurosci.* 2002;5(2):155-161. doi:10.1038/nn791
32. Pizzino G, Irrera N, Cucinotta M, et al. Oxidative Stress: Harms and Benefits for Human Health. *Oxid Med Cell Longev.* 2017;2017:8416763. doi:10.1155/2017/8416763
33. Zhou R, Yazdi AS, Menu P, Tschopp J. A role for mitochondria in NLRP3 inflammasome activation. *Nature.* 2011;469(7329):221-225. doi:10.1038/nature09663
34. Goulopoulou S, Matsumoto T, Bomfim GF, Webb RC. Toll-like receptor 9 activation: a novel mechanism linking placenta-derived mitochondrial DNA and vascular dysfunction in preeclampsia. *Clin Sci Lond Engl 1979.* 2012;123(7):429-435. doi:10.1042/CS20120130
35. Mai S, Klinkenberg M, Auburger G, Bereiter-Hahn J, Jendrach M. Decreased expression of Drp1 and Fis1 mediates mitochondrial elongation in senescent cells and enhances resistance to oxidative stress through PINK1. *J Cell Sci.* 2010;123(Pt 6):917-926. doi:10.1242/jcs.059246
36. Leduc-Gaudet JP, Picard M, St-Jean Pelletier F, et al. Mitochondrial morphology is altered in atrophied skeletal muscle of aged mice. *Oncotarget.* 2015;6(20):17923-17937. doi:10.18632/oncotarget.4235
37. Sun N, Youle RJ, Finkel T. The Mitochondrial Basis of Aging. *Mol Cell.* 2016;61(5):654-666. doi:10.1016/j.molcel.2016.01.028
38. Wang L, Pavlou S, Du X, Bhuckory M, Xu H, Chen M. Glucose transporter 1 critically controls microglial activation through facilitating glycolysis. *Mol Neurodegener.* 2019;14:2. doi:10.1186/s13024-019-0305-9
39. Voloboueva LA, Emery JF, Sun X, Giffard RG. Inflammatory response of microglial BV-2 cells includes a glycolytic shift and is modulated by mitochondrial glucose-regulated protein 75/mortalin. *FEBS Lett.* 2013;587(6):756-762. doi:10.1016/j.febslet.2013.01.067
40. Castanier C, Garcin D, Vazquez A, Arnoult D. Mitochondrial dynamics regulate the RIG-I-like receptor antiviral pathway. *EMBO Rep.* 2010;11(2):133-138. doi:10.1038/embor.2009.258
41. Houle S, Kokiko-Cochran ON. A Levee to the Flood: Pre-injury Neuroinflammation and Immune Stress Influence Traumatic Brain Injury Outcome. *Front Aging Neurosci.* 2022;13:788055. doi:10.3389/fnagi.2021.788055

42. Nair S, Sobotka KS, Joshi P, et al. Lipopolysaccharide-induced alteration of mitochondrial morphology induces a metabolic shift in microglia modulating the inflammatory response in vitro and in vivo. *Glia*. 2019;67(6):1047-1061. doi:10.1002/glia.23587
43. Kalayci M, Unal MM, Gul S, et al. Effect of coenzyme Q10 on ischemia and neuronal damage in an experimental traumatic brain-injury model in rats. *BMC Neurosci*. 2011;12:75. doi:10.1186/1471-2202-12-75
44. Pierce JD, Gupte R, Thimmesch A, et al. Ubiquinol treatment for TBI in male rats: Effects on mitochondrial integrity, injury severity, and neurometabolism. *J Neurosci Res*. 2018;96(6):1080-1092. doi:10.1002/jnr.24210
45. Simon DW, McGeachy M, Bayır H, Clark RSB, Loane DJ, Kochanek PM. Neuroinflammation in the Evolution of Secondary Injury, Repair, and Chronic Neurodegeneration after Traumatic Brain Injury. *Nat Rev Neurol*. 2017;13(3):171-191. doi:10.1038/nrneuro.2017.13
46. Baracaldo-Santamaría D, Ariza-Salamanca DF, Corrales-Hernández MG, Pachón-Londoño MJ, Hernandez-Duarte I, Calderon-Ospina CA. Revisiting Excitotoxicity in Traumatic Brain Injury: From Bench to Bedside. *Pharmaceutics*. 2022;14(1). doi:10.3390/pharmaceutics14010152
47. Hu Y, Mai W, Chen L, et al. mTOR-mediated metabolic reprogramming shapes distinct microglia functions in response to lipopolysaccharide and ATP. *Glia*. 2020;68(5):1031-1045. doi:10.1002/glia.23760
48. Gyoneva S, Ransohoff RM. Inflammatory reaction after traumatic brain injury: Therapeutic potential of targeting cell-cell communication by chemokines. *Trends Pharmacol Sci*. 2015;36(7):471-480. doi:10.1016/j.tips.2015.04.003
49. Ransohoff RM. Chemokines and chemokine receptors: Standing at the crossroads of immunobiology and neurobiology. *Immunity*. 2009;31(5):711-721. doi:10.1016/j.immuni.2009.09.010
50. Bajetto A, Bonavia R, Barbero S, Florio T, Schettini G. Chemokines and their receptors in the central nervous system. *Front Neuroendocrinol*. 2001;22(3):147-184. doi:10.1006/frne.2001.0214
51. Doğanyığıt Z, Erbakan K, Akyuz E, Polat AK, Arulsamy A, Shaikh MohdF. The Role of Neuroinflammatory Mediators in the Pathogenesis of Traumatic Brain Injury: A Narrative Review. *ACS Chem Neurosci*. 2022;13(13):1835-1848. doi:10.1021/acschemneuro.2c00196
52. Pop V, Sorensen DW, Kamper JE, et al. Early brain injury alters the blood–brain barrier phenotype in parallel with β -amyloid and cognitive changes in adulthood. *J Cereb Blood Flow Metab*. 2013;33(2):205-214. doi:10.1038/jcbfm.2012.154

53. Wu Y, Wu H, Guo X, Pluimer B, Zhao Z. Blood–Brain Barrier Dysfunction in Mild Traumatic Brain Injury: Evidence From Preclinical Murine Models. *Front Physiol.* 2020;11. Accessed November 8, 2022. <https://www.frontiersin.org/articles/10.3389/fphys.2020.01030>
54. Kokiko-Cochran ON, Godbout JP. The Inflammatory Continuum of Traumatic Brain Injury and Alzheimer’s Disease. *Front Immunol.* 2018;9:672. doi:10.3389/fimmu.2018.00672
55. Hill CS, Coleman MP, Menon DK. Traumatic Axonal Injury: Mechanisms and Translational Opportunities. *Trends Neurosci.* 2016;39(5):311-324. doi:10.1016/j.tins.2016.03.002
56. Maxwell WL, Bartlett E, Morgan H. Wallerian degeneration in the optic nerve stretch-injury model of traumatic brain injury: a stereological analysis. *J Neurotrauma.* 2015;32(11):780-790. doi:10.1089/neu.2014.3369
57. Bradshaw DV, Knutsen AK, Korotcov A, et al. Genetic inactivation of SARM1 axon degeneration pathway improves outcome trajectory after experimental traumatic brain injury based on pathological, radiological, and functional measures. *Acta Neuropathol Commun.* 2021;9(1):89. doi:10.1186/s40478-021-01193-8
58. Green REA, Colella B, Maller JJ, Bayley M, Glazer J, Mikulis DJ. Scale and pattern of atrophy in the chronic stages of moderate-severe TBI. *Front Hum Neurosci.* 2014;8:67. doi:10.3389/fnhum.2014.00067
59. Cole JH, Leech R, Sharp DJ, Alzheimer’s Disease Neuroimaging Initiative. Prediction of brain age suggests accelerated atrophy after traumatic brain injury. *Ann Neurol.* 2015;77(4):571-581. doi:10.1002/ana.24367
60. Hellewell SC, Yan EB, Agyapomaa DA, Bye N, Morganti-Kossmann MC. Post-traumatic hypoxia exacerbates brain tissue damage: analysis of axonal injury and glial responses. *J Neurotrauma.* 2010;27(11):1997-2010. doi:10.1089/neu.2009.1245
61. Shaw AC, Goldstein DR, Montgomery RR. Age-dependent dysregulation of innate immunity. *Nat Rev Immunol.* 2013;13(12):875-887. doi:10.1038/nri3547
62. Cunningham C, Wilcockson DC, Champion S, Lunnon K, Perry VH. Central and Systemic Endotoxin Challenges Exacerbate the Local Inflammatory Response and Increase Neuronal Death during Chronic Neurodegeneration. *J Neurosci.* 2005;25(40):9275-9284. doi:10.1523/JNEUROSCI.2614-05.2005
63. Henry CJ, Huang Y, Wynne AM, Godbout JP. Peripheral Lipopolysaccharide (LPS) challenge promotes microglial hyperactivity in aged mice that is associated with exaggerated induction of both pro-inflammatory IL-1 β and anti-inflammatory IL-10 cytokines. *Brain Behav Immun.* 2009;23(3):309-317. doi:10.1016/j.bbi.2008.09.002

64. Krukowski K, Chou A, Feng X, et al. Traumatic Brain Injury in Aged Mice Induces Chronic Microglia Activation, Synapse Loss, and Complement-Dependent Memory Deficits. *Int J Mol Sci.* 2018;19(12):3753. doi:10.3390/ijms19123753
65. Holden SS, Grandi FC, Aboubakr O, et al. Complement factor C1q mediates sleep spindle loss and epileptic spikes after mild brain injury. *Science.* 2021;373(6560):eabj2685. doi:10.1126/science.abj2685
66. Ritzel RM, Doran SJ, Glaser EP, et al. Old age increases microglial senescence, exacerbates secondary neuroinflammation, and worsens neurological outcomes following acute traumatic brain injury in mice. *Neurobiol Aging.* 2019;77:194-206. doi:10.1016/j.neurobiolaging.2019.02.010
67. Barrett JP, Knobloch SM, Bhattacharya S, Gordish-Dressman H, Stoica BA, Loane DJ. Traumatic Brain Injury Induces cGAS Activation and Type I Interferon Signaling in Aged Mice. *Front Immunol.* 2021;12:710608. doi:10.3389/fimmu.2021.710608
68. Kumar A, Sidhu J, Goyal A, Tsao JW. Alzheimer Disease. In: *StatPearls.* StatPearls Publishing; 2022. Accessed November 11, 2022. <http://www.ncbi.nlm.nih.gov/books/NBK499922/>
69. Guo Z, Cupples LA, Kurz A, et al. Head injury and the risk of AD in the MIG study. *Neurology.* 2000;54(6):1316-1323. doi:10.1212/wnl.54.6.1316
70. Fleminger S, Oliver D, Lovestone S, Rabe-Hesketh S, Giora A. Head injury as a risk factor for Alzheimer's disease: the evidence 10 years on; a partial replication. *J Neurol Neurosurg Psychiatry.* 2003;74(7):857-862. doi:10.1136/jnnp.74.7.857
71. Wilson L, Stewart W, Dams-O'Connor K, et al. The chronic and evolving neurological consequences of traumatic brain injury. *Lancet Neurol.* 2017;16(10):813-825. doi:10.1016/S1474-4422(17)30279-X
72. Pluta R, Furmaga-Jabłońska W, Maciejewski R, Ułamek-Kozioł M, Jabłoński M. Brain Ischemia Activates β - and γ -Secretase Cleavage of Amyloid Precursor Protein: Significance in Sporadic Alzheimer's Disease. *Mol Neurobiol.* 2013;47(1):425-434. doi:10.1007/s12035-012-8360-z
73. Iadecola C. The pathobiology of vascular dementia. *Neuron.* 2013;80(4):10.1016/j.neuron.2013.10.008. doi:10.1016/j.neuron.2013.10.008
74. Monomer Dynamics of Alzheimer Peptides and Kinetic Control of Early Aggregation in Alzheimer's Disease - PMC. Accessed November 11, 2022. <https://www.ncbi.nlm.nih.gov/pmc/articles/PMC5806154/>
75. Ghiso J, Fossati S, Rostagno A. Amyloidosis Associated with Cerebral Amyloid Angiopathy: Cell Signaling Pathways Elicited in Cerebral Endothelial Cells. *J Alzheimers Dis JAD.* 2014;42(0 3):S167-S176. doi:10.3233/JAD-140027

76. Fossati S, Cam J, Meyerson J, et al. Differential activation of mitochondrial apoptotic pathways by vasculotropic amyloid- β variants in cells composing the cerebral vessel walls. *FASEB J*. 2010;24(1):229-241. doi:10.1096/fj.09-139584
77. Jääntti H, Sitnikova V, Ishchenko Y, et al. Microglial amyloid beta clearance is driven by PIEZO1 channels. *J Neuroinflammation*. 2022;19(1):147. doi:10.1186/s12974-022-02486-y
78. Y Y, Rd Y. Microglial A β receptors in Alzheimer's disease. *Cell Mol Neurobiol*. 2015;35(1). doi:10.1007/s10571-014-0101-6
79. Huang Y, Happonen KE, Burrola PG, et al. Microglia use TAM receptors to detect and engulf amyloid β plaques. *Nat Immunol*. 2021;22(5):586-594. doi:10.1038/s41590-021-00913-5
80. Johnson VE, Stewart W, Smith DH. Axonal Pathology in Traumatic Brain Injury. *Exp Neurol*. 2013;246:35-43. doi:10.1016/j.expneurol.2012.01.013
81. Ramos-Cejudo J, Wisniewski T, Marmar C, et al. Traumatic Brain Injury and Alzheimer's Disease: The Cerebrovascular Link. *EBioMedicine*. 2018;28:21-30. doi:10.1016/j.ebiom.2018.01.021
82. Shin MK, Vázquez-Rosa E, Koh Y, et al. Reducing acetylated tau is neuroprotective in brain injury. *Cell*. 2021;184(10):2715-2732.e23. doi:10.1016/j.cell.2021.03.032
83. Crunkhorn S. Targeting tau in traumatic brain injury. *Nat Rev Drug Discov*. 2021;20(6):424-424. doi:10.1038/d41573-021-00070-2
84. Perea JR, Ávila J, Bolós M. Dephosphorylated rather than hyperphosphorylated Tau triggers a pro-inflammatory profile in microglia through the p38 MAPK pathway. *Exp Neurol*. 2018;310:14-21. doi:10.1016/j.expneurol.2018.08.007
85. Yoshiyama Y, Higuchi M, Zhang B, et al. Synapse loss and microglial activation precede tangles in a P301S tauopathy mouse model. *Neuron*. 2007;53(3):337-351. doi:10.1016/j.neuron.2007.01.010
86. Gratuze M, Leyns CEG, Holtzman DM. New insights into the role of TREM2 in Alzheimer's disease. *Mol Neurodegener*. 2018;13:66. doi:10.1186/s13024-018-0298-9
87. Clusterin in Alzheimer's Disease: Mechanisms, Genetics, and Lessons From Other Pathologies - PMC. Accessed November 11, 2022. <https://www.ncbi.nlm.nih.gov/pmc/articles/PMC6403191/>
88. Lambert JC, Ibrahim-Verbaas CA, Harold D, et al. Meta-analysis of 74,046 individuals identifies 11 new susceptibility loci for Alzheimer's disease. *Nat Genet*. 2013;45(12):1452-1458. doi:10.1038/ng.2802

89. Zhu XC, Yu JT, Jiang T, Wang P, Cao L, Tan L. CR1 in Alzheimer's disease. *Mol Neurobiol.* 2015;51(2):753-765. doi:10.1007/s12035-014-8723-8
90. Ransohoff RM. A polarizing question: do M1 and M2 microglia exist? *Nat Neurosci.* 2016;19(8):987-991. doi:10.1038/nn.4338
91. Cardona AE, Piroo EP, Sasse ME, et al. Control of microglial neurotoxicity by the fractalkine receptor. *Nat Neurosci.* 2006;9(7):917-924. doi:10.1038/nn1715
92. Paolicelli RC, Bolasco G, Pagani F, et al. Synaptic pruning by microglia is necessary for normal brain development. *Science.* 2011;333(6048):1456-1458. doi:10.1126/science.1202529
93. Schafer DP, Stevens B. Microglia Function in Central Nervous System Development and Plasticity. *Cold Spring Harb Perspect Biol.* 2015;7(10):a020545. doi:10.1101/cshperspect.a020545
94. Li Q, Barres BA. Microglia and macrophages in brain homeostasis and disease. *Nat Rev Immunol.* 2018;18(4):225-242. doi:10.1038/nri.2017.125
95. Peng J, Liu Y, Umpierre AD, et al. Microglial P2Y12 receptor regulates ventral hippocampal CA1 neuronal excitability and innate fear in mice. *Mol Brain.* 2019;12(1):71. doi:10.1186/s13041-019-0492-x
96. Cserép C, Pósfai B, Lénárt N, et al. Microglia monitor and protect neuronal function through specialized somatic purinergic junctions. *Science.* 2020;367(6477):528-537. doi:10.1126/science.aax6752
97. Cherry JD, Olschowka JA, O'Banion MK. Are "Resting" Microglia More "M2"? *Front Immunol.* 2014;5. Accessed November 11, 2022. <https://www.frontiersin.org/articles/10.3389/fimmu.2014.00594>
98. Jurga AM, Paleczna M, Kuter KZ. Overview of General and Discriminating Markers of Differential Microglia Phenotypes. *Front Cell Neurosci.* 2020;14. Accessed November 10, 2022. <https://www.frontiersin.org/articles/10.3389/fncel.2020.00198>
99. Boje KM, Arora PK. Microglial-produced nitric oxide and reactive nitrogen oxides mediate neuronal cell death. *Brain Res.* 1992;587(2):250-256. doi:10.1016/0006-8993(92)91004-x
100. He M, Dong H, Huang Y, et al. Astrocyte-Derived CCL2 is Associated with M1 Activation and Recruitment of Cultured Microglial Cells. *Cell Physiol Biochem Int J Exp Cell Physiol Biochem Pharmacol.* 2016;38(3):859-870. doi:10.1159/000443040
101. Corraliza IM, Soler G, Eichmann K, Modolell M. Arginase induction by suppressors of nitric oxide synthesis (IL-4, IL-10 and PGE2) in murine bone-marrow-derived macrophages. *Biochem Biophys Res Commun.* 1995;206(2):667-673. doi:10.1006/bbrc.1995.1094

102. Odegaard JI, Ricardo-Gonzalez RR, Red Eagle A, et al. Alternative M2 activation of Kupffer cells by PPARdelta ameliorates obesity-induced insulin resistance. *Cell Metab.* 2008;7(6):496-507. doi:10.1016/j.cmet.2008.04.003
103. Keren-Shaul H, Spinrad A, Weiner A, et al. A Unique Microglia Type Associated with Restricting Development of Alzheimer's Disease. *Cell.* 2017;169(7):1276-1290.e17. doi:10.1016/j.cell.2017.05.018
104. Krasemann S, Madore C, Cialic R, et al. The TREM2-APOE pathway drives the transcriptional phenotype of dysfunctional microglia in neurodegenerative diseases. *Immunity.* 2017;47(3):566. doi:10.1016/j.immuni.2017.08.008
105. Hammond TR, Dufort C, Dissing-Olesen L, et al. Single-Cell RNA Sequencing of Microglia throughout the Mouse Lifespan and in the Injured Brain Reveals Complex Cell-State Changes. *Immunity.* 2019;50(1):253-271.e6. doi:10.1016/j.immuni.2018.11.004
106. Li Q, Cheng Z, Zhou L, et al. Developmental Heterogeneity of Microglia and Brain Myeloid Cells Revealed by Deep Single-Cell RNA Sequencing. *Neuron.* 2019;101(2):207-223.e10. doi:10.1016/j.neuron.2018.12.006
107. Casali BT, Reed-Geaghan EG. Microglial Function and Regulation during Development, Homeostasis and Alzheimer's Disease. *Cells.* 2021;10(4):957. doi:10.3390/cells10040957
108. Deczkowska A, Keren-Shaul H, Weiner A, Colonna M, Schwartz M, Amit I. Disease-Associated Microglia: A Universal Immune Sensor of Neurodegeneration. *Cell.* 2018;173(5):1073-1081. doi:10.1016/j.cell.2018.05.003
109. Rangaraju S, Dammer EB, Raza SA, et al. Identification and therapeutic modulation of a pro-inflammatory subset of disease-associated-microglia in Alzheimer's disease. *Mol Neurodegener.* 2018;13:24. doi:10.1186/s13024-018-0254-8
110. Wang S, Sudan R, Peng V, et al. TREM2 drives microglia response to amyloid- β via SYK-dependent and -independent pathways. *Cell.* 2022;185(22):4153-4169.e19. doi:10.1016/j.cell.2022.09.033
111. Boche D, Gordon MN. Diversity of transcriptomic microglial phenotypes in aging and Alzheimer's disease. *Alzheimers Dement.* 2022;18(2):360-376. doi:10.1002/alz.12389
112. Frigerio CS, Wolfs L, Fattorelli N, et al. The Major Risk Factors for Alzheimer's Disease: Age, Sex, and Genes Modulate the Microglia Response to A β Plaques. *Cell Rep.* 2019;27(4):1293-1306.e6. doi:10.1016/j.celrep.2019.03.099

113. Condello C, Yuan P, Schain A, Grutzendler J. Microglia constitute a barrier that prevents neurotoxic protofibrillar A β 42 hotspots around plaques. *Nat Commun.* 2015;6:6176. doi:10.1038/ncomms7176
114. Paresce DM, Ghosh RN, Maxfield FR. Microglial cells internalize aggregates of the Alzheimer's disease amyloid beta-protein via a scavenger receptor. *Neuron.* 1996;17(3):553-565. doi:10.1016/s0896-6273(00)80187-7
115. Candlish M, Hefendehl JK. Microglia Phenotypes Converge in Aging and Neurodegenerative Disease. *Front Neurol.* 2021;12. Accessed November 12, 2022. <https://www.frontiersin.org/articles/10.3389/fneur.2021.660720>
116. Hong S, Beja-Glasser VF, Nfonoyim BM, et al. Complement and microglia mediate early synapse loss in Alzheimer mouse models. *Science.* 2016;352(6286):712-716. doi:10.1126/science.aad8373
117. Henry RJ, Ritzel RM, Barrett JP, et al. Microglial Depletion with CSF1R Inhibitor During Chronic Phase of Experimental Traumatic Brain Injury Reduces Neurodegeneration and Neurological Deficits. *J Neurosci Off J Soc Neurosci.* 2020;40(14):2960-2974. doi:10.1523/JNEUROSCI.2402-19.2020
118. Witcher KG, Bray CE, Chunchai T, et al. Traumatic Brain Injury Causes Chronic Cortical Inflammation and Neuronal Dysfunction Mediated by Microglia. *J Neurosci.* 2021;41(7):1597-1616. doi:10.1523/JNEUROSCI.2469-20.2020
119. Yao Z, van Velthoven CTJ, Nguyen TN, et al. A taxonomy of transcriptomic cell types across the isocortex and hippocampal formation. *Cell.* 2021;184(12):3222-3241.e26. doi:10.1016/j.cell.2021.04.021
120. Ding J, Adiconis X, Simmons SK, et al. Systematic comparison of single-cell and single-nucleus RNA-sequencing methods. *Nat Biotechnol.* 2020;38(6):737-746. doi:10.1038/s41587-020-0465-8
121. Lacar B, Linker SB, Jaeger BN, et al. Nuclear RNA-seq of single neurons reveals molecular signatures of activation. *Nat Commun.* 2016;7(1):11022. doi:10.1038/ncomms11022
122. Henry RJ, Ritzel RM, Barrett JP, et al. Microglial Depletion with CSF1R Inhibitor During Chronic Phase of Experimental Traumatic Brain Injury Reduces Neurodegeneration and Neurological Deficits. *J Neurosci Off J Soc Neurosci.* 2020;40(14):2960-2974. doi:10.1523/JNEUROSCI.2402-19.2020
123. Byrnes KR, Loane DJ, Stoica BA, Zhang J, Faden AI. Delayed mGluR5 activation limits neuroinflammation and neurodegeneration after traumatic brain injury. *J Neuroinflammation.* 2012;9:43. doi:10.1186/1742-2094-9-43
124. Cortes-Gutierrez M, sament, Martin C, et al. Frozen Tissue Nuclei Extraction (for 10xV3 snSEQ). protocols.io. Published January 1, 1970. Accessed November 9, 2022.

<https://www.protocols.io/view/frozen-tissue-nuclei-extraction-for-10xv3-snseq-cd2qs8dw>

125. CG000212_SingleCellATAC_Nuclei_Isolation_MouseBrain_DemonstratedProtocol_Rev_C.pdf. Accessed November 9, 2022. https://assets.ctfassets.net/an68im79xiti/zZh2iRV5TgWP8A96Easg6/a8c93762107f2dd635bfcde6978d84f9/CG000212_SingleCellATAC_Nuclei_Isolation_MouseBrain_DemonstratedProtocol_Rev_C.pdf
126. Zheng GXY, Terry JM, Belgrader P, et al. Massively parallel digital transcriptional profiling of single cells. *Nat Commun.* 2017;8(1):14049. doi:10.1038/ncomms14049
127. Satpathy AT, Granja JM, Yost KE, et al. Massively parallel single-cell chromatin landscapes of human immune cell development and intratumoral T cell exhaustion. *Nat Biotechnol.* 2019;37(8):925-936. doi:10.1038/s41587-019-0206-z
128. Hao Y, Hao S, Andersen-Nissen E, et al. Integrated analysis of multimodal single-cell data. *Cell.* 2021;184(13):3573-3587.e29. doi:10.1016/j.cell.2021.04.048
129. Saunders A, Macosko EZ, Wysoker A, et al. Molecular Diversity and Specializations among the Cells of the Adult Mouse Brain. *Cell.* 2018;174(4):1015-1030.e16. doi:10.1016/j.cell.2018.07.028
130. McCarthy DJ, Chen Y, Smyth GK. Differential expression analysis of multifactor RNA-Seq experiments with respect to biological variation. *Nucleic Acids Res.* 2012;40(10):4288-4297. doi:10.1093/nar/gks042
131. Qiu X, Mao Q, Tang Y, et al. Reversed graph embedding resolves complex single-cell trajectories. *Nat Methods.* 2017;14(10):979-982. doi:10.1038/nmeth.4402
132. Granja JM, Corces MR, Pierce SE, et al. ArchR is a scalable software package for integrative single-cell chromatin accessibility analysis. *Nat Genet.* 2021;53(3):403-411. doi:10.1038/s41588-021-00790-6
133. Dijk D van, Sharma R, Nainys J, et al. Recovering Gene Interactions from Single-Cell Data Using Data Diffusion. *Cell.* 2018;174(3):716-729.e27. doi:10.1016/j.cell.2018.05.061
134. Liu T. MACS2: Model Based Analysis for ChIP-Seq data. Accessed November 9, 2022. <http://github.com/taoliu/MACS/>
135. Huynh-Thu VA, Irrthum A, Wehenkel L, Geurts P. Inferring Regulatory Networks from Expression Data Using Tree-Based Methods. *PLOS ONE.* 2010;5(9):e12776. doi:10.1371/journal.pone.0012776

136. Wahane S, Zhou X, Zhou X, et al. Diversified transcriptional responses of myeloid and glial cells in spinal cord injury shaped by HDAC3 activity. *Sci Adv.* 2021;7(9):eabd8811. doi:10.1126/sciadv.abd8811
137. Martinez FO, Gordon S. The M1 and M2 paradigm of macrophage activation: time for reassessment. *F1000prime Rep.* 2014;6:13. doi:10.12703/P6-13
138. Remmerie A, Martens L, Thoné T, et al. Osteopontin Expression Identifies a Subset of Recruited Macrophages Distinct from Kupffer Cells in the Fatty Liver. *Immunity.* 2020;53(3):641-657.e14. doi:10.1016/j.immuni.2020.08.004
139. Schepper SD, Ge JZ, Crowley G, et al. Perivascular SPP1 Mediates Microglial Engulfment of Synapses in Alzheimer's Disease Models. Published online April 5, 2022:2022.04.04.486547. doi:10.1101/2022.04.04.486547
140. Mashaghi A, Marmalidou A, Tehrani M, Grace PM, Pothoulakis C, Dana R. Neuropeptide Substance P and the Immune Response. *Cell Mol Life Sci CMLS.* 2016;73(22):4249. doi:10.1007/s00018-016-2293-z
141. Gil-Yarom N, Radomir L, Sever L, et al. CD74 is a novel transcription regulator. *Proc Natl Acad Sci.* 2017;114(3):562-567. doi:10.1073/pnas.1612195114
142. Lu Y, Tan L, Xie J, Cheng L, Wang X. Distinct microglia alternative splicing in Alzheimer's disease. *Aging.* 2022;14(16):6554-6566. doi:10.18632/aging.204223
143. Sousa C, Golebiewska A, Poovathingal SK, et al. Single-cell transcriptomics reveals distinct inflammation-induced microglia signatures. *EMBO Rep.* 2018;19(11):e46171. doi:10.15252/embr.201846171
144. Lee N, Jae Y, Kim M, et al. A pathogen-derived metabolite induces microglial activation via odorant receptors. *FEBS J.* 2020;287(17):3841-3870. doi:10.1111/febs.15234
145. Liu Q, Zhang Y. PRDX1 enhances cerebral ischemia-reperfusion injury through activation of TLR4-regulated inflammation and apoptosis. *Biochem Biophys Res Commun.* 2019;519(3):453-461. doi:10.1016/j.bbrc.2019.08.077
146. Srinivasan K, Friedman BA, Larson JL, et al. Untangling the brain's neuroinflammatory and neurodegenerative transcriptional responses. *Nat Commun.* 2016;7(1):11295. doi:10.1038/ncomms11295
147. Makinde HM, Winter DR, Procissi D, et al. A Novel Microglia-Specific Transcriptional Signature Correlates With Behavioral Deficits in Neuropsychiatric Lupus. *Front Immunol.* 2020;11. Accessed November 10, 2022. <https://www.frontiersin.org/articles/10.3389/fimmu.2020.00230>
148. Dordoe C, Chen K, Huang W, et al. Roles of Fibroblast Growth Factors and Their Therapeutic Potential in Treatment of Ischemic Stroke. *Front Pharmacol.* 2021;12.

149. Li Y, Lu B, Sheng L, et al. Hexokinase 2-dependent hyperglycolysis driving microglial activation contributes to ischemic brain injury. *J Neurochem.* 2018;144(2):186-200. doi:10.1111/jnc.14267
150. Zhao Y, Ma C, Chen C, et al. STAT1 Contributes to Microglial/Macrophage Inflammation and Neurological Dysfunction in a Mouse Model of Traumatic Brain Injury. *J Neurosci.* 2022;42(39):7466-7481. doi:10.1523/JNEUROSCI.0682-22.2022
151. Levy DR, Udgata A, Turlomousis P, et al. The Parkinson's disease-associated kinase LRRK2 regulates genes required for cell adhesion, polarization, and chemotaxis in activated murine macrophages. *J Biol Chem.* 2020;295(31):10857-10867. doi:10.1074/jbc.RA119.011842
152. Lau SF, Cao H, Fu AKY, Ip NY. Single-nucleus transcriptome analysis reveals dysregulation of angiogenic endothelial cells and neuroprotective glia in Alzheimer's disease. *Proc Natl Acad Sci.* 2020;117(41):25800-25809. doi:10.1073/pnas.2008762117
153. Mitroi DN, Tian M, Kawaguchi R, Lowry WE, Carmichael ST. Single-nucleus transcriptome analysis reveals disease- and regeneration-associated endothelial cells in white matter vascular dementia. *J Cell Mol Med.* 2022;26(11):3183-3195. doi:10.1111/jcmm.17315
154. Hecht I, Toporik A, Podojil JR, et al. ILDR2 Is a Novel B7-like Protein That Negatively Regulates T Cell Responses. *J Immunol.* 2018;200(6):2025-2037. doi:10.4049/jimmunol.1700325
155. Zöller T, Attaai A, Potru PS, Ruß T, Spittau B. Aged Mouse Cortical Microglia Display an Activation Profile Suggesting Immunotolerogenic Functions. *Int J Mol Sci.* 2018;19(3):706. doi:10.3390/ijms19030706
156. Grabert K, Michoel T, Karavolos MH, et al. Microglial brain region-dependent diversity and selective regional sensitivities to ageing. *Nat Neurosci.* 2016;19(3):504-516. doi:10.1038/nn.4222
157. Hohsfield LA, Najafi AR, Ghorbanian Y, et al. Subventricular zone/white matter microglia reconstitute the empty adult microglial niche in a dynamic wave. *eLife.* 2018;7:e66738. doi:10.7554/eLife.66738
158. Srinivasan K, Friedman BA, Etxeberria A, et al. Alzheimer's Patient Microglia Exhibit Enhanced Aging and Unique Transcriptional Activation. *Cell Rep.* 2020;31(13):107843. doi:10.1016/j.celrep.2020.107843

159. Zöller T, Schneider A, Kleimeyer C, et al. Silencing of TGF β signalling in microglia results in impaired homeostasis. *Nat Commun.* 2018;9(1):4011. doi:10.1038/s41467-018-06224-y
160. Zhou HJ, Wang LQ, Wang DB, et al. Long noncoding RNA MALAT1 contributes to inflammatory response of microglia following spinal cord injury via the modulation of a miR-199b/IKK β /NF- κ B signaling pathway. *Am J Physiol Cell Physiol.* 2018;315(1):C52-C61. doi:10.1152/ajpcell.00278.2017
161. Otani Y, Yamaguchi Y, Sato Y, et al. PLD4 Is Involved in Phagocytosis of Microglia: Expression and Localization Changes of PLD4 Are Correlated with Activation State of Microglia. *PLoS ONE.* 2011;6(11):e27544. doi:10.1371/journal.pone.0027544
162. Lively S, Schlichter LC. Microglia Responses to Pro-inflammatory Stimuli (LPS, IFN γ +TNF α) and Reprogramming by Resolving Cytokines (IL-4, IL-10). *Front Cell Neurosci.* 2018;12:215. doi:10.3389/fncel.2018.00215
163. Lam D, Schlichter LC. Expression and contributions of the Kir2.1 inward-rectifier K $^+$ channel to proliferation, migration and chemotaxis of microglia in unstimulated and anti-inflammatory states. *Front Cell Neurosci.* 2015;9:185. doi:10.3389/fncel.2015.00185
164. Rangaraju S, Dammer EB, Raza SA, et al. Quantitative proteomics of acutely-isolated mouse microglia identifies novel immune Alzheimer's disease-related proteins. *Mol Neurodegener.* 2018;13:34. doi:10.1186/s13024-018-0266-4
165. Zang J, Wu Y, Su X, et al. Inhibition of PDE1-B by Vinpocetine Regulates Microglial Exosomes and Polarization Through Enhancing Autophagic Flux for Neuroprotection Against Ischemic Stroke. *Front Cell Dev Biol.* 2021;8:616590. doi:10.3389/fcell.2020.616590
166. O'Brien JJ, O'Callaghan JP, Miller DB, et al. Inhibition of calcium-calmodulin-dependent phosphodiesterase (PDE1) suppresses inflammatory responses. *Mol Cell Neurosci.* 2020;102:103449. doi:10.1016/j.mcn.2019.103449
167. McQuown S, Xia S, Baumgärtel K, et al. Phosphodiesterase 1b (PDE1B) Regulates Spatial and Contextual Memory in Hippocampus. *Front Mol Neurosci.* 2019;12. Accessed November 11, 2022. <https://www.frontiersin.org/articles/10.3389/fnmol.2019.00021>
168. Zhang L, Guo K, Yin S, et al. RNA-Seq Reveals Underlying Transcriptomic Mechanisms of Bone Marrow-Derived Mesenchymal Stem Cells in the Regulation of Microglia-Mediated Neuroinflammation After Subarachnoid Hemorrhage. *Stem Cells Dev.* 2020;29(9):562-573. doi:10.1089/scd.2019.0216
169. Yeh H, Ikezu T. Transcriptional and epigenetic regulation of microglia in health and disease. *Trends Mol Med.* 2019;25(2):96-111. doi:10.1016/j.molmed.2018.11.004

170. Cronk JC, Derecki NC, Ji E, et al. Methyl-CpG binding protein 2 regulates microglia and macrophage gene expression in response to inflammatory stimuli. *Immunity*. 2015;42(4):679-691. doi:10.1016/j.immuni.2015.03.013
171. Ebert DH, Gabel HW, Robinson ND, et al. Activity-Dependent Phosphorylation of MeCP2 T308 Regulates Interaction with NCoR. *Nature*. 2013;499(7458):341-345. doi:10.1038/nature12348
172. Zhang B, Gaiteri C, Bodea LG, et al. Integrated systems approach identifies genetic nodes and networks in late-onset Alzheimer's disease. *Cell*. 2013;153(3):707-720. doi:10.1016/j.cell.2013.03.030
173. Microglia pathogen phagocytosis pathway (Homo sapiens) - WikiPathways. Accessed November 11, 2022. <https://www.wikipathways.org/instance/WP3937>
174. Finelli MJ, Oliver PL. TLDC proteins: new players in the oxidative stress response and neurological disease. *Mamm Genome*. 2017;28(9):395-406. doi:10.1007/s00335-017-9706-7
175. Guebel DV, Torres NV. Sexual Dimorphism and Aging in the Human Hypocampus: Identification, Validation, and Impact of Differentially Expressed Genes by Factorial Microarray and Network Analysis. *Front Aging Neurosci*. 2016;8:229. doi:10.3389/fnagi.2016.00229
176. Sidiropoulos PNM, Mieke M, Bock T, et al. Dynamin 2 mutations in Charcot-Marie-Tooth neuropathy highlight the importance of clathrin-mediated endocytosis in myelination. *Brain J Neurol*. 2012;135(Pt 5):1395-1411. doi:10.1093/brain/aws061
177. Uronen RL, Huttunen HJ. Genetic risk factors of Alzheimer's disease and cell-to-cell transmission of Tau. *J Neurol Neuromedicine*. 2016;1(2). Accessed November 11, 2022. <https://www.jneurology.com/articles/genetic-risk-factors-of-alzheimers-disease-and-cellto-cell-transmission-of-tau.html>
178. Mellai M, Annovazzi L, Boldorini R, et al. SEL1L plays a major role in human malignant gliomas. *J Pathol Clin Res*. 2019;6(1):17-29. doi:10.1002/cjp2.134
179. Denk F, Crow M, Didangelos A, Lopes DM, McMahon SB. Persistent Alterations in Microglial Enhancers in a Model of Chronic Pain. *Cell Rep*. 2016;15(8):1771-1781. doi:10.1016/j.celrep.2016.04.063
180. Butovsky O, Jedrychowski MP, Moore CS, et al. Identification of a unique TGF- β -dependent molecular and functional signature in microglia. *Nat Neurosci*. 2014;17(1):131-143. doi:10.1038/nn.3599
181. Wang Y, Luo W, Wang X, Ma Y, Huang L, Wang Y. MAMDC2, a gene highly expressed in microglia in experimental models of Alzheimer's Disease, positively regulates the innate antiviral response during neurotropic virus infection. *J Infect*. 2022;84(2):187-204. doi:10.1016/j.jinf.2021.12.004

182. Dean RA, Cox JH, Bellac CL, Doucet A, Starr AE, Overall CM. Macrophage-specific metalloelastase (MMP-12) truncates and inactivates ELR+ CXC chemokines and generates CCL2, -7, -8, and -13 antagonists: potential role of the macrophage in terminating polymorphonuclear leukocyte influx. *Blood*. 2008;112(8):3455-3464. doi:10.1182/blood-2007-12-129080
183. Lipman AR, Fan X, Shen Y, Chung WK. Clinical and genetic characterization of CACNA1A-related disease. *Clin Genet*. 2022;102(4):288-295. doi:10.1111/cge.14180
184. Brenner E, Tiwari GR, Kapoor M, Liu Y, Brock A, Mayfield RD. Single cell transcriptome profiling of the human alcohol-dependent brain. *Hum Mol Genet*. 2020;29(7):1144-1153. doi:10.1093/hmg/ddaa038
185. Brunialti E, Villa A, Mekhaeil M, et al. Inhibition of microglial β -glucocerebrosidase hampers the microglia-mediated antioxidant and protective response in neurons. *J Neuroinflammation*. 2021;18(1):220. doi:10.1186/s12974-021-02272-2
186. Castro-Sánchez S, García-Yagüe AJ, Kügler S, Lastres-Becker I. CX3CR1-deficient microglia shows impaired signalling of the transcription factor NRF2: Implications in tauopathies. *Redox Biol*. 2019;22:101118. doi:10.1016/j.redox.2019.101118
187. Zusso M, Methot L, Lo R, Greenhalgh AD, David S, Stifani S. Regulation of postnatal forebrain amoeboid microglial cell proliferation and development by the transcription factor Runx1. *J Neurosci Off J Soc Neurosci*. 2012;32(33):11285-11298. doi:10.1523/JNEUROSCI.6182-11.2012
188. Logan TT, Villapol S, Symes AJ. TGF- β superfamily gene expression and induction of the Runx1 transcription factor in adult neurogenic regions after brain injury. *PLoS One*. 2013;8(3):e59250. doi:10.1371/journal.pone.0059250
189. Deng XL, Feng L, Wang ZX, et al. The Runx1/Notch1 Signaling Pathway Participates in M1/M2 Microglia Polarization in a Mouse Model of Temporal Lobe Epilepsy and in BV-2 Cells. *Neurochem Res*. 2020;45(9):2204-2216. doi:10.1007/s11064-020-03082-3
190. Liu H, Sun Y, Zhang Q, et al. Pro-inflammatory and proliferative microglia drive progression of glioblastoma. *Cell Rep*. 2021;36(11):109718. doi:10.1016/j.celrep.2021.109718
191. Sams EC. Oligodendrocytes in the aging brain. *Neuronal Signal*. 2021;5(3):NS20210008. doi:10.1042/NS20210008
192. Rodríguez-Callejas J de D, Cuervo-Zanatta D, Rosas-Arellano A, Fonta C, Fuchs E, Perez-Cruz C. Loss of ferritin-positive microglia relates to increased iron, RNA oxidation, and dystrophic microglia in the brains of aged male marmosets. *Am J Primatol*. 2019;81(2):e22956. doi:10.1002/ajp.22956

193. García-Revilla J, Boza-Serrano A, Espinosa-Oliva AM, et al. Galectin-3, a rising star in modulating microglia activation under conditions of neurodegeneration. *Cell Death Dis.* 2022;13(7):1-11. doi:10.1038/s41419-022-05058-3
194. Boza-Serrano A, Ruiz R, Sanchez-Varo R, et al. Galectin-3, a novel endogenous TREM2 ligand, detrimentally regulates inflammatory response in Alzheimer's disease. *Acta Neuropathol (Berl).* 2019;138(2):251-273. doi:10.1007/s00401-019-02013-z
195. Jin C, Shao Y, Zhang X, et al. A Unique Type of Highly-Activated Microglia Evoking Brain Inflammation via Mif/Cd74 Signaling Axis in Aged Mice. *Aging Dis.* 2021;12(8):2125-2139. doi:10.14336/AD.2021.0520
196. Yang HS, Onos KD, Choi K, et al. Natural genetic variation determines microglia heterogeneity in wild-derived mouse models of Alzheimer's disease. *Cell Rep.* 2021;34(6). doi:10.1016/j.celrep.2021.108739
197. Wang Y, Luo W, Wang X, Ma Y, Huang L, Wang Y. MAMDC2, a gene highly expressed in microglia in experimental models of Alzheimers Disease, positively regulates the innate antiviral response during neurotropic virus infection. *J Infect.* 2022;84(2):187-204. doi:10.1016/j.jinf.2021.12.004
198. Griciuc A, Patel S, Federico AN, et al. TREM2 Acts Downstream of CD33 in Modulating Microglial Pathology in Alzheimer's Disease. *Neuron.* 2019;103(5):820-835.e7. doi:10.1016/j.neuron.2019.06.010
199. Liu Y, Zhang M, Hao W, et al. Matrix metalloproteinase-12 contributes to neuroinflammation in the aged brain. *Neurobiol Aging.* 2013;34(4):1231-1239. doi:10.1016/j.neurobiolaging.2012.10.015